PROBING THE STRUCTURAL DYNAMICS AND MEMBRANE INTERACTIONS OF THE REGULATORY REGION OF PKC BY SOLUTION NMR

A Dissertation

by

TAYLOR RAZER COLE

Submitted to the Office of Graduate and Professional Studies of
Texas A&M University
in partial fulfillment of the requirements for the degree of

DOCTOR OF PHILOSOPHY

Chair of Committee,	Tatyana I. Igumenova
Committee Members,	Vytas A. Bankaitis
	Jae-Hyun Cho
	Frank M. Raushel
Head of Department,	A. Joshua Wand

December 2019

Major Subject: Biochemistry

ABSTRACT

Protein Kinase C (PKC) family of isoenzymes are critical players in signal transduction at the membrane surface. Its aberrant activity has been associated with Alzheimer's disease, cancer, and mood disorders. Significant efforts have been made to understand how PKC is regulated in order to design drugs to modulate activity. This has proved challenging due to the dynamic nature of PKCs.

The key event in PKC activation is the translocation of its regulatory region to anionic membranes in response to second messengers. This region in conventional isozymes contains three peripheral membrane binding modules: twin C1 domains that penetrate the membrane in response to diacylglycerol and a C2 domain that binds to anionic lipids upon association with up to three Ca^{2+}ions. The objective of this dissertation is to provide mechanistic insight into PKC activation by probing the regulatory region's structure, function, and interactions with toxic substances.

Paramagnetic solution NMR revealed that the C1B-C2 region from PKCα primarily samples open conformations, with both membrane binding sites exposed. In several of these conformations, the membrane binding loops of C1B and C2 are in relative orientations that are compatible with simultaneous membrane insertion. This suggested that C1 and C2 domains coordinate membrane binding. Consistent with this, functional studies showed that C1 ligands lowered the amount of Ca^{2+} needed to traffic C2 to membrane mimics.

Studies with membrane mimics revealed that the regulatory region responded differently to C1 ligands, diacylglycerol and tumor-promoting phorbol ester, PDBu. Preliminary data indicated that diacylglycerol drives the C1 domain deeper into the bilayer. Furthermore, the presence of the low abundance signaling lipid, phosphatidylinositol 4,5-bisphosphate, was required for bivalent binding of C1 and C2 in the presence of diacylglycerol but not PDBu.

Finally, previous studies have shown that PKCs are targeted by xenobiotic metal ions, Pb^{2+} and Cd^{2+}. This work shows that both metals drive self-assembly of the C1B-C2 regulatory region into large oligomers, enhancing membrane binding functionality. A new mode of Pb^{2+} and Cd^{2+} binding is identified. Both bind opportunistically to the linker region and C-terminal helix. Collectively this work adds to the understanding of PKC activation and its interactions with toxic substances.

ACKNOWLEDGEMENTS

I would like to thank my committee chair and principle investigator, Dr. Tatyana Igumenova and committee members, Dr. Frank Raushel, Dr. Vytas Bankaitis, and Dr. Jae-Hyun Cho for their training, support, and feedback throughout my graduate studies.

I would also like to express my thanks to past and present members of the Igumenova lab for their support and scientific discussions. My sincerest thanks go to Drs. Krystal Morales, Mikaela Stewart, and Yuan Yang for their guidance, training, and friendship.

Finally, I would like to thank my family and friends for their love and support throughout the years. In particular, I would like to thank my parents for raising me to believe that I can accomplish anything that I work hard for and my husband, Buddy, for always supporting me, believing in me, and pushing me.

CONTRIBUTORS AND FUNDING SOURCES

Contributors

I would like to thank all who contributed to the work presented in this dissertation: Dr. Krystal Morales for assigning the backbone NMR spectra for C1B-C2 and collecting part of the relaxation data presented in Chapter IV; Dr. Min Woo Sung and Dr. Andreas Holzenburg for collecting electron microscopy data; my undergraduate student, Samuel Erickson, for helping construct and collect analytical gel filtration data for the C1B-C2 variants in Chapter III; Dr. Mauricio Lasagna for advice and help with troubleshooting fluorescence experiments; Dhanusree Viswanathan for collecting the protein-to-membrane FRET data for C1B-C2 linker variants in Chapter V; Dr. Lawrence Dangott for training in MALDI-TOF spectrometry; and the first year rotation students that have contributed to my projects. In addition, my thanks go to past and present members of the Biochemistry and Biophysics department.

Funding Sources

This work was made possible by funding from the Welch Research Foundation, Biochemistry and Biophysics Department, and National Institutes of Health.

NOMENCLATURE

ACN	acetonitrile
APR	aprotinin
C1	conserved homology 1
C2	conserved homology 2
CA	carbonic anhydrase
CMBL	calcium membrane binding loop
CPMG	Carr-Purcell-Meiboom-Gill
CSP	chemical shift perturbations
DAG	diacylglycerol
Dansyl-PE	1,2-dioleoyl-sn-glycero-3-phosphoethanolamine-N-(5-dimethylamino-1-naphthalenesulfonyl)
DHPC	1,2-dihexanoyl-sn-glycero-3-phosphocholine
DHPS	1,2-dihexanoyl-sn-glycero-3-phospho-L-serine
DMPC	1,2-dimyristoyl-sn-glycero-3-phosphocholine
DMPS	1,2-dimyristoyl-sn-glycero-3-phospho-L-serine
DMSO	dimethyl sulfoxide
DOG	1,2-dioctanoyl-sn-glycerol
DOSY	diffusion ordered spectroscopy
DPC	dodecylphosphocholine
DPS	2-dihexanoyl-sn-glycero-3-[phospho-L-serine]

DTT	1,4-dithiothreitol
EM	electron microscopy
EGTA	ethylene glycol-bis(β-aminoethyl ether)-N,N,N′,N′-tetraacetic acid
FRET	Förster resonance energy transfer
fHSQC	fast heteronuclear single quantum coherence
FPLC	fast protein liquid chromatography
GST	glutathione S-transferase
HEPES	4-(2-hydroxyethyl)-1-piperazineethanesulfonic acid
HSQC	heteronuclear single quantum coherence
IMAC	Immobilized metal affinity chromatography
IP3	inositol triphosphate
IPAP	in-phase anti-phase
IPTG	isopropyl β-D-thiogalactoside
LB	Luria-Bertani
LRC	lysine rich cluster
LUV	large unilamellar vesicle
MALDI-TOF	matrix-assisted laser desorption/ionization time-of-flight
MBP	maltose binding protein
MES	2-(N-morpholino)ethanesulfonic acid
MO	Maximum Occurrence
NMR	nuclear magnetic resonance
NOE	nuclear Overhauser effect

PC	phosphatidylcholine
PCR	polymerase chain reaction
PCS	pseudocontact shift
PDB	protein data bank
PDB ID	protein data bank identification number
PDBu	phorbol 12,13-dibutyrate
PIP2	phosphatidylinositol (4,5) bisphosphate
PIP3	phosphatidylinositol (3,4,5)-trisphosphate
PKC	protein kinase C
PMA	phorbol 12-myristate 13-acetate
POPC	1-palmitoyl-2-oleoyl-sn-glycero-3-phosphocholine
POPS	1-palmitoyl-2-oleoyl-sn-glycero-3-phospho-L-serine
PRE	paramagnetic relaxation enhancement
PS	phosphatidylserine
RDC	residual dipolar couplings
SAXS	small angle x-ray scattering
SDS-PAGE	sodium dodecyl sulfate polyacrylamide gel electrophoresis
SEP	solubility enhancement peptide
SUMO	small ubiquitin-like modifier
Syt I	synaptotagmin I
TCEP	tris(2-carboxyethyl)phosphine
TFA	trifluoroacetic acid

TROSY	transverse relaxation-optimized spectroscopy

TABLE OF CONTENTS

Page

LIST OF FIGURES

Page

LIST OF TABLES

Page

CHAPTER I

INTRODUCTION

Protein Kinase C comprises a family of Ser/Thr kinases that participate in cellular signaling at the membrane surface. PKCs are members of the AGC (PKA, PKG, PKC) family of kinases. It was first discovered in 1977 as "PKM", a cyclic nucleotide-independent protein kinase produced by a proteolytic reaction.[1,2] Later studies determined that full-length PKC is activated by Ca^{2+} and phospholipids.[3] The field of research on PKC exploded when PKCs were discovered as receptors for tumor-promoting phorbol esters.[4,5] PKC isoenzymes are ubiquitously expressed in many different tissues (reviewed in [6]) and have been implicated in many human diseases such as heart disease[7,8], Alzheimer's disease[9], cancer [10-14], and mood disorders.[15] In addition, PKC has been identified as a player in heavy metal toxicity.[16-19]

PKC isoenzymes serve as integral components in multiple cellular processes such as cell proliferation, migration, and apoptosis.[20-22] Studies have shown that different PKC isoforms often play opposing roles in both diseased states and normal function.[6] Their role in disease sparked the interest in finding modulators of PKC activity. However, to design these, structural information is needed for different stages in the activation pathway. Mature PKC exists in the cytosol in a compact, latent form (Figure I.1). In this form, an N-terminal pseudosubstrate region is bound to the active site of the kinase domain. This region is designed to mimic targets of PKC[23,24], with an alanine residue instead of Ser/Thr at the phospho-acceptor site.[25] When an extracellular signal binds to a G-protein coupled receptor, phospholipase Cβ is activated and

hydrolyzes phosphatidylinositol 4,5-bisphosphate (PIP2) to generate diacylglycerol (DAG) and inositol 1,4,5-trisphosphate (IP_3). DAG remains in the membrane while IP_3 goes on to the endoplasmic reticulum to release Ca^{2+}. The hallmark of PKC activation is the recruitment of the PKC regulatory domain to the plasma membrane by these two second messengers (DAG and Ca^{2+}). The resulting conformational rearrangements mediate the expulsion of the pseudo substrate region from the active site (Figure I.1), generating a fully active kinase. Currently, there is no structural information available for the latent nor the membrane-bound enzyme, despite over forty years passing since the discovery of PKC. This is largely in part due to the nature of PKC. PKCs are multi-modular, flexible, and hydrophobic, all traits which present challenges for conventional biophysical techniques. Herein lies the primary motivation for this work: to overcome these challenges and increase the understanding of the structure of the PKC regulatory region during activation. Furthermore, toxic metal ions and phorbol esters have been shown to interfere with the normal activation pathway. Additional work presented is aimed at understanding the mechanisms for this. The following subsections will provide an introduction to the existing knowledge in the field about PKC structure, function, activation, and the foreign substances that interfere with them.

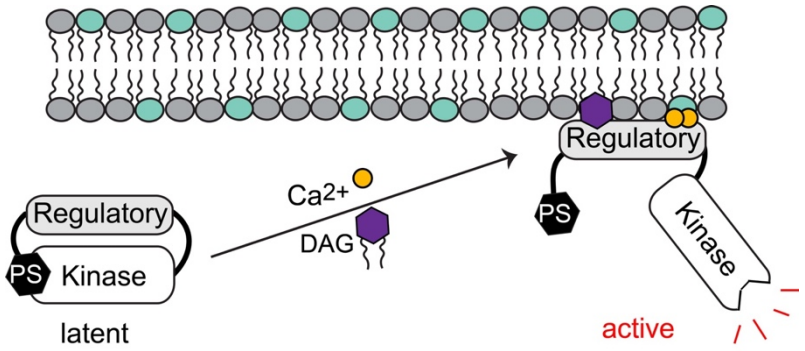

Figure I.1 Current model for the activation of the conventional isoform PKCα. Second messengers Ca^{2+} and diacylglycerol (DAG) target the PKCα regulatory domains (C2, C1A, and C1B) to the cell membrane.

PKC Isoforms and Substructure

PKC isoenzymes are divided into three subgroups based on their activation requirements: conventional, novel, and atypical. Conventional isozymes (α, β, βII, and γ) are activated by both diacylglycerol and Ca^{2+}. Novel isoforms (ε, δ, θ, and η) are activated by DAG only and atypical isoforms (ζ and ι/λ) do not require either second messenger to be activated. All three subgroups have a regulatory domain and a catalytic domain connected by a proteolytically-sensitive hinge. Figure I.2 shows the multimodular structure of each region.

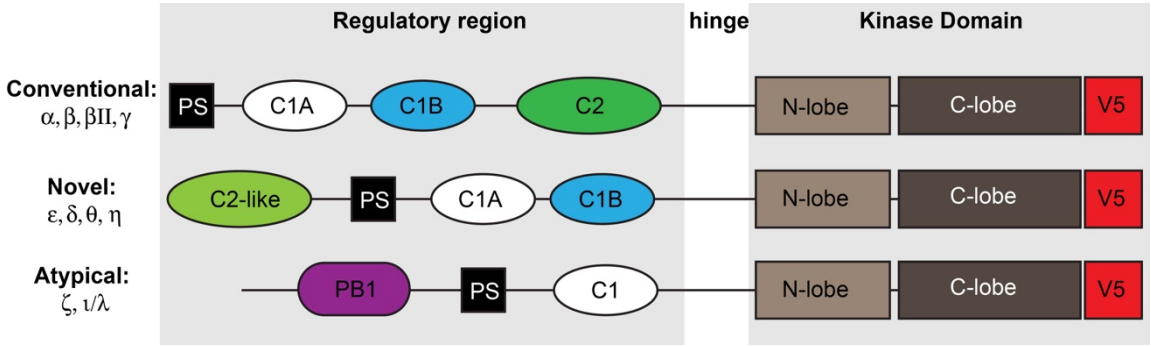

Figure I.2 Linear diagrams illustrating the multimodular structure of PKC isoforms.

All subgroups have a conserved kinase domain with N- and C-terminal lobes and an intrinsically disordered variable 5 domain at the C-termini. All isoforms have the pseudosubstrate region within their regulatory domains that binds to the active site of the kinase in the latent form, although its placement within the regulatory domain varies. Structural differences are found in the regulatory regions, variable linkers, and the C-terminal tail, making these regions attractive targets for isoform-specific modulators.

The regulatory region of conventional isoforms contains twin C1 domains that bind to membrane-embedded diacylglycerol and a C2 domain that associates with anionic membranes upon sensing its cofactor, Ca^{2+}. Novel isoforms have diacylglycerol-binding, twin C1 domains following a C2-like domain that lacks the residues needed for Ca^{2+} coordination. Finally, atypical PKCs have only one atypical C1 domain that does not have diacyglycerol binding ability and instead binds to ceramide or phosphatidylinositol (3,4,5)-trisphosphate (PIP3) and a protein-protein interaction box, PB1. Each of the individual regulatory domains is functionally autonomous. The hinge between the regulatory domains is sensitive to proteases[26,27] and cleavage at this site

generates a constitutively active kinase for some isoforms.[28] The majority of this work focuses on the regulatory regions of conventional isoform, α, and Chapter 2 also focuses on novel isoform, δ. Therefore, the remainder of the introduction will focus on these isoforms.

C1 domains

Structure

Both novel and conventional isoforms have two conserved homology 1 (C1) domains that bind to DAG and biologically active forms of phorbol esters, phorbol 12-myristate 13-acetate (PMA) and phorbol 12,13-dibutyrate (PDBu). Although these domains were originally identified in PKC, they exist in other signaling proteins such as Munc-13 isoforms and chimaerins (reviewed in [29]). The primary structure of these domains contains the sequence motif: His-X_{12}-Cis-X_2-Cis-$X_{(13\text{ or }14)}$-Cis-X_2-Cis-X_4-His-X_2-Cis-X_7-Cis, where X can be any residue. Two structural Zn^{2+} ions are coordinated by the six cysteines and two histidines and are essential to the proper folding of C1 domains.[30] A reactive cysteine (C151) was discovered for C1B of PKCα, an uncommon feature for structural Zn-sites.[31] It is unknown if other C1 domains feature this trait. Crystal structures and solution Nuclear Magnetic Resonance (NMR) structures exist for the C1 domains of isoforms δ[30], α[32], γ[33], and θ.[34] These structures reveal that C1 domains adopt the canonic treble-clef fold common to Zn-finger proteins, with two "unzipped" β-sheets and a C-terminal α-helix. The tops of C1 domains are very hydrophobic and insert into the membrane. The crystal structure of PKCδ in the presence of a phorbol ester showed that ligands bind in a pocket of the two loops (Figure

I.3), serving to cap hydrophilic residues in the ligand-binding loops and completing the hydrophobic surface that facilitates membrane penetration. The middle of C1 domains has positively charged residues that mediate interactions with anionic phospholipids, with some isoforms having a preference for phosphatidylserine.[35]

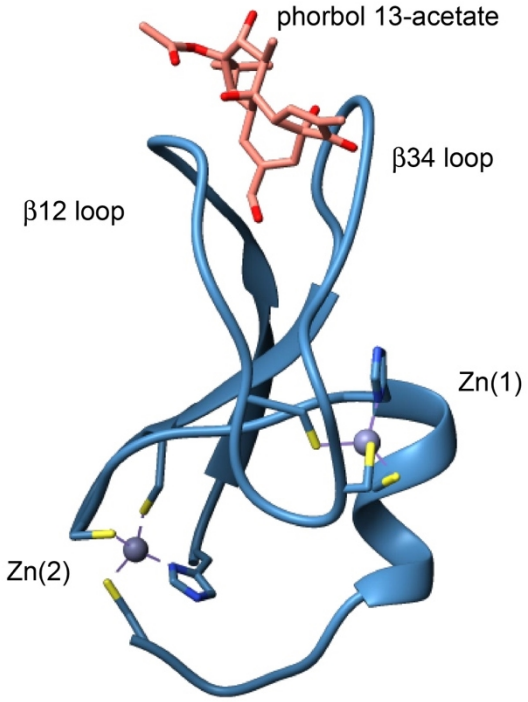

Figure I.3 C1 domain architecture and ligand-binding. Crystal structure of C1B domain from PKCδ in complex with phorbol 13-acetate (1PTR).

Membrane Interactions

Despite high sequence identities (36-46% within the folded core), C1 domains have varying affinities for DAG and phorbol esters, even within the same isoform.[36-38]

Studies have shown that the C1A domains of both PKCα and PKCδ have high affinities for DAG and play a primary role in DAG-mediated activation of PKC.[37,39] Within the same isoforms, C1B domains have low affinities for DAG and are implicated in phorbol ester-mediated activation of their full-length counterparts, with high affinities.[38] The affinities of C1 domains to diacylglycerol have been found to correlate with the identity of a single residue in the loop region that is a Tyr in C1 domains with low affinity to DAG and Trp in C1 domains with high affinity for DAG.[40] The high-affinity interactions of C1 domains in novel isoforms stabilize the membrane-bound form in the absence of a membrane-binding C2 domain.[41]

C2 domains

Like C1 domains, conserved homology 2 domains serve as one of the building blocks of many different proteins including synaptotagmins[42], involved in synaptic vesicle exocytosis; phospholipase C, another key player in signal transduction; and Munc 13, also involved in exocytosis. C2 domains were first discovered in PKC isozymes as ~130 amino acid long Ca^{2+} and phospholipid binding motifs.[43-45] Their ability to bind Ca^{2+} and phospholipids was first discovered in Synaptotagmin I.[46] The basic structure of C2 domains consists of eight, conserved, anti-parallel β-strands connected by more variable loop regions.[47] Structural and functional studies on PKCα found that 2 or 3 Ca^{2+} ions bind cooperatively to highly conserved aspartic acid residues in the Ca^{2+} metal-binding loops that connect the β-sheets.[48] In conventional isoforms, Ca^{2+} -binding and subsequent trafficking of PKC to the membrane serve as the first step of activation.[49] Ca^{2+} binding is proposed to serve three purposes in modulating C2

affinity for membranes: (1) contributing to the change of electrostatic potential of C2, (2) coordinating the head groups of anionic lipids with a preference for phosphatidylserine (PS), and (3) contributing to interdomain rearrangements in the regulatory region that primes the enzyme for membrane association.[44] In addition to Ca^{2+}, C2 domains have been shown to be targeted by toxic metal ions with varying consequences for function. While Pb^{2+} was able to drive the membrane association of C2 almost as effectively as Ca^{2+}[50], Cd^{2+} binding to the loops of the C2 domain completely abolished membrane association.[51]

C2 domains from conventional isoforms also bind to PIP2 through a positive patch on the β-strands 3 and 4 called the lysine-rich cluster (LRC) (Figure I.4). PIP2 binding to the LRC has been shown to change the membrane binding geometry of C2 domains [52] and significantly lowers the Ca^{2+}-requirements for membrane recruitment of C2.[53-55] In contrast to the C2 domains of conventional isoforms, C2 domains of novel isoform, δ, do not bind to Ca^{2+} and do not traffic the parent enzyme to membranes.[41] Instead, the relatively high affinity of the PKCδ C1 domains compensate for the lack of membrane binding C2 domain.[41]

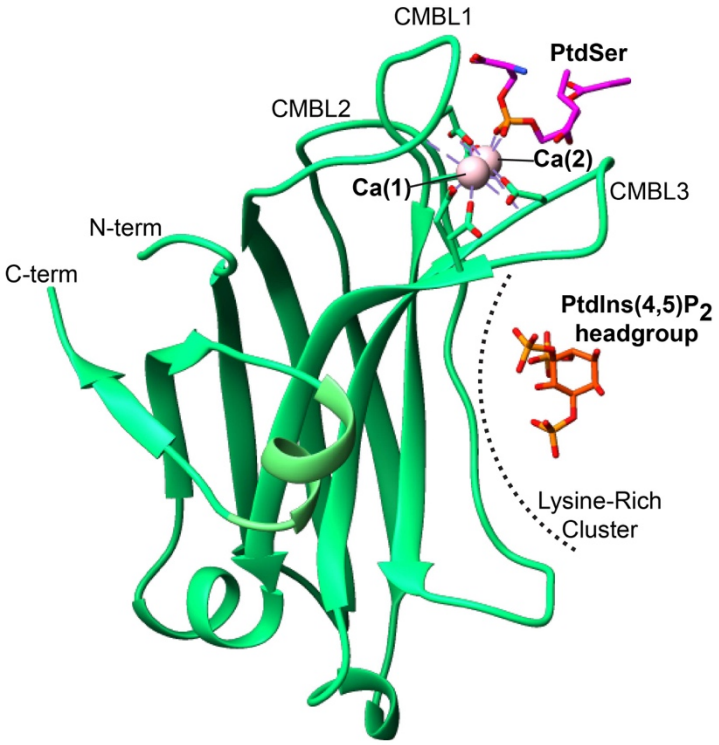

Figure I.4 C2 domain architecture and ligand-binding. Ribbon diagram showing the structure of C2 domain from PKCα in complex with PS (1DSY). The coordinates for PtdIns(4,5)P_2 (PIP2) were taken from 3GPE.

PKC Regulation

Intramolecular Interactions

The hallmark of PKC activation is translocation of the regulatory region to membranes. This process is regulated by ligands (Ca^{2+} and DAG), phosphorylation, protein-protein interactions, and intramolecular interactions. A host of intermolecular interactions that stabilize the latent form of PKC are summarized in Figure I.5. It has been shown that the ligand binding sites of C1A and C1B domains of conventional isoforms PKCβII and PKCα were masked in the mature enzyme.[56] One interaction that

stabilizes the latent form of PKC is between the pseudosubstrate region and the kinase domain[24], however, several intermolecular interactions involving C1 and C2 domains are also important. The most notable of these interactions is the proposed autoinhibitory interaction between C1A and C2 of PKCα.[57,58] Evidence for this interaction comes from mutagenesis and docking studies that identified three interacting pairs of residues between the C1A and C2 domains[57]: Asp55-Arg252, Arg42-Glu282, and Phe72-Phe255. Furthermore, a surface plasmon resonance study showed that the C2 domain from PKCα bound to a construct containing the PKCα C1A and C1B domains.[58] The same study concluded that fusion proteins containing C1 domains from isoform α and novel isoform δ were able to activate the full-length enzyme of the corresponding isoform, indicating their abilities to compete for the intermolecular interaction sites.[58] Additionally, the C2 domain from PKCα has also been shown to interact with the C-terminal tail of the kinase domain.[59,60] This interaction is proposed to serve two purposes: to maintain the auto-inhibited form of PKC and to sensitize the C2 domain to intracellular Ca^{2+} levels.[59]

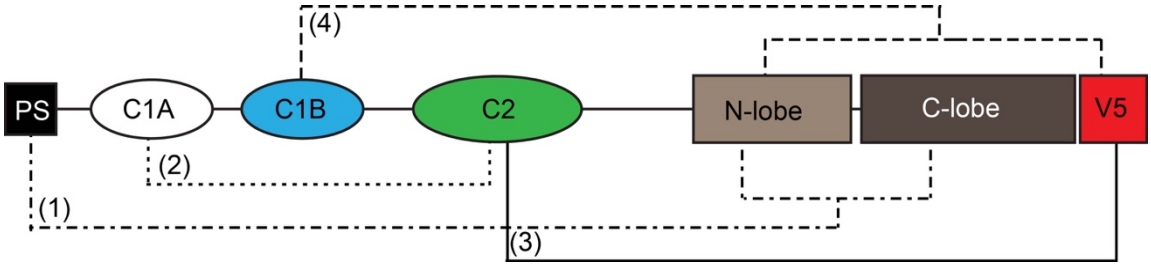

Figure I.5 Intramolecular interactions stabilize the latent form of PKC. Proposed intramolecular interactions indicated on the linear diagram for conventional PKC isozymes: (1) pseudosubstrate region and the active site of the kinase domain, (2) C1A and C2 (3) C2/V5 (4) C1B/kinase domain.

A partial crystal structure of PKC βII revealed a "C1B clamp" consisting of interactions between the C1B domain, N-lobe of the kinase domain, and the variable 5 (V5) domain.[61] This interaction involves the side chains of Leu125 and Ile126 which are involved in membrane binding. Furthermore, it blocks the DAG binding site, pointing to the autoinhibitory nature of the interaction. Mutations designed to destabilize this interface lowered the concentration of PMA needed for membrane translocation of full-length PKCβII.[61]

PKC self-association

An additional layer of regulation is thought to come through self-association. PKC activity was found to be concentration dependent, consistent with oligomerization.[58] A peptide containing the C1A and C1B domains from PKCα was found to be able to activate the corresponding parent enzyme in the presence of phorbol ester.[58] Furthermore, the maximum specific activity of PKCα in the presence of its own C1A-C1B peptide was equivalent to the activity in the presence of saturating activators:

phospholipids, phorbol esters, and Ca^{2+}, which indicates that self-association is potent in activation. Crosslinking studies found that conventional PKCs form homodimers in the presence of activators, phospholipids and Ca^{2+}, with phosphatidylserine having the most profound effect.[62] This was found to occur independently of the substrate binding site and in parallel with activation, likely due to exposure of interfaces masked in the latent form.

More recent studies using intermolecular Förster resonance energy transfer (FRET) pairs suggest that homodimerization serves to regulate PKC activity by sequestering intramolecular interaction sites.[63] Furthermore, this study identifies the regulatory domain in addition to the V5 domain as the sites of interaction in the homodimer. Yet another study found that Ca^{2+} was minimally sufficient for PKC to self-associate in vitro and that the clustered state of PKC depends on which ligands are used to stimulate oligomerization.[64] Despite accumulating evidence of PKC dimerization, further investigation is needed to understand the molecular details of the interactions.

Foreign Substances Modulate PKC Activity

Foreign substances interfere with the physiological activity of PKC with adverse effects on human health. This work deals with two types of these: toxic metal ions and tumor-promoting phorbol esters. An introduction to the consequences of PKC exposure to both is given below.

Toxic Metal Ions

Heavy metals are naturally occurring in trace amounts but become enriched in our environment through industrial, technological, and agricultural applications.[65,66] Human exposure to these metals, even in small amounts has been shown to cause cancer, neurological defects, and other health problems.[65-70] PKC is a known player in heavy metal toxicity. Pb^{2+} has been shown to activate PKC at low concentrations and inhibit PKC at higher concentrations.[71,72] Cu^{2+}, Cd^{2+}, Mn^{2+}, Zn^{2+}, and Hg^{2+} were all shown to inhibit phorbol ester binding.[73,74] Cd^{2+} has been shown to interfere with multiple cellular processes through PKC signal transduction pathways.[18,75] Due to the dependence of PKC activity on Ca^{2+} which can be mimicked by divalent toxic metals, studies on PKC and heavy metals have focused on the C2 domain. Pb^{2+}, for example, was found to be as effective as Ca^{2+} in driving the C2 domain to the membrane.[50] In stark contrast, Cd^{2+} treatment of C2 abolished binding to anionic membranes.[51] Despite the lack of C2-membrane binding in the presence of Cd^{2+}, it was shown to activate nuclear PKC.[17]

Phorbol Esters

Phorbol esters refer to a class of compounds naturally occurring in croton oil and plants from the family Euphorbiaceae.[76] Phorbol esters can make their way into our diet through the consumption of animals that are exposed to the plants. It was found that treatment of mice with phorbol esters promoted the formation of skin tumors, making them the focus of intensive research.[77] PKCs are the primary target for tumor-promoting phorbol esters although other receptors have been identified. For example, Munc 13-1, a regulator in synaptic function in mammals, is a well-established phorbol ester receptor.[78]

The discovery that PKCs were receptors for phorbol-esters was the initial motivation for intense studying of PKCs.[79] The cocarcinogenic effect comes from PKCs involvement in cell growth and proliferation. The potency of the response of PKC to phorbol esters is due to the high affinity to C1 domains and the inability of phorbol esters to be metabolized by the cell like it's native agonist, DAG, rendering PKC constitutively active.

Challenges associated with structural studies on PKC

To date, there is no mechanistic understanding of PKC activation. This is largely due to the challenges associated with studying PKCs. The full-length enzyme is ~80 kDa, large for solution structural studies by NMR and adding in membrane mimetics to study the membrane-associated form only increases the effective size and makes studying PKC more difficult. X-ray crystallography has been indispensable in obtaining information about the isolated regulatory domains. However, the multi-modular structure and dynamic nature of PKC, while essential to function, have prevented attainment of a full-length crystal structure. Only one partial crystal structure of PKC exists.[61] In this structure of PKC βII, the C1A domain is completely missing and although Ca^{2+} is bound to the C2 domain, the kinase is in an inactive conformation, indicating that the conformation represents an intermediate along the activation pathway. In particular, the peripheral membrane binding domains of the regulatory region present challenges in obtaining concentrations high enough for biophysical studies. C1A domains are notoriously insoluble and have a propensity to aggregate.[80,81] A common approach in studying PKC isozymes is to express C1-containing constructs as fusion partners with

highly soluble tags such as maltose binding protein (MBP) or glutathione S-transferase (GST) and retain the tag after purification.[58,81,82] However, large tags can influence the native conformation and behavior of the protein of interest and these tags often add a considerable amount of molecular weight to the constructs. This approach is not viable for structural studies by NMR due to the increase in the molecular tumbling time and the line broadening that occurs as a result. [83] The work presented in this thesis is largely aimed at overcoming these challenges to gain insight into the structure and function of the regulatory region during different steps of the activation process.

CHAPTER II

EXPRESSION AND PURIFICATION OF THE N-TERMINAL REGULATORY DOMAIN OF PROTEIN KINASE C FOR BIOPHYSICAL STUDIES[*]

Background

This chapter details efforts towards obtaining full-length PKC regulatory region constructs suitable for biophysical studies. Given the pivotal role of PKCs in signal transduction and human disease, significant efforts have been directed at altering their activity in therapeutically productive ways (reviewed in [84]). Structural information is needed for this but has eluded scientists for decades.

The hallmark of PKC activation is their translocation to lipid membranes in response to second messengers that are generated in the upstream signaling event. Conventional PKC isozymes (α, βI, βII, and γ) translocate to membranes in response to both diacylglycerol (DAG) and Ca^{2+}, while novel PKC isozymes (δ, ε, θ, and η) respond to DAG only. The membrane-binding functionality of conventional and novel PKCs resides on their N-terminal regulatory region that has a multi-modular structure. This region contains tandem C1 domains, C1A and C1B, which target PKCs to DAG-containing membranes. Another membrane-targeting domain of conventional PKCs, C2, binds anionic phospholipids – with high specificity towards phosphatidylserine – in

---

[*] Reprinted with permission from Cole, T.R., and Igumenova, T.I. (2015) Expression and purification of the N-terminal regulatory domain of Protein Kinase C for biophysical studies, *Protein Expr Purif 110*, 14-21. doi: 10.1016/j.pep.2014.12.018.

a Ca^{2+}-dependent manner. In novel PKC isozymes, the C2-like domains lack the residues required for Ca^{2+}/membrane association and serve as protein interaction modules.[85,86] All C1 and C2 domains are independently folded protein modules that preserve their functional properties when expressed in the isolated form.

The membrane-binding step relieves the auto-inhibitory interaction between a short pseudosubstrate region (black bars in Figure II.1A) and the active site of the C-terminal catalytic domain. [87-90] The structural basis of the membrane association step, which includes the rearrangement within the N-terminal regulatory domain followed by membrane insertion, remains poorly understood. The functional autonomy of the N-terminal region [91-93] makes it an attractive candidate for structural studies of the membrane association process, including the domain rearrangement that accompanies insertion and the geometry of protein-membrane interactions.

Liquid-state Nuclear Magnetic Resonance (NMR) techniques are ideally suited to probe the structure and dynamics of inherently dynamic multi-modular systems, such as the N-terminal regulatory region. An additional advantage of NMR methods is that they can provide access to both, solution and membrane-bound states of the N-terminal regulatory region, the latter through incorporation of membrane mimics and hydrophobic ligands. The objective of this work was to develop a robust and cost-effective protocol that would enable the generation of sufficient protein quantities for future NMR studies. Analysis of the existing literature revealed that large-scale preparation of these proteins is challenging. The C1A domain from conventional isozymes, PKCβI/βII has been referred to as "notoriously insoluble". [80] This finding was subsequently extended to the

C1A domain from PKCα. [94] Because of the low solubility of C1A domains from α and βI/βII isozymes, they are targeted to inclusion bodies during heterologous over-expression in *E. coli*; this requires implementation of purification protocols that include a protein-refolding step in the presence of Zn^{2+}. [95] When placed in the context of its primary structure neighbors, such as C1B, the C1A domain imposes its unfavorable solubility properties on the entire construct. [96]

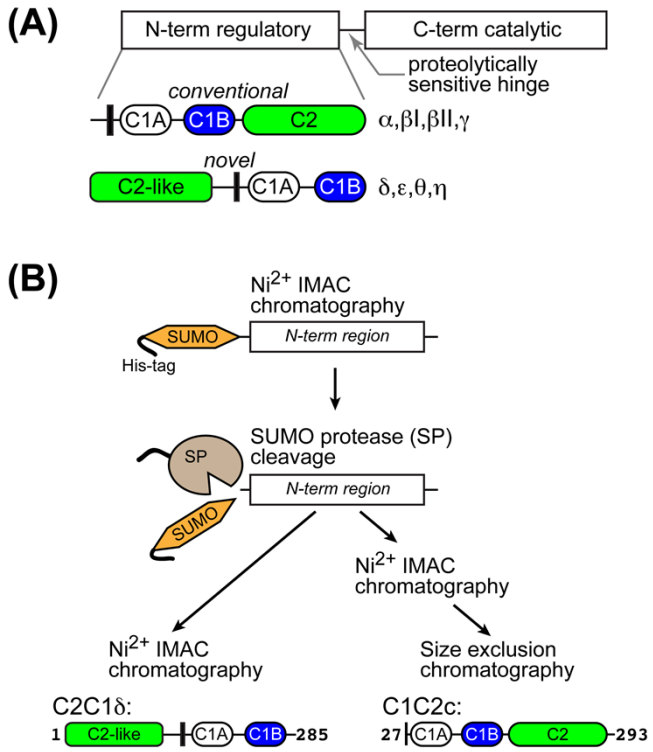

Figure II.1 Regulatory regions purified in this Chapter. (A) Linear diagram illustrating the multi-modular structure of conventional and novel PKC isoforms. Black bar indicates a short pseudo-substrate region. (B) Schematic view of the purification procedures used in this study. *Reused with proper permission from ref[97].

For the biochemical studies of PKC, fusing the N-terminal regulatory region and its individual domains to glutathione S-transferase (GST) and maltose binding protein (MBP) results in high expression of soluble proteins and facilitates the purification. Moreover, the GST and MBP tags are almost always retained after purification to improve the solubility and stability of the proteins. [36,58,81,82] These tags add a considerable amount of molecular mass to the target proteins, ≥100 % in the case of ~30 kDa N-terminal regulatory domains. This presents challenges for NMR spectroscopy because the increase in the rotational diffusion coefficient and number of amino acids in the fusion protein diminishes the resolution and signal-to-noise ratios of the spectra. In this chapter, the expression and purification protocols for two N-terminal regulatory domain constructs suitable for NMR studies are reported: C2-C1A-C1B from the novel isozyme PKCδ (C2C1δ) and the chimeric C1Aγ-(C1B-C2)α (C1C2c, where "c" stands for conventional PKC isozymes).

Materials and methods

Cloning and site-directed mutagenesis

The cDNA of PKCα (*R. norvegicus*), PKCγ (*M. musculus*), and PKCδ (*R. norvegicus*) was purchased from Open Biosystems/GE Healthcare. The amino acid sequences of PKCγ from *M. musculus* and *R. norvegicus* are identical. pET-SUMO plasmid (Novagen) was used as the expression vector for all PKC constructs. The cloning strategy involved inserting the target gene downstream from SUMO, thereby placing the expression of the fusion protein gene under the control of an inducible T7 promoter.

The regulatory region, C2C1δ, comprising residues 1-285 of PKCδ was cloned into pET-SUMO using the In-Fusion PCR Cloning Kit (Clontech), according to the manufacturer's instructions. The cloning of C1C2c that comprises the C1A domain from PKCγ (residues 27-98) and the C1B-C2 domain from PKCα (residues 100-293) into pET-SUMO was outsourced to GenScript. The F83S mutation was introduced into C1C2c using a QuikChange® Site-Directed Mutagenesis kit (Stratagene) with the appropriate primers. Using the same procedure, a positively charged amino acid tag, $G(K)_6$, was added to the C-terminus of C2C1δ to generate the C2C1δ-$G(K)_6$ variant. The sequences of all constructs were verified by DNA sequencing.

Induction and solubility tests

A single colony was picked from a transformation plate of the appropriate PKC plasmid and used to inoculate 5 mL of LB broth supplemented with 50 μg/mL kanamycin. For the pLysS and Rosetta cell lines, chloramphenicol was added to a final concentration of 34 μg/mL to maintain the pLysS and pRARE plasmids, respectively. Cultures were grown to an OD_{600}=0.6 at 37 °C, followed by incubation at the appropriate temperature for 15 minutes and subsequent induction of protein expression with isopropyl β-D-thiogalactoside (IPTG). Samples of cell culture were taken pre- and post-induction. Cells were harvested at the end of the induction period by centrifugation at 3,400 g for 10 minutes. Cell pellets were re-suspended and lysed at room temperature with 0.3 mL of B-PER protein extraction reagent (Thermo Scientific). Soluble and insoluble fractions were separated by centrifugation at 13,520 g for 5 minutes. 12%

SDS-PAGE was used to assess the amount of total PKC fusion proteins pre- and post-induction, and the amount of soluble protein after lysis.

Protein expression

Rosetta™ 2(DE3)pLysS competent cells (Novagen) were used as the *E. coli* expression strain. All cell cultures were supplemented with 50 μg/mL kanamycin and 34 μg/mL chloramphenicol and grown with shaking at 250 rpm. For natural abundance protein preparations, 5 mL starter cultures in LB broth (Fisher Scientific) were grown at 37 °C to reach an $O.D._{600}$=0.6. The starter cultures were subsequently transferred to 30 mL of fresh LB medium and grown to an OD_{600}=0.8-1 at 30 °C. As a final step, 30 mL cultures were transferred to 1 L of fresh LB medium and grown to an OD_{600}=0.4. The temperature was then reduced to 20 °C, to allow 1 L cell cultures to equilibrate at a lower temperature and reach $O.D._{600}$=0.6. The expression of fusion protein was induced with IPTG at a final concentration of 0.5 mM for 16 hours at 20°C. Immediately prior to induction, 100 μM $ZnSO_4$ was added to the growth medium to facilitate the proper folding of C1 domains.

For the preparation of ^{15}N-enriched proteins, the 5 mL starter LB cultures were spun down and re-suspended in 30 mL of M9 medium containing 1 g/L of ammonium chloride (^{15}N, 99 %)(Cambridge Isotopes) and 3 g/L D-glucose (Macron Chemicals) as nitrogen and carbon sources, respectively. The growth medium was supplemented with Kao and Michayluk Vitamin Solution (Sigma-Aldrich), 100 μM $ZnSO_4$, and 1 g/L of ISOGRO®-^{15}N Powder-Growth Medium (^{15}N, 98 %)(Sigma-Aldrich). The cell culture growth and induction of protein expression was conducted as described for the natural-

abundance preparation. Cells were harvested by centrifugation at 4000 g for 30 min at 4 °C. Cell pellets were stored at -20 °C.

Protein purification

Cell pellets were re-suspended in ice-cold lysis buffer containing 20 mM Tris-HCl at pH 7.5, 10% (w/v) sucrose, 50 μM $ZnSO_4$, 5 mM β-mercaptoethanol (β-ME), and 1 M NaCl. For the C1C2c construct and its F83S variant, 50 μM $CaCl_2$ was added to stabilize the C2 domain. The cells were disrupted with a Microfluidizer® processor (Microfluidics Corporation) pre-packed with ice and equilibrated for 30 minutes. The lysate was clarified by centrifugation at 15,300 g for 30 minutes at 4 °C.

All preparative and analytical chromatography experiments were carried out using an ÄKTA FPLC system and appropriate columns (GE Healthcare Life Sciences). For IMAC chromatography, the composition of loading/wash Buffer A was 20 mM Tris-HCl at pH 7.5, 0.5 M NaCl, 5 mM β-ME, and 5 mM imidazole. The composition of Buffer B was identical except for the addition of 1 M imidazole. The SUMO fusion protein carrying the N-terminal histidine tag was purified from cell lysate on a 2 x 5 mL HisTrap™ HP Ni^{2+} affinity column, using a 0-50 % gradient of Buffer B over 15 column volumes (Figure II.1B).

Fractions containing the fusion protein were pooled, concentrated to 10 mL using a 10 kDa cutoff Vivaspin® 15R concentrator (VIVAproducts), and diluted 5 times with Buffer A to reduce the imidazole concentration. The SUMO fusion tag was cleaved from the target protein using 170 nM histidine-tagged SUMO protease at 25°C in the presence of 10 mM β-ME. To follow the progress of the reaction, small-volume aliquots

of the reaction mixture were taken at specific times and quenched by mixing with the SDS-PAGE loading buffer and subsequent freezing. The aliquots were run on a 12% SDS-PAGE gel to assess the amount of cleaved protein. Cleavage was > 90% complete after 3 hours for all constructs. The products of the SUMO protease cleavage reaction were separated on a 2 x 5 mL HisTrap™ HP Ni^{2+} affinity column. The target proteins were collected in the flow through, while His-tagged SUMO protease and SUMO were retained on the column. The SDS-PAGE analysis of concentrated C2C1δ and its serial dilutions showed that the purity of the target protein is > 95%, which is suitable for NMR work. The conventional PKC constructs, C1C2c and its F83S variant, required an additional purification step (Figure II.1B). Gel-filtration chromatography was carried out using a HiLoad 16/600 Superdex 200 gel filtration column (GE Healthcare Life Sciences), in 20 mM Tris-HCl at pH 7.5, 0.5 M NaCl, 5 mM β-ME, and 100 μM $CaCl_2$. The purity of the C1C2c and its F83S variant was >95%, as determined by the SDS-PAGE.

Analytical gel-filtration

Analytical gel-filtration was carried out for all PKC constructs using a Superdex 75 10/300 GL column (GE Healthcare Life Sciences). The column was calibrated with protein standards from the Gel Filtration LMW Calibration Kit (GE Healthcare/Life Sciences) according to the manufacturer's protocol. 100 μl of 0.1-0.2 mM protein sample was loaded onto the column that was run with a flow rate of 0.5 mL/min. The composition of the gel-filtration buffer for C2C1δ was 20 mM Imidazole, 500 mM KCl, and 5 mM β-ME and 20 mM NaH_2PO_4, 150 mM L-arginine and L-glutamate, 10 μM

$ZnSO_4$, and 5 mM β-ME for C2C1δ-$G(K)_6$. C1C2c and its F83S variant showed strong interactions with the gel-filtration resin at low salt concentrations. A high-salt buffer containing 20 mM Tris-HCl at pH 7.5, 0.5 M NaCl, 100 μM $CaCl_2$, and 5 mM β-ME was used for these samples.

Mass-spectrometry

MALDI-TOF experiments were carried out using a Shimadzu/Kratos MALDI-TOF mass spectrometer in linear mode at the Protein Chemistry Laboratory (Texas A&M University). Samples were concentrated to > 2mg/mL and processed with a ZipTip® pipette tip (Millipore) to remove excess salt. The ZipTip® was washed with acetonitrile (ACN) and equilibrated with 0.1% trifluoroacetic acid (TFA). 10 μL of concentrated sample was bound to the ZipTip® and eluted with a 20 mg/mL solution of sinapic acid (Sigma-Aldrich) in 50/50 0.1% TFA/ACN. The instrument was calibrated with either cytochrome c or a mixture of cytochrome c/aldolase, both from Sigma-Aldrich.

Sample preparation and Nuclear Magnetic Resonance (NMR) experiments

To prepare NMR samples, all proteins were concentrated and buffer exchanged using 10 kDa cutoff Vivaspin® 15R concentrators (VIVAproducts). The buffers used for NMR experiments are listed in Table II.1. The experiments were carried out on Avance III HD NMR spectrometers (Bruker Biospin) operating at the ^1H Larmor frequencies of 800 (18.8 Tesla) and 600 MHz (14.1 Tesla). The 800 and 600 MHz systems were equipped with a cryogenically cooled and room temperature probes, respectively. The temperature was calibrated using deuterated (D4, 98%) and protonated

methanol samples. The ^{15}N-^{1}H chemical shift correlation spectra were collected using the fHSQC method. [98]

Table II-1. NMR buffers used for PKC constructs. Reprinted with permission from ref [97].

NMR buffer	PKC construct	pH	Composition
N1	C2C1δ	6.5	20 mM Imidazole (D4, 98%), 500 mM KCl, 70 μM $ZnSO_4$, 1 mM TCEP, 8% D_2O, and 0.02% NaN_3
N2	C2C1δ-$G(K)_6$	6.3	20 mM NaH_2PO_4, 150 mM L-arginine and L-glutamate, 10 μM $ZnSO_4$, 1 mM TCEP, 8% D_2O, and 0.02% NaN_3
N3	C1C2c	6.0	10 mM MES, 150 mM KCl, 1 mM TCEP, 8% D_2O, and 0.02% NaN_3
N4	F83S C1C2c	7.0	1 M glycine (D5, 98%), 2 mM $CaCl_2$, 1 mM TCEP, 8% D_2O, and 0.02% NaN_3

Results

Construction of chimeric protein enables expression of the tag-free soluble N-terminal regulatory region from conventional PKC

In conventional PKC isoenzymes the C1A domain is the least soluble of the three peripheral membrane modules that comprise the N-terminal regulatory region. Inspection of the primary structures reveals an unusually high content of Phe residues – 10, or 20%, in the 50-residue folded core of C1A domain from α (C1Aα) and βI/βII (C1Aβ) isoenzymes. Recently, the structure of C1A from human PKCγ (C1Aγ, PDB ID: 2E73, identical to the *R. norvegicus* C1Aγ) was determined using solution NMR

methods by the RIKEN Structural Genomics/Proteomics Initiative in Japan (Figure II.2 A). Although the experimental protocol has not been published, the header of the PDB file indicates that the isotopically enriched protein was generated using cell-free synthesis rather than heterologous expression in *E. coli*. Comparison of the primary structures of C1Aα and C1Aγ shows that only 6 amino acid residues are different in the domain core (Figure II.2B). Based on these data, it was concluded that the construction of chimeric proteins is a viable approach to overcome the detrimental effect of C1A on the expression and solubility behavior of the N-terminal regulatory region from conventional isoenzymes. In this work, the expression and purification of the chimeric C1C2c, which is a fusion of C1Aγ with the (C1B-C2)α, and its F83S variant (Figure II.1A) that has superior solubility properties is reported. The N-terminal regulatory region of PKCδ, C2C1δ, was cloned "as is". SUMO was chosen as a fusion partner for all PKC constructs because of the high expression yields of fusion proteins and the specificity of the SUMO protease cleavage reaction.

Figure II.2 The C1A domain from PKCγ has a high sequence identity to C1Aα. (A) NMR structure of C1Aγ from *H. sapiens* (PDB ID: 2E73). The first structure of the ensemble is shown. Diacylglycerol and phorbol esters bind in the cleft formed by the two ligand-binding loops. There are two structural Zn^{2+} that stabilize the structure. (B) Alignment of the C1A primary structures from γ and α PKC isoenzymes from *R. norvegicus*. Zn^{2+}-coordinating residues and residues that are different between the isoenzymes are highlighted with yellow and gray, respectively.

Expression of soluble N-terminal regulatory region is exquisitely sensitive to experimental conditions

Expression and lysis of C1C2c required optimization of several parameters, as only a very narrow set of conditions yielded soluble protein in sufficient quantities for NMR work. These parameters include the expression cell line, Zn^{2+} supplementation of the growth medium, temperature of induction, and cell disruption method.

The induction and solubility tests were conducted at 4 temperatures: 37 °C (4 hours), 30 °C (6 hours), 24 °C (16 hours), and 15 °C (16 hours) in the following 5 cell lines: BL21(DE3), BL21 (DE3)pLysS, Rosetta™, Rosetta™ (DE3)pLysS, and Rosetta™ 2(DE3)pLysS. In previous experiments with isolated C1Aγ, it was found that supplementation of growth medium with Zn^{2+} was essential for maximizing the amount of soluble protein. Therefore, the concentration of $ZnSO_4$ was varied in the range from

10 to 1000 μM using a set of small-volume LB cell cultures expressing C1Aγ. While the overall induction levels remained approximately the same, even small amounts of Zn^{2+} resulted in significant increase of the soluble protein yield. The intermediate value of 100 μM Zn^{2+} was chosen for inducing the expression of both isolated C1Aγ and the N-terminal regulatory domains. The appropriately buffered solution of $ZnSO_4$ was added to the growth medium immediately prior to induction.

The expression level of SUMO-C1C2c fusion protein was high at 37°C for all cell lines, but most of the protein was insoluble. Induction tests at 15 °C resulted in very low overall expression. At intermediate temperatures, only pLysS strains produced significant amounts of soluble fusion protein, approximately 50% of the total at 30 °C and 80-90% of the total at 24°C. The optimum temperature range for a balance between expression and solubility was determined to be 20-24°C. Ultimately, the Rosetta™ 2(DE3)pLysS cell line was chosen for further experiments because of its slightly higher levels of protein expression compared to other pLysS strains.

While B-PER lysis reagent worked well for the small-scale C1C2c tests, upon scaling up to larger cell cultures, cell disruption with a Microfluidizer® processor led to higher yields of soluble protein. B-PER was effective in lysing the cells expressing C2C1δ, but the protein began to precipitate out of solution within 10 minutes after lysis. Therefore, the Microfluidizer® processor was used to disrupt cells expressing all PKC constructs.

Tag-free C1C2c and C2C1δ can be obtained with moderate-to-high yields

The SDS-PAGE gels illustrating the expression and purification for the conventional and novel PKC constructs are shown in Figures II.3A and II.3B, respectively. The corresponding SUMO fusion proteins were highly soluble illustrating the applicability of the SUMO system [99] to the expression of regulatory regions from PKCs. The highly specific SUMO protease cleavage reaction proceeded to completion in a matter of hours. The yields from the protein preparations that were carried out in this study are summarized in Table II.2. For the C2C1δ variants, 17-18 mg of > 95% pure protein were obtained per 1 liter of LB broth. For the C1C2c variants, the yields were ~3-4-fold lower at 5-6 mg of > 95% pure protein per 1 liter of LB broth.

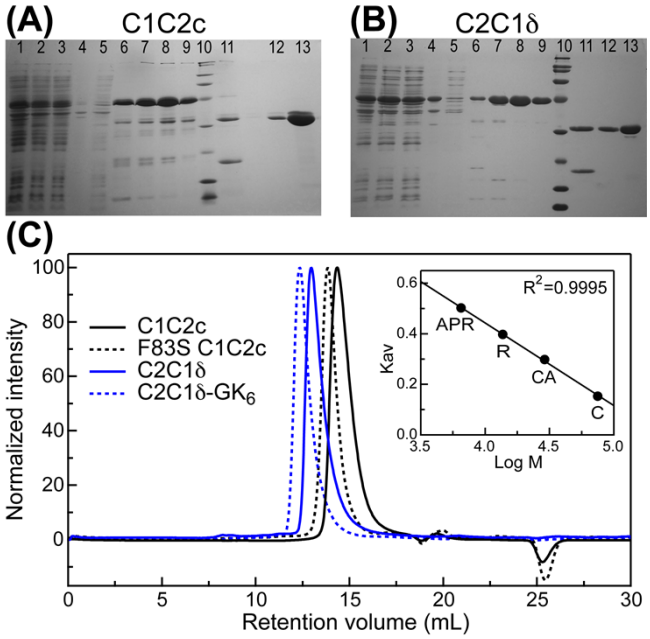

Figure II.3 Regulatory region preparations are mono-disperse. SDS-PAGE gels illustrating expression and purification of (A) C1C2c and (B) C2C1δ. The gel labels correspond to: (1) induced cells; (2) cell lysate; (3) supernatant; (4) pellet; (5) flow-through of the first Ni^{2+} affinity column; (6-9) eluted fusion proteins; (10) molecular weight marker (five bottom bands are: 6.5, 14.4, 21.5, 31, and 45 kDa); (11) SUMO protease cleavage reaction; (12) elution from the gel-filtration column (A) and flow-through of the second Ni^{2+} affinity column (B); and (13) concentrated protein sample to show purity. (C) Elution profiles of four PKC constructs that illustrate mono-dispersity of the samples. Inset: calibration of the analytical Superdex 75 10/300 column using standard proteins: APR, aprotinin, 6.5 kDa; R, ribonuclease A, 13.7 kDa; CA, carbonic anhydrase, 29.0 kDa; and C, conalbumin, 75.0 kDa. Reprinted with permission from ref [97].

For all constructs, milligram quantities of soluble proteins that are free of bulky solubility tags were obtained.

Preparation of samples for NMR studies

NMR experiments typically require milligram quantities of isotopically enriched proteins that are soluble to > 100 μM. The isotope enrichment is usually carried out in the M9 minimal medium, where the ^{15}N-enriched ammonium chloride and ^{13}C-enriched

D-glucose serve as sole nitrogen and carbon sources, respectively. However, the maximum attainable cell mass and protein expression yields are lower in M9 compared to the rich medium such as LB broth. This problem can be alleviated by re-suspension of LB-grown cultures at high cell densities in M9 with subsequent induction of expression[100]; the use of algal lysate-derived complex labeling medium such as ISOGRO® (Sigma-Aldrich) or BioExpress® 1000 (Cambridge Isotope Laboratories); and the supplementation of M9 medium with either ISOGRO® or BioExpress® 1000. For the preparation of uniformly ^{15}N-enriched N-terminal regulatory regions of PKCs, it was found that 10% (w/v) supplementation of M9 with ISOGRO® resulted in the final cell mass and protein yields that are comparable to those obtained in LB broth (Table II-2). This provides a cost-effective method to produce isotopically enriched domains of PKC.

Protein aggregation is problematic for biophysical studies in general and NMR in particular. To assess the oligomerization state of the PKC samples, analytical gel filtration experiments were conducted using a size-exclusion column with a fractionation range between 3 and 60 kDa (Figure II.3C). The concentration of analyzed samples was between 100 and 200 μM, which are within the range suitable for NMR spectroscopy. All protein species eluted in a single peak, indicating the mono-dispersity of the samples. The calibration of the gel-filtration column with globular protein standards enabled evaluation of the apparent molecular mass of the PKC constructs, which was similar to the theoretical values for the C2C1δ variants. However, C1C2c and its F83S variant have larger than expected retention volumes with apparent molecular masses of 15.8

kDa and 19.7 kDa, respectively. This behavior can be attributed to the interactions of proteins with the column matrix. Consistent with this, the elution volume increased even further upon omitting salt in the running buffer and substituting with 1 M glycine. Given the propensity of the PKC regulatory domain to interact with the column matrix, definitive information about their Stokes radii will have to await detailed biophysical studies.

Table II-2. Properties of N-terminal PKC constructs. Reprinted with permission from ref [97].

PKC construct	pI	Mol. mass (calc., Da)	Mol. mass (exp., Da)	Yield, mg/(1L of LB)	Yield, mg/(1L of M9)
C2C1δ	8.9	32,664	32,725	17-18	18
[U-^{15}N] C2C1δ-GK$_6$	9.2	33,902	33,888	17-18	18
C1C2c F83S	8.8	30,517	30,547	5-6	4
C1C2c	8.8	30,577	30,595	5-6	4

C1C2c: improvement of solubility and stability

Proper folding of the PKC N-terminal regulatory regions was evaluated using NMR spectroscopy. The ^{15}N-^{1}H chemical shift correlation spectra of [U-^{15}N] C1C2c contained regions with poor chemical shift dispersion that may indicate partial misfolding of the protein (Figure II.4A). A comparison of the C1C2c NMR spectra with that of a well-behaved C1B-C2 construct revealed that the C1A domain is the likely "problem site" of this three-domain protein. In previous work on isolated C1Aγ (unpublished), it was found that addition of glycine, a naturally occurring osmolyte [101],

stabilizes the domain and results in well-dispersed NMR spectra. It was previously shown that addition of up to 2 M glycine enhances protein folding and stability, without significant perturbations to the native fold and function.[102] Therefore it was incorporated at 1 M into the NMR buffer N4 (Table II-1).

To further improve the solubility properties of the C1C2c construct, the differences between the C1A domains and highly soluble C1B domains from conventional PKC isoforms were investigated. The main difference is the phenylalanine content, a total of 8-10 in C1A and only 2 in C1B. A surface-exposed phenylalanine at position 83 (Figure II.2), which is close to the linker region and away from the ligand-binding loops, is a conserved serine in C1B domains. To decrease the hydrophobicity of the C1Aγ domain in C1C2c, this phenylalanine at position 83 was mutated to a serine. Because this residue is not a part of any secondary structure element and is not involved in ligand/membrane interactions in homologous C1 domains[103,104], its mutation to a hydrophilic residue is unlikely to affect the fold of C1Aγ. A combination of 1 M glycine and the F83S mutation significantly improved the quality of NMR spectra (Figure II.4B), as evidenced by the number of cross-peaks and their dispersion. The ^{1}H cross-sections taken at the ^{15}N chemical shifts of 116.4 ppm (C1C2c) and 116.2 ppm (F83S) illustrate the differences in signal intensity and the number of cross-peaks between the two spectra. The data were scaled to account for the differences in protein concentration, receiver gain, and the number of points in the direct and indirect dimensions. While the exact quantitative comparison is not feasible due to a rather drastic change in protein state and buffer conditions, the improvement of data quality

due to the F83S mutation and glycine are evident. The use of glycine also enabled acquiring data at an increased sample temperature of 35 °C. Higher temperatures are beneficial for protein NMR experiments due to the reduction of the rotational correlation time of the molecule with the concomitant reduction in the line-widths.

An overlay of the F83S C1C2c NMR spectrum with those of the individual components, C1B-C2α and C1Aγ, shows the general similarity of the chemical shift patterns (Figure II.5). This indicates that individual domains are properly folded in the full-length construct of the regulatory domain.

C2C1δ: improvement of solubility

Compared to the C1C2c variants, C2C1δ has more favorable solubility properties albeit under high salt conditions, ≥ 0.5 M. The ^{15}N-^{1}H chemical shift correlation spectrum of C2C1δ in high-salt buffer N1 (Table II-1), collected using the room-temperature NMR probe showed good chemical shift dispersion indicative of a fully folded protein (Figure II.4C). However, to take full advantage of the sensitivity enhancement afforded by the cryogenically cooled NMR probes, the concentration of salt in the sample needed to be reduced.

For this, two strategies were implemented: introduction of a solubility enhancement peptide (SEP) tag and incorporation of osmolytes in the NMR buffer. SEP tags comprising short stretches of either negatively[105] or positively[106] charged amino acids were shown to improve protein solubility. Taking into consideration the "basic" isoelectric point of C2C1δ, the C2C1δ-G$(K)_6$ construct was generated by adding six lysines to the C-terminus. The effect of glycine on the solubility of C1C2δ-G$(K)_6$ was

investigated. Addition of ≥ 0.5 M glycine to the NMR buffer resulted in protein precipitation. In contrast, a buffer additive comprising a mixture of 150 mM L-glutamate and L-arginine enabled the reduction of the salt concentration to 150 mM NaCl (Table II.1, buffer N2), while maintaining the protein concentration at 0.2 mM for NMR measurements. To prepare the NMR sample, buffer N2 was added to the protein sample under dilute conditions and not directly to the concentrated sample, as prescribed by Golovanov et al. [107] This step was crucial to achieving the maximum benefits afforded by the Arg/Glu mixture. However, both the Arg/Glu osmolytes as well as the SEP were needed to improve the behavior of the δ regulatory region. A combination of SEP with L-arginine/L-glutamate and moderate concentrations of salt enabled acquisition of a high-quality 800 MHz NMR spectrum with a cryogenically cooled probe (Figure II.4D).

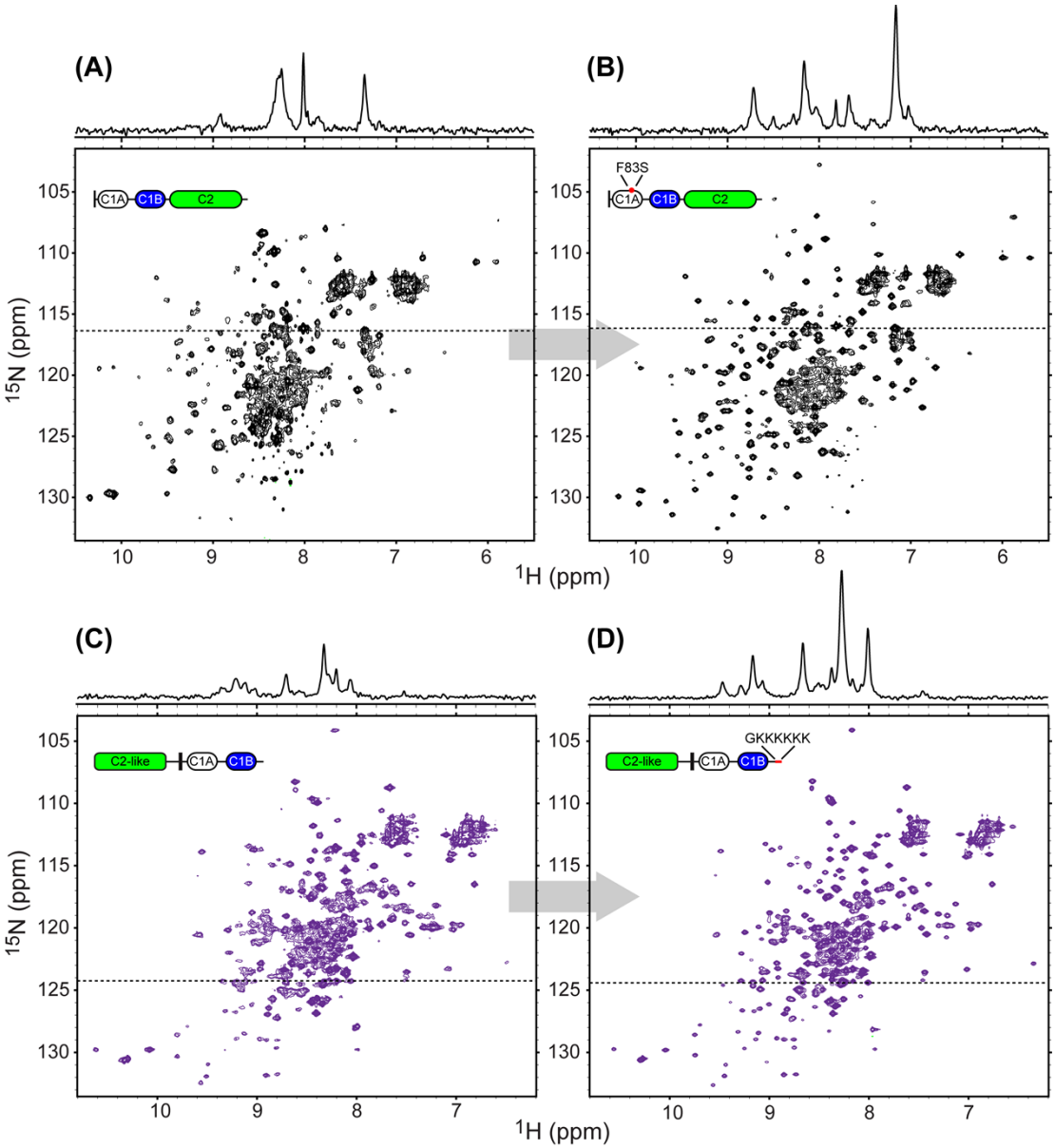

Figure II.4 Use of osmolytes, SEP, and targeted mutations improves the quality of NMR spectra of N-terminal regulatory regions of PKCs. ^{15}N-^{1}H HSQC spectra of (A) C1C2c in buffer N3, 25°C, 18.8 Tesla; (B) F83S C1C2c in buffer N4, 35°C, 18.8 Tesla; (C) C2C1δ in buffer N1, 25°C, 14.1 Tesla; (D) C1C2δ-G(K)$_6$ in buffer N2, 25°C, 18.8 Tesla. The buffer compositions are given in Table II.1. The 1D ^{1}H cross-sections were taken at the ^{15}N chemical shift positions indicated with dashed lines. The chosen cross-sections go through at least one cross peak whose (^{1}H, ^{15}N) position is similar in the pair of spectra being compared. Reprinted with permission from ref **[97]**.

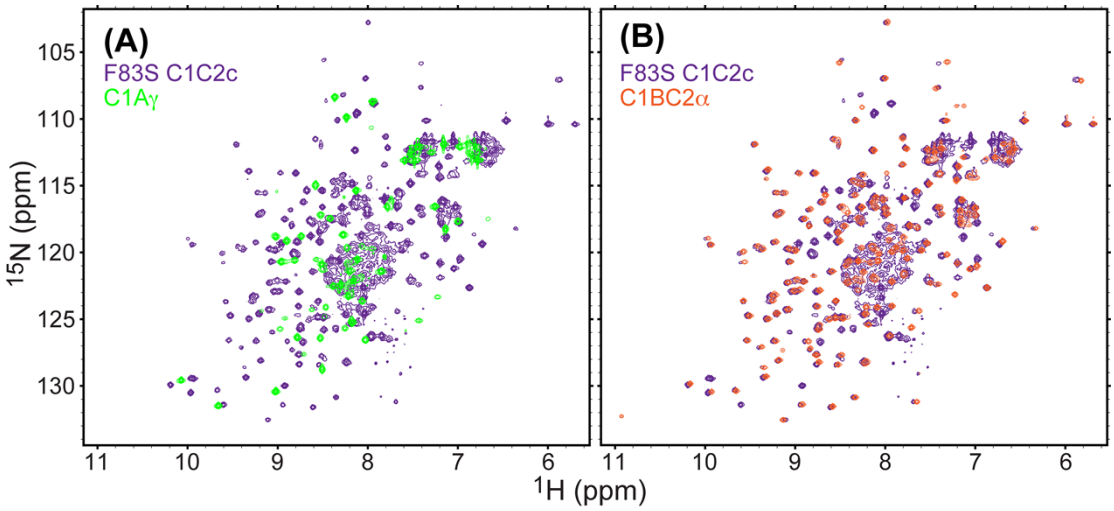

Figure II.5 Individual domain resonances are present in the ^{15}N-^{1}H HSQC spectrum of F83S C1C2c. This is demonstrated by its overlays with the spectra of C1Aγ (A) and (B) C1BC2α. The data for individual domains were collected under buffer conditions that matched those of F83S C1C2c (Tables II-1 and II-2), except that the C1Aγ spectrum was collected at 25° C. Reprinted with permission from ref [97].

Conclusion

This chapter describes the expression, purification, and NMR characterization of the N-terminal regulatory regions from PKC isozymes. Challenges associated with purification of these regions were overcome by optimization of expression, purification, and buffer conditions as well as carefully designed modifications to the regions. Although the modifications are not expected to interfere with function, future work is needed to determine the effect of these mutations. These represent the first fusion-partner-free full-length regulatory domains of PKC to be purified in sufficient quantities for structural and biophysical studies. The successful purification of these proteins will

enable scientists to gain insight into the tertiary structure of the regulatory domains and evaluate the structural changes that they undergo upon association with membranes. The NMR spectra of the N-terminal regulatory regions are indicative of fully folded protein species. It is worth noting that the quality of the NMR spectra can be improved even further by using deuteration and implementation of transverse-relaxation optimized NMR techniques.

CHAPTER III

OPPORTUNISTIC CD(II) AND PB(II) BINDING TRIGGERS THE SELF-ASSOCIATION OF PERIPHERAL MEMBRANE BINDING DOMAINS FROM PROTEIN KINASE C[†]

Background

This chapter describes the structural and functional consequences of the exposure of the PKC regulatory region to xenobiotic metal ions, Cd(II) and Pb(II). Cd(II) and Pb(II) are potent environmental toxins that have elevated levels in the environment due to human activity. Cd(II) is a known carcinogen, with its chronic exposure leading to kidney damage[66-69] and lead has adverse effects on all organs in the body and is associated with long-term effects on the ability to learn in children.[65,70] These deleterious effects are compounded by the relatively long half-lives of both metals in the human body. [66,108,109] Despite this, the molecular mechanisms of toxicity remain poorly understood, although it is well documented that divalent Pb^{2+} and Cd^{2+} can mimic native metal ions in the cell. For example, Cd^{2+} and Pb^{2+} ions have been shown to replace Ca^{2+} in many different proteins with various structural and functional consequences. In studies with calmodulin, Pb^{2+} was as effective as Ca^{2+} in binding and activation while Cd^{2+} was much less potent. [110,111] In contrast, while Pb^{2+} was able to bind with higher

---

[†] Portions of this chapter are adapted with permission from Cole, T.R., Erickson, S.G., et al. (2019) Cd(II)- and Pb(II)-Induced Self-Assembly of Peripheral Membrane Domains from Protein Kinase C, *Biochemistry* 58, 509-513. Copyright 2019 American Chemical Society.

affinity than Ca^{2+} and drive phospholipid association of Synaptotagmin I (Syt I), it was unable to support interactions with its binding partner, Syntaxin. [112]

Toxic metal ions can also target Zn-finger proteins resulting in diverging impacts on structure and function. [113-115] Due to the high affinity of Cd^{2+} for thiol groups, it readily replaces Zn^{2+} in structural Zn-sites. While in most systems Cd^{2+} supports the global fold, it does not always preserve the function of Zn-finger containing proteins[114] and due to the larger ionic radius, has been shown to cause reorientation of secondary structural elements and side chains. [116] Pb^{2+} also has high affinity for cysteine residues in structural Zn^{2+} sites but in most cases cannot support the fold or function.[117] The diversity of protein-responses to non-essential metal ions highlights the need for system specific studies on their molecular targets.

Protein Kinase C is a well-documented target of both Pb^{2+} and Cd^{2+}. [118-120] While it has been shown that Pb^{2+} and Cd^{2+} can have both activating and inhibitory effects on PKCs[17,18,118,121], the molecular details are not well understood.

PKCs have a multi-modular structure with a conserved kinase domain and membrane-binding regulatory domain. The key step in PKC activation is translocation of the regulatory domains to anionic membranes upon sensing its ligands, Ca^{2+} and diacylglycerol embedded in the membrane. This region of PKC relies on divalent metal ions, Zn^{2+} and Ca^{2+} for structure and function of the regulatory domain[122,123] and previous studies have shown that the regulatory domain of protein kinase C is targeted by toxic metal ions such as Pb^{2+} and Cd^{2+}. [17,120,124-126] The objective of this chapter is to illustrate the effect of toxic metal ions Pb^{2+} and Cd^{2+} on the structure and function of the

membrane-binding regulatory region of PKC and investigate their ability to replace Zn^{2+} and Ca^{2+}.

Efforts were focused on a regulatory domain construct from PKCα, consisting of two, independently folded and functionally autonomous peripheral membrane-binding domains, C1B and C2 (Figure III.1). These domains represent the minimal machinery of the PKCα region needed to bind both lipid and metal ligands and fully activate the parent enzyme. The conventional, full-length regulatory region construct from Chapter II was used to ensure that the behavior of C1B-C2 is a faithful representation of the behavior of the full-region. The structure and function of this region relies on divalent metal ions. C1A and C1B both require two structural Zn^{2+} ions, each with a Cys(3)His coordination sphere to properly fold and bind diacylglycerol embedded in the membrane. The C2 domain binds up to three Ca^{2+} ions and interacts with anionic lipids. An understanding of how metal ions affect this region is needed to understand the mechanism of toxicity. In addition, C1 and C2 motifs are the basic building blocks of many proteins in the cell and the knowledge gained from this study can be applied to other C1 and C2 containing proteins, leading to a more complete understanding of heavy metal toxicity. [127-129]

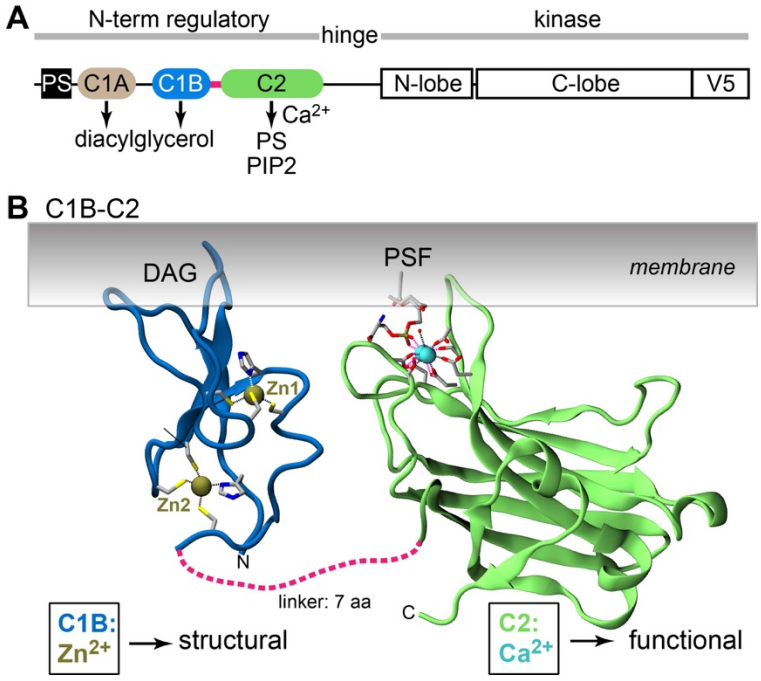

Figure III.1 Modular structure and peripheral domains of conventional PKC isoenzymes. Shown is the linear diagram of conventional PKCs (A) and ribbon representation of C1B (NMR structure, 2ELI) with highlighted structural Zn^{2+} sites, and C2 (crystal structure, 1DSY) in complex with Ca^{2+} and phosphatidylserine analogue, PSF (B). DAG stands for diacylglycerol.

Using solution nuclear magnetic resonance (NMR) spectroscopy, it is shown that Cd^{2+}, but not Pb^{2+} is able to spontaneously replace Zn^{2+} in the C1B domain. Additionally, it is demonstrated that opportunistic binding of Cd^{2+} and Pb^{2+} leads to the self-association of C1B-C2 which has a profound impact on its membrane binding functionality. This work indicates that ionic mimicry is insufficient to explain the interactions of Pb^{2+} and Cd^{2+} with PKC and demonstrates the potential diversity of responses of signaling proteins to toxic metal ions.

Methods

Buffer and metal ion solutions

For the majority of experiments reported in this work, "MES buffer" was used and prepared in HPLC-grade water (Avantor) and comprising 10 mM 2-(N-morpholino)ethanesulfonic acid (MES) at pH 6.0, 150 mM KCl, and 1 mM tris(2-carboxyethyl)phosphine (TCEP). The pH was chosen to minimize (i) the formation of Pb(II) hydroxides that becomes prominent at higher pH values; and (ii) the broadening of amide hydrogen cross-peaks in the NMR spectra due to exchange with water. In addition, several Cd^{2+} experiments were conducted in the "HEPES buffer" comprising 10 mM HEPES at pH 7.4, 100 mM KCl, and 1 mM TCEP. The buffer solutions were passed through the Chelex® 100 (Sigma-Aldrich) column to remove residual divalent metal ions. The stock solutions of metal ions were prepared by dissolving either $Cd(NO_3)_2 \cdot 4H_2O$ (>99% purity, Sigma-Aldrich) in the appropriate buffer or $Pb(CH_3CO_2)_2 \cdot 3H_2O$ (99.999% purity, Sigma-Aldrich) in the HPLC-grade water.

Protein purification

The DNA sequence encoding residues 100-293 of PKCα (M. musculus) was amplified by PCR using the cDNA clone of PKCα (Open Biosystems) as a template and cloned into the pET-SUMO vector (Invitrogen). Protein expression was carried out in E. coli BL21(DE3) cells. Cell cultures were grown to an OD600 of 0.6 and induced with 0.5 mM Isopropyl β-D-1-thiogalactopyranoside (FisherBioreagents) for 16 hours at 15 °C, with 10 μM $ZnCl_2$ added to the growth medium prior to induction. For the preparation of ^{15}N-enriched proteins, 5 mL starter LB cultures were spun down and re-

suspended in 1 L of M9 medium containing 1 g/L of ammonium chloride (^{15}N, 99%) (Cambridge Isotopes) and 3 g/L d-glucose (Macron Chemicals) as nitrogen and carbon sources, respectively. The growth medium was supplemented with Kao and Michayluk Vitamin Solution (Sigma–Aldrich), 100 μM $ZnSO_4$, and 1 g/L of ISOGRO®-^{15}N Powder-Growth Medium (^{15}N, 98%) (Sigma–Aldrich). The cell culture growth and induction of protein expression were conducted as described for the natural-abundance preparation. The re-suspension method of Marley et al[130] was used to generate [U-^{13}C,^{15}N, 55%-^{2}H] C1B-C2 sample for resonance assignment experiments. Cells were harvested by centrifugation at 4,000 g for 30 min at 4 °C and stored at −20 °C. Cell pellets were re-suspended in B-PER™ Bacterial Protein Extraction Reagent (Thermo-Fisher Scientific) supplemented with Halt™ Protease Inhibitor Cocktail (Thermo-Fisher Scientific) and 0.25 mg/mL lysozyme. The lysate was clarified by centrifugation at 15,300 g for 30 min at 4 °C. The histidine-tagged SUMO-C1B-C2 fusion protein was purified using a HisTrap™ HP Ni^{2+} affinity column (GE Healthcare Life Sciences). Fractions containing fusion protein were desalted on a HiPrep 26/10 column (GE Healthcare Life Sciences). C1B-C2 was obtained by cleaving the fusion protein for 1 hour with histidine-tagged SUMO protease at room temperature, followed by another Ni^{2+} affinity purification step to remove the histidine-tagged SUMO and SUMO protease. The final purification step was cation-exchange chromatography on a Source 15S column (GE Healthcare Life Sciences), carried out in 10 mM 2-(N-morpholino)ethanesulfonic acid (MES) buffer at pH 6.5, 0.1 mM $CaCl_2$, and 1 mM tris(2-carboxyethyl)phosphine (TCEP) with a linear concentration gradient of NaCl. The

purity of C1B-C2 was evaluated using SDS-PAGE. The molecular weight was verified by MALDI-TOF mass spectrometry. Fractions containing C1B-C2 were transferred to a 10 kDa VivaSpin 15R spin concentrator (Sartorius) where C1B-C2 decalcification was carried out. A total of 3 washes with 10 μM EGTA containing buffer (10 mM MES pH 6.0, 150 mM KCl, 1 mM TCEP, and 10 μM EGTA), followed by 3 washes into the final, EGTA-free buffer. C1B-C2 variants were generated either using the QuikChange (Agilent) or Q5® (NEB) mutagenesis kits. Full regulatory region of PKC (C1C2c, comprising C1Aγ/C1B/C2 domains harboring the F83S stabilizing mutation) and isolated C1B and C2 were expressed and purified as described previously[97,103,126] and as described in Chapter II.

Analytical gel-filtration

Superdex 75 10/300 GL column (GE Healthcare Life Sciences) and Superdex 200 Increase 10/300 GL column were calibrated with protein standards from the Gel Filtration LMW Calibration Kit (GE Healthcare/Life Sciences), supplemented with alcohol dehydrogenase and apo ferritin (Sigma-Aldrich) for the Superdex 200 calibration. 150-200 μM C1B-C2 samples were dialyzed overnight against the Cd^{2+}-containing MES or HEPES buffers to ensure removal of displaced Zn^{2+}. Pb^{2+}/C1B-C2 samples were prepared by adding up to 2 mM $Pb(Ac)_2$ from a concentrated stock solution to 0.3 mM [U-^{15}N] C1B-C2 and diluting the sample to 150 μM just prior to injection. The gel-filtration buffers were supplemented with 2% glycerol to prevent non-specific interactions with the column, and either 1 mM Cd^{2+}, 1 mM Ca^{2+}, or 0.5 mM Pb^{2+}. Typically, 100 μl of 100-150 μM protein sample was loaded onto the column that

was run with a flow rate of 0.5 mL/min; proteins were eluted with 1.5 column volumes of buffer.

UV-vis spectroscopy

UV-vis spectra were collected on a Beckman DU 640 spectrophotometer. 25 μM protein (C1B-C2, C2, or C1B) solution or "MES buffer" (for metal ion-only reference experiments) were placed in the sample cuvette; the reference cuvette always contained metal ion-free MES buffer. Pb^{2+} or Cd^{2+} were added stepwise from the corresponding stock solutions to the sample cuvette. The samples were incubated for 5 minutes prior to the start of the measurements for Pb^{2+} experiments and 1 hour for Cd^{2+} experiments. The post-acquisition processing included the subtraction of the spectra of free Pb^{2+} and Cd^{2+} from the spectra of protein-containing samples. The difference spectra were obtained by subtracting the spectrum of the apo protein from the spectra of the metal ion containing protein. All spectra were corrected for dilution prior to subtraction.

C1B refolding

[U-^{15}N]-enriched C1B was dissolved in 6 M guanidine hydrochloride (Acros Organics) and the "refolding buffer" comprising 20 mM MES at pH 6.0 and 1 mM TCEP. The final protein concentration was between 15 μM and 35 μM during the denaturation step. The refolding was conducted in three dialysis steps, all of them carried out in the refolding buffer: (1) against 8 M urea at room temperature, for 8 hours; (2) against 1.5 M urea and 100 μM of either Cd(II) nitrate or Pb(II) acetate at 4 °C, overnight; and (3) against urea-free buffer at 4 °C, for 3 days to ensure complete removal of all urea. The refolded protein was concentrated in a spin concentrator with a

3 kDa cutoff and subsequently exchanged into an NMR buffer (10 mM MES pH 6.0, 150 mM KCl, 1 mM TCEP, 0.02% NaN_3, and 8% D_2O (Cambridge Isotopes)) using a Midi-Trap G25 desalting column (GE Healthcare). Successful refolding of the protein was achieved in the presence of Cd^{2+} only.

NMR spectroscopy

All proteins were concentrated and buffer exchanged using 10 kDa (C1B-C2), 3 kDa (C1B) and 5 kDa (C2) cutoff Vivaspin® 15R concentrators into an MES buffer containing 0.02% (w/v) NaN_3, and 8% (v/v) D_2O. The experiments were carried out on Avance III HD NMR spectrometers (Bruker Biospin), operating at the ^1H Larmor frequencies of 800 (18.8 Tesla) and 600 MHz (14.1 Tesla) equipped with cryogenically cooled probes, and 500 MHz (11.7 Tesla) equipped with a room temperature probe. The temperature was calibrated using deuterated (D4, 98%) methanol for cryogenically cooled probes and protonated methanol for the room temperature probe. Spectra were processed using nmrPipe.[131] The cross-peak intensities were obtained using Sparky.[132] Sequence-specific assignments of the ^1H and ^{15}N resonances for apo C1BC2 were obtained using ^2H-decoupled 3D HN(CA)CB, HNCA(CB), HN(COCA)CB, and HN(CO)CA[133] experiments on a [U-^{13}C,^{15}N; 55%-^2H] C1B-C2 sample. Assignments for Cd^{2+}-substituted C1B ($C1B^{Cd}$) were transferred from the native Zn^{2+}-containing protein ($C1B^{Zn}$) and verified using 3D CBCA(CO)NH and HNCACB[134] spectra collected at 14.1 Tesla. Assignments for Cd^{2+}-bound C1B-C2 were transferred from the isolated C1B and C2[124] domains. Chemical shift perturbations Δ between Cd^{2+}-free and Cd^{2+}-containing C1B-C2 were calculated according to the following equation:

Equation 1

$$\Delta = \sqrt{\Delta\delta_H^2 + (0.152\Delta\delta_N)^2}$$

where $\Delta\delta_H$ and $\Delta\delta_N$ are residue-specific ^1H_N and ^{15}N chemical shift differences.

For NMR-detected binding experiments, the C1B ligand phorbol-12,13-dibutyrate (PDBu, Sigma-Aldrich) was dissolved in [$^2H_6$] DMSO (Cambridge Isotopes) and added to the sample containing 94 μM of [U-^{15}N] enriched $C1B^{Cd}$ in the presence of 10 mM mixed micelles. Mixed micelles comprising [$^2H_{38}$] dodecylphosphocholine, (DPC, Cambridge Isotopes) and 2-dihexanoyl-sn-glycero-3-[phospho-l-serine] (DPS, Avanti Polar Lipids) at a molar ratio of 7 to 3 were prepared as previously described.[103] The final concentration of PDBu in the NMR sample was 100 μM.

Small-angle X-ray scattering (SAXS) data collection

SAXS experiments were conducted on the SIBYLS[135] beamline at the Advanced Light Source synchrotron at the Lawrence Berkeley National Laboratory. Full regulatory region of PKC (C1C2c[97], comprising C1Aγ-C1B-C2 domains) and C1B-C2 were concentrated and dialyzed against the appropriate metal-ion containing buffer (Table III-1) for 48 hours. 24 μL of protein solution at three different concentrations (1, 2.5, and 4.5 mg/mL) was placed in a 96-well plate (Axygen). SAXS data were collected continuously with q ranging from 0.013 to 0.328 with exposures of 0.5, 1, 2, and 5 s. Buffer blanks were performed both before and after each sample exposure and subtracted from the sample signal for each condition tested. Data analysis was carried out using ScÅtter.

Small Angle X-ray Scattering (SAXS) measurements: buffer conditions and data analysis procedures

The scattering curves I(q) were examined for signatures of aggregation, concentration dependence, and radiation damage. Data sets that were free from radiation damage and concentration dependence were merged using the software package ScÅtter. For conditions that had greater than 5 data sets that could be merged the median value was taken to avoid bias from outliers. Conditions with less than 5 data sets that could be merged were averaged. The pair-distance distribution function, P(r); the "real space" radius of gyration, R_g; and maximum particle dimension, D_{max}, were obtained from I(q) using Indirect Fourier transform, as implemented in ScÅtter. The molecular mass for each sample was estimated using the method of Rambo and Tainer.[136] For the analysis of protein flexibility and shape, the dimensionless Kratky plots, $(qRg)^2I(q)/I(0)$ versus (qRg), were constructed as described by Durand et al.[137]

In contrast to the data obtained on the full-length regulatory region C1C2c (see Table III-1), the Pb^{2+}/C1B-C2 data were not useable for quantitative analysis because of aggregation and severe signs of inter-particle interference. It is assumed that that the SAXS experiments on the Pb^{2+}-containing sample of C1C2c were successful because glycine was used as a buffer. 1 M glycine serves not only as an osmolyte that is required to stabilize the C1C2c structure,[97] but also as a ligand that can sequester excess Pb^{2+} [138] and thereby prevent the formation of high-molecular-weight aggregates.

Table III-1. Sample conditions for SAXS experiments.

Metal ion/protein	pH	Buffer Components	Merged data sets/method
Ca^{2+}/C1B-C2	6.0	10 mM MES, 150 mM KCl, 1 mM TCEP, 2% glycerol, 0.02 % NaN_3, 2 mM $CaCl_2$	4.5 mg/mL; exposure 0.5 and 1 s; 2.5 mg/mL; exposure 0.5, 1, and 2 s; 1.0 mg/mL; exposure 2 and 5 s; median
Cd^{2+}/C1B-C2	6.0	10 mM MES, 150 mM KCl, 1 mM TCEP, 2% glycerol, 0.02% NaN_3, 1 mM $Cd(NO_3)_2$	4.5 mg/mL; exposure 0.5 and 1 s; 2.5 mg/mL; exposure 0.5, 1, and 2 s; median
Pb^{2+}/C1B-C2	6.0	10 mM MES, 150 mM KCl, 1 mM TCEP, 2% glycerol, 0.02% NaN_3, 1 mM $Pb(Ac)_2$	Not useable for analysis due to aggregation and inter-particle interference
Ca^{2+}/C1Aγ-C1B-C2	7.0	1 M Glycine, 1 mM TCEP, 2% Glycerol, 0.02% NaN_3, 2 mM $CaCl_2$	4.5 mg/mL; exposure 0.5, 1, and 2 s; 2.5 mg/mL; exposure 0.5, 1, and 2 s; median
Cd^{2+}/C1Aγ-C1B-C2	7.0	1 M Glycine, 1 mM TCEP, 2% Glycerol, 0.02% NaN_3, 1 mM $Cd(NO_3)_2$	2.5 mg/mL; exposure 0.5, 1, and 2 s; average
Pb^{2+}/C1Aγ-C1B-C2	7.0	1 M Glycine, 1 mM TCEP, 2% Glycerol, 0.02% NaN_3, 1 mM $Pb(Ac)_2$	1.0 mg/mL 0.5, 1, 2, and 5 s; average

Analytical gel-filtration and sedimentation experiments

Analytical gel-filtration experiments were carried out on a Superdex 75 10/300 or a Superdex 200 Increase 10/300 GL columns as described in the SI. Sedimentation velocity experiments on Cd^{2+}-complexed and Pb^{2+}-complexed C1B-C2 were conducted at the Center for Analytical Ultracentrifugation of Macromolecular Assemblies at the University of Texas Health Science Center at San Antonio. The experiments with Cd^{2+} were conducted at pH 6.0 and 7.4 for two C1B-C2 samples with 1 mM Cd^{2+} containing buffer: a "low" concentration sample, 7 μM/OD_{280}=0.3, and a "high" concentration sample, 23 μM/OD_{280}=0.9. Samples were centrifuged for 12 hours 27 minutes and 13 seconds at 25,000 rpm at 20 °C in a Beckman Optima analytical ultracentrifuge. Experiments in the presence of 0.1 mM Pb^{2+} were conducted in MES buffer with 7 μM/OD_{280}=0.3, and a "high" concentration sample, 23 μM/OD_{280}=0.9. Pb^{2+} concentrations were limited by the strong absorbance of $Pb[Cl_3]^-$ and $Pb[Cl_4]^{2-}$ species at

280 nm. [139] The data were analyzed using the van-Holde Weischet method[140] for heterogeneous systems, as implemented in the UltraScan software package.[141]

Electron microscopy

Cd^{2+}/C1B-C2 samples were prepared as described for SAXS measurements and then passed through the Superdex 200 GL 10/300 column to isolate the oligomer fraction. The Pb^{2+}/C1BC2 oligomers were prepared by incubation of 150 μM C1B-C2 with 1 mM Pb^{2+} in the MES buffer supplemented with 2% glycerol. The concentration of Pb^{2+}/C1BC2 oligomers in the gel-filtration fraction was not high enough to observe them in the EM experiments; the appropriate dilution of the pre-incubated protein-metal ion mixture was used instead. The C1B-C2 oligomers were negatively stained according to Valentine et al.[142] Specimens were observed in a JEOL 1200 EX transmission electron microscope operated at an acceleration voltage of 100 kV. Electron micrographs were recorded at a calibrated magnification of ×50,000 using a 3k slow-scan CCD camera (model 15C, SIA) resulting in 5.1 Å/pixel at the specimen level. The images were processed using the EMAN single particle analysis package. Class averages were obtained using reference-free classification with a box size of 32.6 nm for Cd^{2+} (1834 particles) and 22.4 nm for Pb^{2+} (2903 particles). Averages were low-pass filtered to 11 Å. The maximum particle dimensions were estimated using ImageJ. Histograms of Feret diameters were constructed using 24,237 (Pb^{2+}) and 25,289 (Cd^{2+}) C1B-C2 particles.

Protein-to-membrane FRET

Large unilamellar vesicles (LUVs) were prepared as previously described[126] using 1-Palmitoyl-2-oleoyl-sn-glycero-3-phosphocholine (POPC), 1-palmitoyl-2-oleoyl-sn-glycero-3-phospho-L-serine (POPS), and 1,2-dioleoyl-sn-glycero-3-phosphoethanolamine-N-(5-dimethylamino-1-naphthalenesulfonyl) (dansyl-PE), all from Avanti Polar Lipids. The composition of LUVs was POPC:POPS:dansyl-PE=(73-75):20:(7-5) molar %. FRET experiments using Trp residues in C1B-C2 as a donor and dansyl-PE as an acceptor were conducted as previously described, with excitation at 295 nm.[124] FRET experiments were carried out on an ISS PC1 fluorometer (ISS, Champaign, IL) at 25 °C. Cd^{2+} or Pb^{2+} from the respective concentrated stock solutions were added to 0.5 μM protein (C1B-C2 or C2) pre-incubated with 150 μM LUVs. The cuvettes were coated with Sigmacote® (Sigma Aldrich) siliconizing reagent to prevent protein adsorption on the cuvette walls.

Estimation of the relative affinities for Cd^{2+} and Zn^{2+} to C1B

Three residues (I145, V147, and H140) in both the C1B (Figure III.10) and C1B-C2 (Figure III.7C, expansions shown for I145 and V147) regions had four exchange peaks associated with each residue. These correspond to four distinct species that coexist in solution: Zn(1,2), Zn(1)Cd(2), Cd(1)Zn(2), and Cd(1,2). The intensity of the Cd(1,2) exchange peak increased, while the Zn(1,2) crosspeak intensity decreased, as more Cd^{2+} was added. The relative populations of each species were used, determined from the intensities of the corresponding crosspeaks, to obtain the affinity of each site for Cd^{2+} relative to Zn^{2+}. Consistent with Cd^{2+} binding to the loops of C2[124], C2 residues in C1B-

C2 also shifted in response to Cd^{2+} addition (Figure III.9) indicating Cd^{2+} is simultaneously populating both the loops of C2 and the Zn-sites of C1B. Therefore, for the analysis, the isolated C1B domain was used which is only affected by Cd^{2+} replacing Zn^{2+}.

For any given concentration of Cd^{2+} the fractional populations, f, are defined by:

Equation 2

$$f_{Zn(1,2)} = \frac{I_{Zn(1,2)}}{\Sigma}, f_{PZn(1)Cd(2)} = \frac{I_{Zn(1)Cd(2)}}{\Sigma}, f_{PCd(1)Zn(2)} = \frac{I_{Cd(1)Zn(2)}}{\Sigma}, f_{Cd(1,2)} = \frac{I_{Cd(1,2)}}{\Sigma}$$
$$\Sigma = I_{Zn(1,2)} + I_{Zn(1)Cd(2)} + I_{Cd(1)Zn(2)} + I_{Cd(1,2)}$$

where I is the intensity of the corresponding species identified in Figure III.10 in Cd^{2+} containing ^{15}N-^{1}H HSQC for H140, I145, and V147.

The concentrations of free Cd^{2+} and Zn^{2+} are estimated from the fractional populations assuming a starting stoichiometry of 2 Zn^{2+} per C1B domain:

Equation 3

$$\frac{[Cd^{2+}]_0}{P_0} = \frac{[Cd^{2+}]}{P_0} + 2f_{PCd(1,2)} + f_{PZn(1)Cd(2)} + f_{PCd(1)Zn(2)}$$

Equation 4

$$2 = \frac{[Zn^{2+}]}{P_0} + 2f_{PZn(1,2)} + f_{PZn(1)Cd(2)} + f_{PCd(1)Zn(2)}$$

where P_0 is the total protein concentration and $[Cd^{2+}]_0$ is the total Cd^{2+} concentration.

In the presence of Cd^{2+}, each site exists in an equilibrium between free, Zn-coordinated, and Cd-coordinated:

$$PZn(2) + Zn^{2+} \underset{}{\overset{K_a Zn(1)}{\rightleftharpoons}} PZn(1,2)$$

$$PZn(2) + Cd^{2+} \underset{}{\overset{K_a Cd(1)}{\rightleftharpoons}} PCd(1)Zn(2)$$

$$PZn(1) + Zn^{2+} \underset{}{\overset{K_aZn(2)}{\rightleftharpoons}} PZn(1,2)$$

$$PZn(1) + Cd^{2+} \underset{}{\overset{K_aCd(2)}{\rightleftharpoons}} PZn(1)Cd(2)$$

The binding equilibria in terms of fractional population are described by:

Equation 5

$$K_aZn(1) = \frac{f_{Zn(1,2)}}{f_{Zn(2)}[Zn^{2+}]}$$

Equation 6

$$K_aCd(1) = \frac{f_{Cd(1)Zn(2)}}{f_{Zn(2)}[Cd^{2+}]}$$

Equation 7

$$K_aZn(2) = \frac{f_{Zn(1,2)}}{f_{Zn(1)}[Zn^{2+}]}$$

Equation 8

$$K_aCd(2) = \frac{f_{Zn(1)Cd(2)}}{f_{Zn(1)}[Cd^{2+}]}$$

and the relative affinity of Cd^{2+} and Zn^{2+} to each site can be estimated by taking the ratio of association constants for each site:

Equation 9

$$\frac{K_aCd(1)}{K_aZn(1)} = \frac{[Zn^{2+}]f_{Cd(1)Zn(2)}}{[Cd^{2+}]f_{Zn(1,2)}}$$

Equation 10

$$\frac{K_aCd(2)}{K_aZn(2)} = \frac{[Zn^{2+}]f_{Zn(1)Cd(2)}}{[Cd^{2+}]f_{Zn(1,2)}}$$

In addition, Cd^{2+} and Zn^{2+} can bind to one site of a C1B molecule that is already populated by Cd^{2+} at the other site:

$$PCd(1) + Zn^{2+} \underset{}{\overset{K_a'Zn(2)}{\rightleftharpoons}} PCd(1)Zn(2)$$
$$PCd(1) + Cd^{2+} \underset{}{\overset{K_a'Cd(2)}{\rightleftharpoons}} PCd(1,2)$$

$$PCd(2) + Zn^{2+} \underset{}{\overset{K_a'Zn(1)}{\rightleftharpoons}} PZn(1)Cd(2)$$
$$PCd(2) + Cd^{2+} \underset{}{\overset{K_a'Cd(1)}{\rightleftharpoons}} PCd(1,2)$$

and the relative affinity to each site when Cd^{2+} is bound at the other site can be estimated by:

Equation 11

$$\frac{K_a'Cd(1)}{K_a'Zn(1)} = \frac{[Zn^{2+}]f_{Cd(1,2)}}{[Cd^{2+}]f_{Zn(1)Cd(2)}}$$

Equation 12

$$\frac{K_a'Cd(2)}{K_a'Zn(2)} = \frac{[Zn^{2+}]f_{Cd(1,2)}}{[Cd^{2+}]f_{Cd(1)Zn(2)}}$$

These values describe how population at one structural site influences the population of the other site.

For a 0.1 mM sample of isolated C1B with 0.1 mM Cd^{2+} equilibrated overnight, the fractional populations of each species and the concentrations of free Cd^{2+} and Zn^{2+} were determined in solution for all residues that showed four exchange peaks (Table III-2).

Table III-2. Fractional populations of each C1B species in solution for a 0.1 mM C1B sample with 0.1 mM Cd^{2+}.

Residue	f_{PZn_2}	f_{PZnCd}	f_{PCdZn}	f_{PCd_2}	[Zn^{2+}], μM	[Cd^{2+}], μM
H140	0.387	0.205	0.271	0.138	75.1	24.9
I145	0.400	0.215	0.247	0.138	73.8	26.2
V147	0.389	0.211	0.264	0.136	74.6	25.4
Average	0.392± 0.007	0.210± 0.005	0.260± 0.012	0.137± 0.001	74.5± 0.7	25.5± 0.7

Results

Pb^{2+} and Cd^{2+} promote self-assembly of the regulatory region

Two divalent metal ions, Zn^{2+} and Ca^{2+}, are essential components of the membrane-binding regulatory region of PKCα. Zn^{2+} is required for the proper folding and structural integrity of the C1 domains, C1A and C1B. Ca^{2+} is not needed for the C2 domain folding but is essential for its association with acidic phospholipids. In fully activated PKCα, the interaction of both C2 and C1 domains with membranes, schematically illustrated in Figure III.1, is required for full activation of the enzyme.[143] Therefore, while only Zn^{2+} plays a structural role in PKC, both metal ions are absolutely essential for the PKC function. For the majority of the work reported here, a two-domain C1B-C2 membrane-binding region was used (Figure III.1) that faithfully reproduces the behavior of the full-length region.

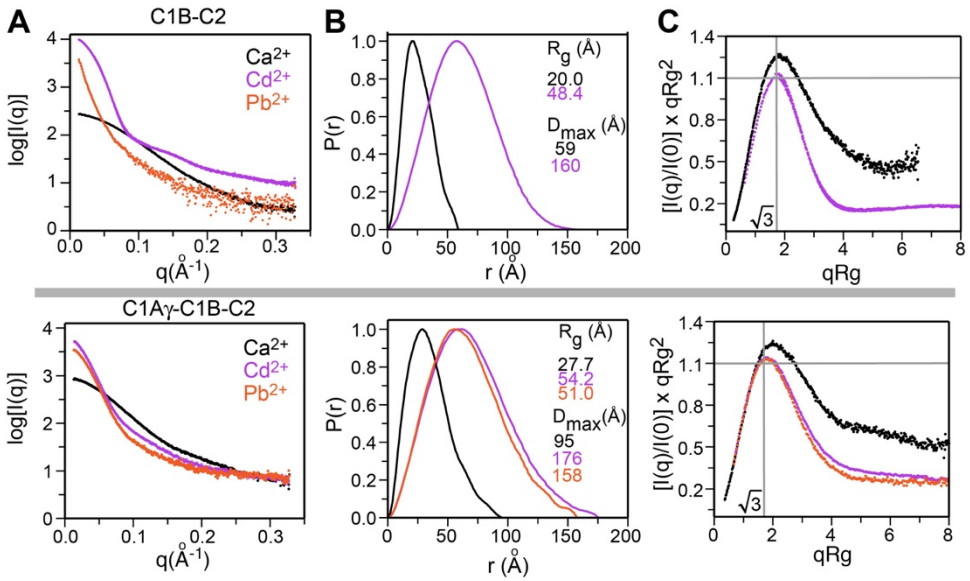

Figure III.2 Treatment of PKC regulatory region with Cd^{2+} or Pb^{2+} results in self-association, loss of conformational flexibility, and formation of globular species. (A) SAXS scattering curves of the 2- and 3-domain regulatory regions showing the differences between Ca^{2+} and Cd^{2+}/Pb^{2+}-bound proteins. The changes in size and flexibility/shape caused by Cd^{2+} and Pb^{2+} are evident from the comparison of pair-distance distribution functions P(r) (B) and dimensionless Kratky plots (C), respectively.

To determine how toxic metal ions influence the shape and size of the membrane-binding regulatory region of PKCα, SAXS experiments were conducted on the C1B-C2 and the full regulatory region C1C2c that additionally contains the C1A domain.[97] Three metal ions: Cd^{2+}, Pb^{2+}, and native cofactor Ca^{2+} were introduced into protein solutions via dialysis during the SAXS sample preparation procedure (see Table III-1 for the composition of all samples). A comparison of the scattering curves illustrates that the morphology of the protein species in the presence of Cd^{2+} and Pb^{2+} is drastically different from that of the Ca^{2+}-complexed proteins that are monomeric (Figure III.2A). Surprisingly, the scattering curves of Cd^{2+}/C1C2s and Pb^{2+}/C1C2s are similar, indicating that these metal ions interact with the regulatory region in a similar

manner. The Pb^{2+}/C1B-C2 scattering curves showed signs of aggregation and inter-particle repulsion and were not used for quantitative analysis (see Methods for details).

Analysis of the pair-distance distribution functions P(r) revealed that interactions with Cd^{2+} and Pb^{2+} promote self-association of the regulatory regions (Figure III.2B). The radii of gyration, R_g, of the Cd^{2+} complexes exceeded those of the Ca^{2+}-bound species ~2-fold. The maximum distance present in the scattering particle, D_{max}, increased 1.9- and 2.7-fold for the C1B-C2 and C1C2c, respectively. The behavior of Pb^{2+}-bound C1C2c sample closely mirrored that of the Cd^{2+}-complexed species.

Dimensionless Kratky plots[137] were constructed to evaluate the flexibility and shape of the protein complexes. The plots of globular proteins converge to zero at high scattering angles and have a maximum of 1.1 at qRg = √3. Ca^{2+}-complexed C1B-C2 and C1C2c lack these features and have a plateau-like region at high qRg that is typical of flexible multi-domain proteins (Figure III.2C). In contrast, all Cd^{2+} and Pb^{2+} plots have maxima at (√3, 1.1) and show a significant decrease in intensity at high qRg values. It's conclude that Ca^{2+}-complexed regulatory region behaves as a flexible monomer in solution, as one would expect based on its modular structure with unstructured linkers. Interactions with Cd^{2+} and Pb^{2+} result in formation of oligomeric species that are more globular in shape, with attenuated mobility of the linker regions.

Characterization of Pb^{2+}- and Cd^{2+}-containing C1B-C2 oligomers

Negative-stain electron microscopy experiments were conducted to visualize the oligomers (Figure III.3). The overall globular shape of Cd^{2+}- and Pb^{2+}-containing C1B-C2 oligomers is evident from the inspection of characteristic class averages (bottom

panel of Figure III.3). The maximum dimension of Cd^{2+}-containing particles is 15-18 nm. They appear to be composed of 4 spherical densities, each with an estimated molecular mass of 80 kDa. Given that the molecular mass of the monomer is 22.34 kDa, this would correspond to a 320 kDa oligomer consisting of ~16 monomers. Pb^{2+}-containing particles are smaller. Their footprint appears as two parallel ellipsoids, with each ellipsoid having an estimated molecular mass of ~40 kDa. This arrangement would produce an 80 kDa tetramer. In addition to large particles that were used to generate the class-averages, a sub-population of smaller particles were observed that could be dissociation products of the oligomeric species. The overall distributions of particle sizes are centered at ~12.5 and ~15.0 nm for the Pb^{2+}- and Cd^{2+}-containing particles, respectively (Figure III.3C).

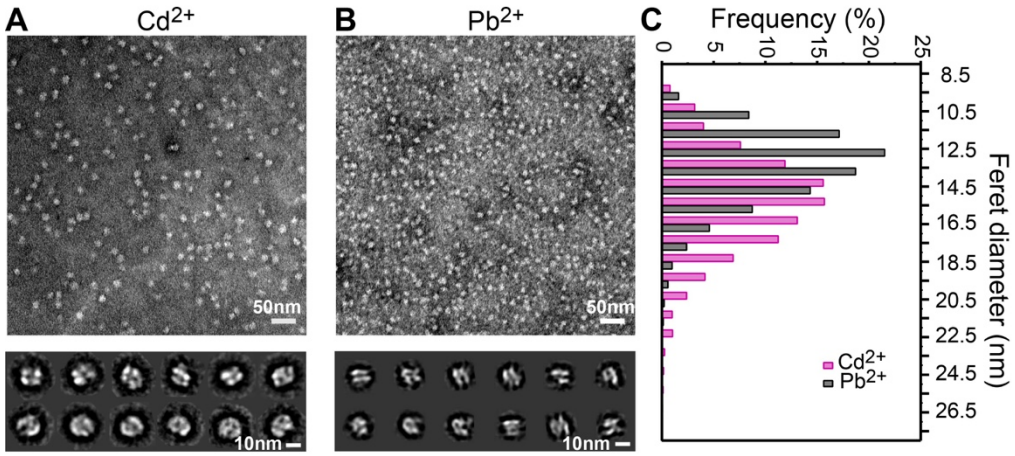

Figure III.3 C1B-C2 forms spherical oligomers in the presence of Cd^{2+} and Pb^{2+}. Electron micrographs and class averages of (A) Cd^{2+}- and (B) Pb^{2+}-complexed C1B–C2. (C) Distribution of Feret diameters in Cd^{2+}- and Pb^{2+}-complexed C1B–C2. The data were obtained at pH 7.4 (Cd^{2+}) and 6.0 (Pb^{2+}).

To characterize the distribution of oligomeric species in solution, sedimentation velocity experiments were conducted on C1B-C2 in the presence of Cd^{2+} and Pb^{2+}. The conditions of sedimentation experiments did not favor the formation of Pb^{2+}-containing C1B-C2 oligomers (Figure III.4), presumably due to lower protein and Pb^{2+} concentration than those used for preparation of EM samples. After one day of incubation, the majority of C1B-C2 in the presence of Pb^{2+} has sedimentation coefficients consistent with monomeric C1B-C2. With two additional days of incubation, 15-20% of the boundary has significantly larger sedimentation coefficients, which indicates the formation of large aggregates over time.

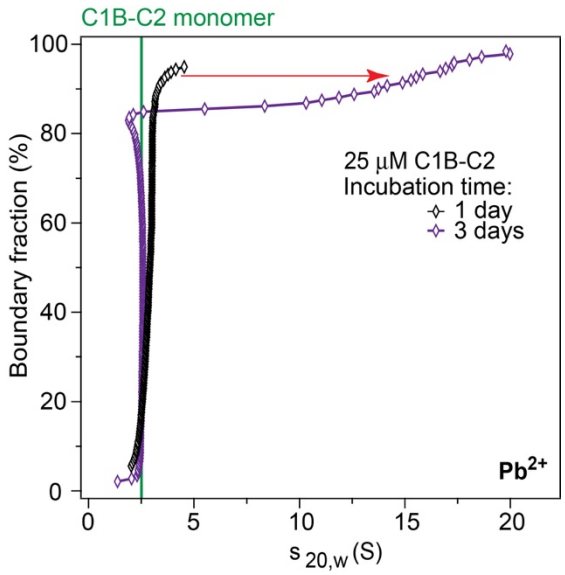

Figure III.4 Pb^{2+} causes aggregation of C1B-C2 over time. Distribution of sedimentation coefficients determined from van-Holde Weischet analysis of sedimentation velocity experiments of C1B-C2 in the presence of 0.1 mM Pb^{2+} at pH 6.0. The increase in the size of aggregated particles over time is indicated with an arrow.

In contrast, Cd^{2+} caused the formation of oligomeric C1B-C2 species in a process that is reversible and pH-dependent (Figure III.5). The sedimentation data are presented in two ways: as integral distribution of $s_{20,w}$, and as the envelopes of the $s_{20,w}$ frequency histograms (Figure III.5). Two distinct populations of oligomeric species are observed. Changing the total protein concentration causes the redistribution of populations, indicating that: (i) Cd^{2+}-dependent oligomerization process is reversible; and (ii) the apparent dissociation constant K_d is in the range of protein concentrations tested, 7–23 μM, at pH 6.0, and is < 7 μM at pH 7.4.

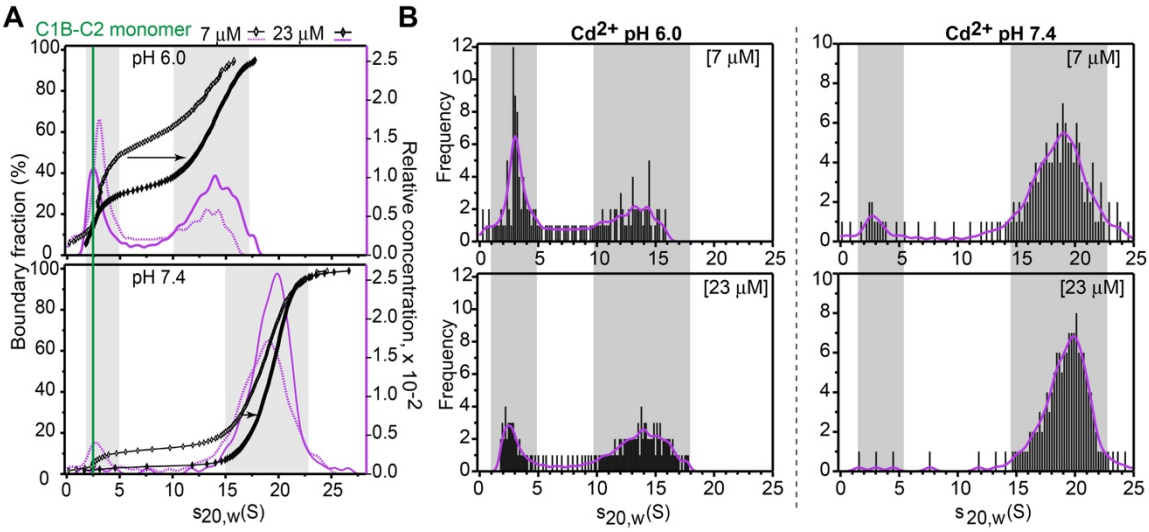

Figure III.5 Cd^{2+}-mediated self-association of C1B-C2 is reversible and pH-dependent. (A) Distribution of sedimentation coefficients determined from the van-Holde Weischet analysis of sedimentation velocity experiments at pH 6.0 (top) and pH 7.4 (bottom). Black symbols represent the integral distribution of $s_{20,w}$; purple lines represent the envelopes of the frequency histograms (B). The shift towards larger sedimentation coefficients upon increasing protein concentration from 7 to 23 μM is indicated with an arrow.

The slow-sedimenting population with $s_{20,w}$ values in the 2-5 S range contains a monomer and lower-order oligomers, potentially up to a tetramer. The fast-sedimenting population showed broad distributions centered at ~14 S (pH 6.0) and ~19 S (pH 7.4), consistent with at least >10 monomers per oligomer. Higher pH value resulted in the shift towards higher molecular mass species. This was also evident in analytical gel-filtration experiments (Figure III.6). Analytical gel filtration data were collected for two, identically prepared C1B-C2 samples at pH 6.0 in MES buffer and pH 7.4 in HEPES buffer with Cd^{2+}. For both conditions, C1B-C2 elutes in two peaks corresponding to monomeric C1B-C2 and high molecular weight oligomers. Changes in the elution profiles at different pH are consistent with size and apparent affinity changes observed in sedimentation velocity experiments. The amount of monomer that elutes from the column decreases with increasing pH (Figure III.6). Furthermore, the retention volume of the oligomer peak decreased at higher pH, which is consistent with the formation of larger species and a higher affinity for oligomer formation at physiological pH.

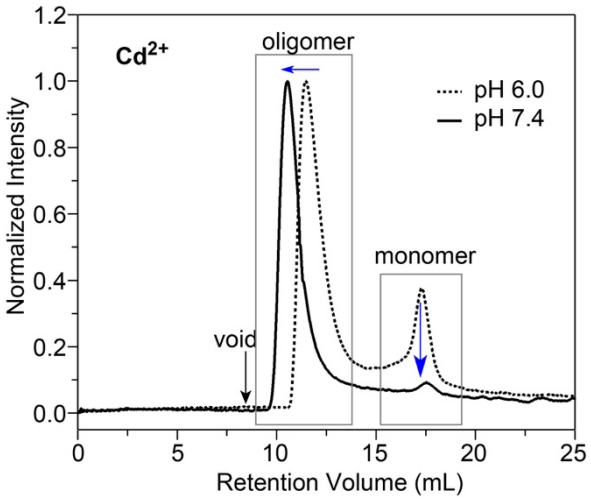

Figure III.6 More self-association is observed at physiological pH with Cd^{2+}. 100 μM C1B-C2 analytical gel filtration profiles on a Superdex 200 10/300 size exclusion column in the presence of 1 mM Cd^{2+} in MES buffer at pH 6.0 and HEPES buffer at pH 7.4. Red arrows indicate the changes in the elution profile under the different conditions.

Mechanism of Cd^{2+}- and Pb^{2+} induced self-association

The next set of experiments was designed to determine: (i) which regions of C1B-C2 interact with Cd^{2+} and Pb^{2+}, and (ii) how these interactions contribute to self-association. From previous studies, it is known that isolated C2 domain binds Pb^{2+} [50] and Cd^{2+} [124] through its calcium-binding loops; there is an additional weak Cd^{2+} site that is formed by the N- and C-terminal residues. Neither binding event causes the self-association of the isolated C2. Therefore, the goal was to determine how C1B and C2 domains interact with Cd^{2+} and Pb^{2+} in the context of the regulatory region.

C1B: Cd^{2+} displaces Zn^{2+} to form a functional "Cd finger"

Addition of Cd^{2+} to the C1B-C2 domain resulted in the appearance of the absorption shoulder near λ=270 nm (Figure III.7A). The wavelength range is consistent

with the position of thiolate-Cd^{2+} charge transfer bands observed in other studies.[144] C2 domain is cysteine-free and therefore does not contribute to the difference absorption spectrum. Based on this information and previous studies of Zn^{2+}-containing proteins with Cys-rich sites, it was concluded that Cd^{2+} forms coordination bonds with the cysteine residues of the C1B domain. Two modes of coordination are possible: peripheral, shared coordination with Zn^{2+} or replacement of Zn^{2+}. To determine if Cys coordination by Cd^{2+} is accompanied by the ejection of Zn^{2+} from the protein, 4 molar equivalents of Cd^{2+} were added to the C1B-C2 domain in the presence of a highly selective Zn^{2+} fluorophore, FluoZin-3. A steady increase in the fluorescence intensity at 516 nm was observed, indicating that Zn^{2+} is being displaced from the protein as a result of Cd^{2+} treatment (Figure III.7B).

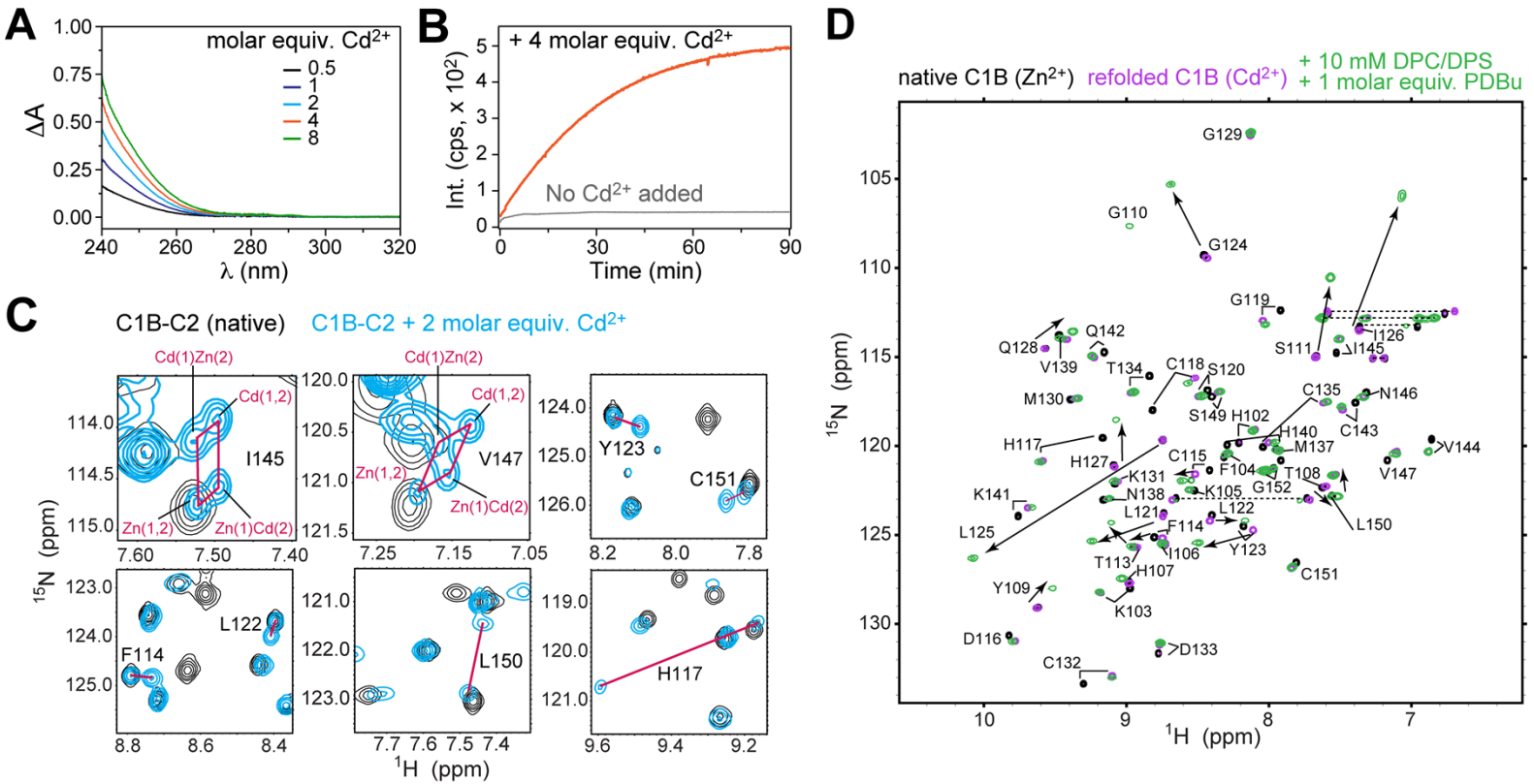

Figure III.7 Cd^{2+} replaces Zn^{2+} in the C1B domain without loss of fold and function. (A) Difference UV-vis absorption spectra of C1B-C2 with increasing molar equivalents of Cd^{2+}. (B) Cd^{2+}-stimulated Zn^{2+} release from the C1B-C2 domain monitored using fluorescence intensity of FluoZin-3 at 516 nm (red). No-Cd^{2+} control is shown in gray. (C) Expansions of the ^{15}N-^{1}H HSQC spectra of native (black) and Cd^{2+}-treated C1B-C2 (blue). The N-H cross-peaks of Cd^{2+}- and Zn^{2+} containing species are connected with red lines. Ile145 and V147 have 4 distinct cross-peaks corresponding to the Zn(1,2), Zn(1)Cd(2), Cd(1)Zn(2), and Cd(1,2) C1B-C2 species. (D) Expansions of the ^{15}N-^{1}H HSQC spectra of isolated native C1B domain (black), C1B "Cd finger" (purple), and "Cd finger" complexed to PDBu and mixed micelles.

NMR experiments conducted on the C1B-C2 and the isolated C1B domain revealed that the replacement of Zn^{2+} with Cd^{2+} occurs at both sites 1 and 2 (see Figure III.1 for the site definitions) without the loss of secondary structure. The expansions of the 2D ^{15}N-^{1}H HSQC spectra illustrate the appearance of a new subset of well-dispersed C1B cross-peaks upon addition of Cd^{2+} to C1B-C2 (Figure III.7C). The same chemical shift pattern was observed in the isolated C1B (Figure III.8), which was used to assign the cross-peaks of the Cd^{2+}-containing protein species. The N-H groups of many residues, including those coordinating Zn1 and Zn2 experience large chemical shift perturbations compared to the native Zn^{2+}-containing protein (Figure III.9). While the majority of the N-H groups had two sets of cross-peaks, there were three residues: His140, Ile145, and Val147, whose N-H groups had four cross-peaks (expansion of Ile145 and Val147 in Figure III.7B; also Figure III.10**)**. This means that all four possible Cd/Zn protein species coexist in solution: Zn(1,2), Zn(1)Cd(2), Cd(1)Zn(2), and Cd(1,2), where "1" and "2" denote the structural zinc sites. The ability to detect distinct Cd^{2+}- and Zn^{2+}-containing protein populations indicates that they interconvert on a timescale that is slow on the NMR chemical shift scale.

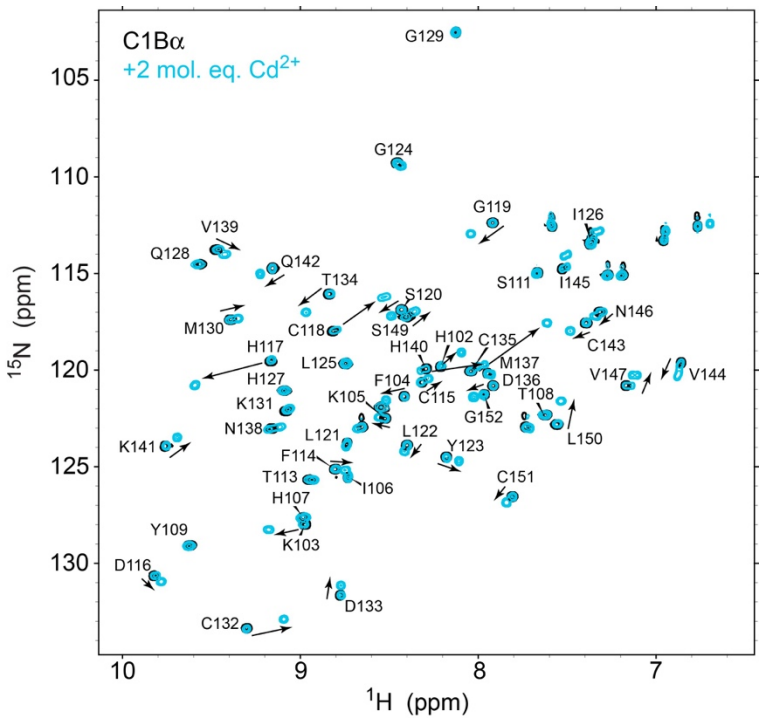

Figure III.8 Cd^{2+} replaces Zn^{2+} in C1B-C2. ^{15}N-^{1}H HSQC of 0.1 mM [U-^{15}N] C1B in apo state and in the presence of 2 molar-equivalents of Cd^{2+}. The same signatures of Cd^{2+} replacement at structural Zn-sites are observed for isolated C1B.

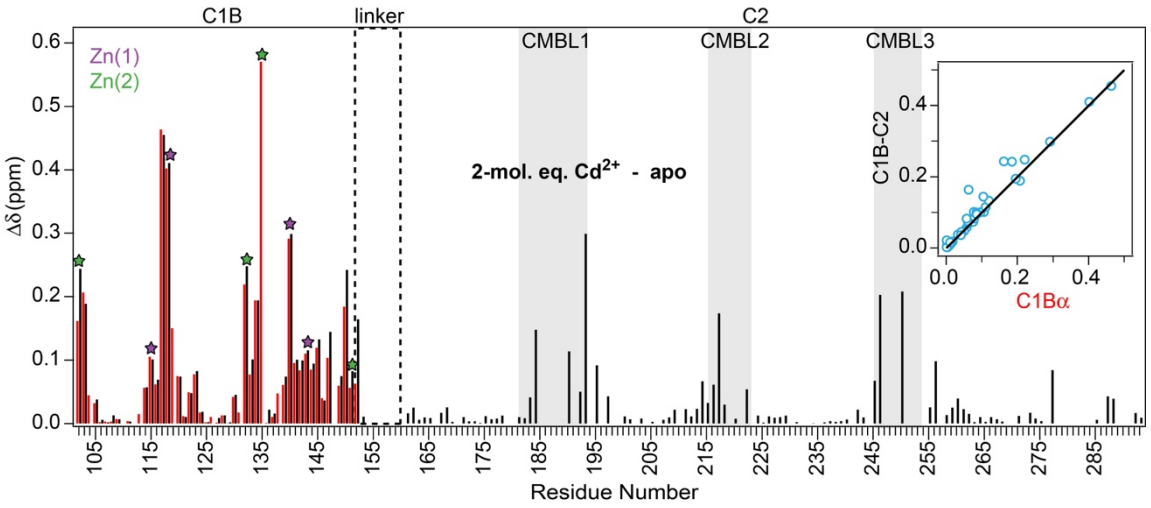

Figure III.9 Cd^{2+} binds to the loop regions of the C2 domains and the structural Zn-sites of the C1B-C2. Chemical shift perturbation (CSP) from ^{15}N-^{1}H HSQC in the presence and absence of Cd^{2+} for C1B-C2 (black) and isolated C1B (red). *Inset:* Correlation of the CSPs for C1B residues in the C1B-C2 region versus the isolated C1B domain.

Based on the relative cross-peak intensities and the peak positions in the refolded Cd(1,2) C1B (Table III-2), all four cross-peaks were assigned to specific Cd/Zn C1B species. The relative intensities of the four cross-peaks enabled determination of the ratio of the association constants for Zn^{2+} and Cd^{2+} binding to the C1B domain. Cd^{2+} has a 1.9-fold higher affinity to site 1 and 1.5-fold higher affinity to site 2 on C1B (Table III-3); these values are independent of the metal ion identity that occupied the other site.

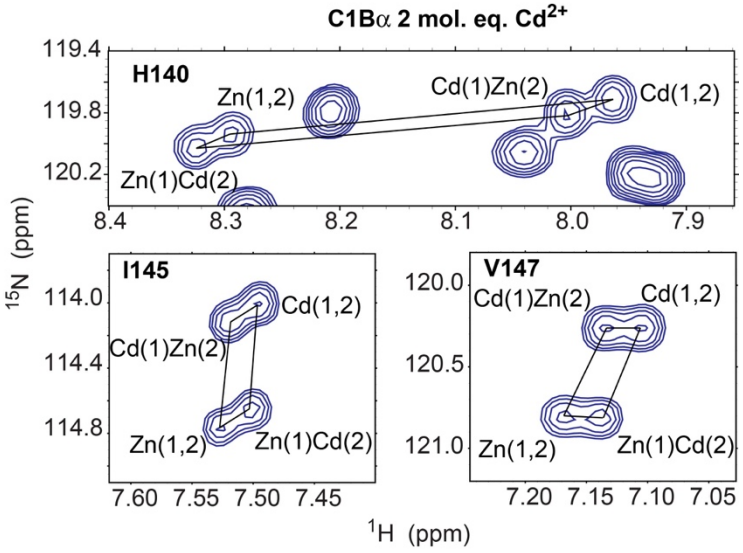

Figure III.10 Four distinct C1B species form upon treatment with Cd^{2+}. Expansions of ^{15}N-^{1}H HSQC for three residues in isolated C1B that have 4 exchange peaks in the presence of Cd^{2+}.

A potent activator of PKC, phorbol ester PDBu, was used to test if the C1B "Cd finger" is functional. C1B was successfully refolded in the presence of Cd^{2+}, as evidenced by large chemical shift dispersion observed in the NMR spectrum of the resulting "Cd finger" (Figure III.7D). Upon addition of PDBu and mixed micelles as a membrane mimic, the loop residues of C1B experienced significant chemical shift

perturbations that were essentially identical to those previously reported for the native Zn(1,2) protein. It is concluded that Cd(1,2) C1B interacts with PDBu and partitions into micelles in a manner identical to that of the native C1B. Taken together, these results demonstrate that Cd^{2+} is able to replace Zn^{2+} at both structural sites and thereby support the fold and function of C1B. The presence of the second domain, C2, has little influence on this process.

Table III-3. Relative affinities of Cd^{2+} to each C1Ba Zn-site. Error is reported as the standard deviation of all three residues.

Residue	$\frac{K_a Cd(1)}{K_a Zn(1)}$	$\frac{K_a Cd(2)}{K_a Zn(2)}$	$\frac{K'_a Cd(1)}{K'_a Zn(1)}$	$\frac{K'_a Cd(2)}{K'_a Zn(2)}$
H140	2.11	1.59	2.02	1.53
I145	1.74	1.51	1.81	1.57
V147	1.99	1.60	1.89	1.52
Average	1.94± 0.19	1.57± 0.05	1.91± 0.11	1.54± 0.03

C1B: Pb^{2+} coordinates Cys residues but can neither displace Zn^{2+} nor support the treble-clef fold

UV-vis absorption spectroscopy was used to monitor Pb^{2+} interactions with C1B-C2. Addition of Pb^{2+} to the C1B-C2 domain resulted in the appearance of absorption bands at 245 and 330 nm (Figure III.11A). To attribute these spectral changes to individual domains, Pb^{2+}-binding experiments were conducted on isolated C1B and C2. Addition of Pb^{2+} to C2 resulted in the increase of absorbance at 245 nm (Figure III.11B), which is consistent with the formation of Pb-O coordination bonds.[145] This observation

is in agreement with previous structural work showing that Pb^{2+} populates two sites on the C2 domain – one high- and one low-affinity, both having an all-oxygen coordination environment.[126] Addition of Pb^{2+} to the isolated C1B domain resulted in the appearance of two bands at 245 nm and 330 nm (Figure III.11C). These represent lead-thiolate charge-transfer bands that were previously detected upon treating Zn^{2+}-binding peptides with Pb^{2+}.[146] Therefore, the C1B-C2 data reflect two types of Pb^{2+} binding events: one to the loop region of C2, and the other one to the cysteine residues of C1B.

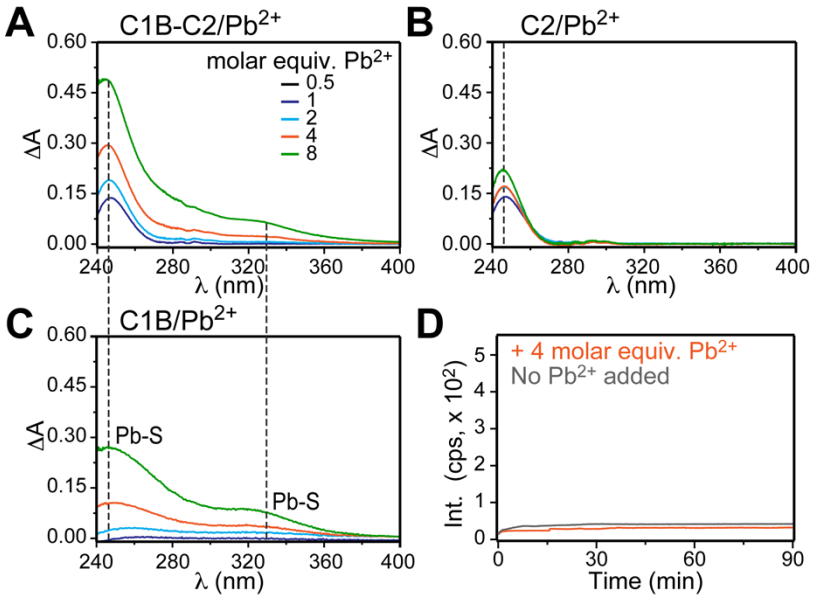

Figure III.11 Pb^{2+} coordinates C1B cysteines but does not cause Zn^{2+} release from C1B-C2. (A) Difference UV-vis absorption spectra of C1B-C2 obtained at increasing molar equivalents of Pb^{2+}. The position of the absorption bands at 245 and 330 nm is consistent with the formation of Cd^{2+}-thiolate bonds. (B,C) Difference UV-vis absorption spectra that show the response of isolated C2 (C) and C1B (D) to Pb^{2+} binding. (D) Treatment with Pb^{2+} does not cause Zn^{2+} release from the C1B-C2 domain, evidenced by unchanged fluorescence intensity of FluoZin-3 at 516 nm (red). No-Pb^{2+} control is shown in gray.

Unlike Cd^{2+}, Pb^{2+} did not cause the release of Zn^{2+} from the structural C1B sites. No increase in FluoZin-3 fluorescence was observed upon treating the protein with 4 molar equivalents of Pb^{2+} (Figure III.11D). Attempts to refold the C1B domain in the presence of Pb^{2+} were unsuccessful, indicating that Pb^{2+} is unable to support the treble-clef fold of C1B. Therefore, the observed changes in the UV-VIS spectra have to come from external coordination of cysteines by Pb^{2+}, without displacement of Zn^{2+}. Because C1B relies on Zn^{2+} for the proper fold, cysteine residues cannot be altered without disturbing the fold. Therefore, to determine how the individual residues of C1B respond to interactions with Pb^{2+}, a series of ^{15}N-^{1}H HSQC NMR experiments were recorded on isolated C1B in the presence of increasing molar equivalents of Pb^{2+}. While little chemical shift perturbation was observed in the spectra, there was a significant decrease in peak intensities, accompanied by modest line broadening, upon increasing Pb^{2+} concentration (Figure III.12). The peak intensities are fully recovered upon EGTA treatment. This behavior is consistent with the reversible formation of high-molecular weight C1B oligomers that are not detectable in NMR spectra due to extreme line broadening. It is concluded that Pb^{2+} promotes self-association of C1B domains through coordination of surface-exposed cysteine residues, with Zn^{2+} structural sites remaining intact. The most likely candidates are Cys132, Cys143, and Cys151 (see Figure III.1B); it was recently demonstrated that the backbone amides of cysteines at equivalent positions are highly solvent exposed in the C1B domain from PKCδ.[147]

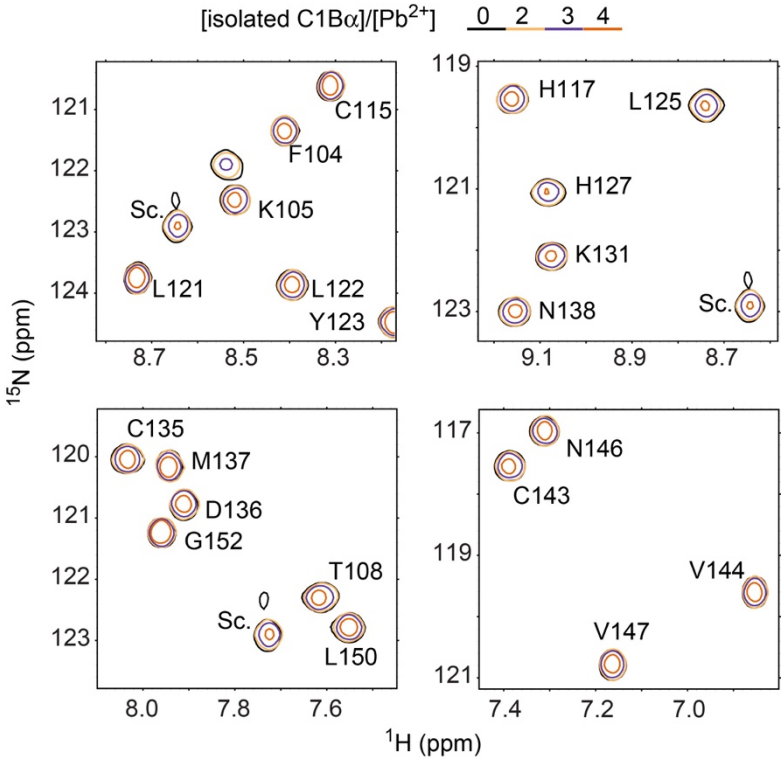

Figure III.12 Pb^{2+} interactions with isolated C1Bα. Expansions of ^{15}N-^{1}H HSQC for 0.1 mM [U-^{15}N] isolated C1B in the presence of increasing molar equivalents of Pb^{2+}.

C2: Cd^{2+} and Pb^{2+} drive the association of C1B-C2 oligomers with acidic membranes

Ca^{2+} binding to the C2 domain is a prerequisite for its association with phosphatidylserine-containing membranes. The C2 domain binds Pb^{2+} and Cd^{2+} through its loop regions; however, in the isolated C2 domain only Pb^{2+126} but not Cd^{2+124} can act as a functional Ca^{2+} mimic and support the membrane interactions.

Protein-to-membrane FRET was used to determine how self-association of the regulatory region influences its membrane binding-properties. The tryptophan residues of the C2 domains served as a donor, while the dansyl-labeled lipid incorporated into large unilamellar vesicles served as an acceptor (Figure III.13A). Upon addition of Pb^{2+}

to the C1B-C2 pre-incubated with LUVs, an appearance of dansyl emission peak was observed due to protein-membrane FRET (Figure III.13B). The Trp emission peak also decreased in intensity due to the combined effect of metal ion binding and resonance energy transfer to dansyl group. Addition of EGTA eliminated the dansyl emission peak indicating that the protein dissociated from the membrane upon sequestration of Pb^{2+} ions. The intensity of the Trp peak did not fully recover upon EGTA treatment because C2 domain has one high-affinity Pb^{2+} site[126] that remains populated even after EGTA treatment.

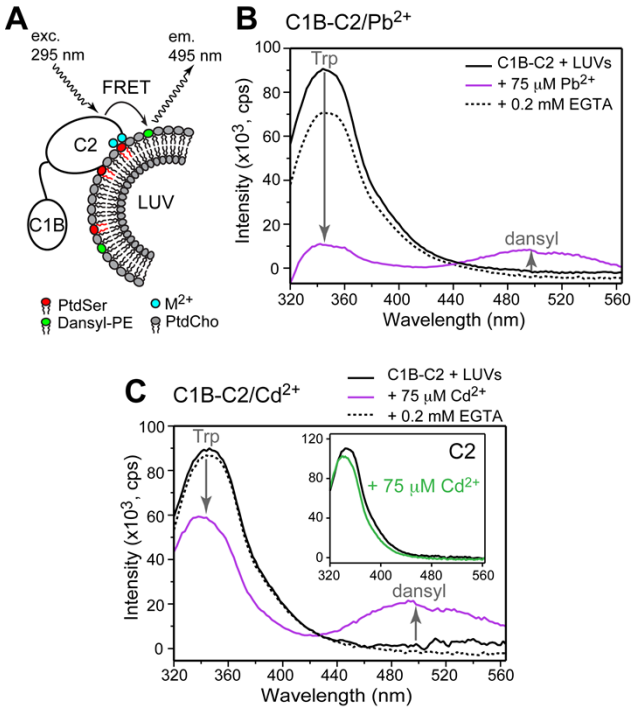

Figure III.13 Pb^{2+} and Cd^{2+} support the interactions of C1B-C2 domain with membranes. (A) Schematic representation of FRET experiments. (B,C) Fluorescence emission spectra of C1B-C2 conducted in the presence of LUVs as a membrane mimic. FRET is manifested as the appearance of the dansyl emission peak and concomitant decrease of the Trp emission peak. The inset in (C) represents the spectra collected on the isolated C2 domain in the presence of LUVs and Cd^{2+}.

It was previously demonstrated that isolated C2, despite binding a full complement of Cd^{2+} ions, does not appreciably associate with membranes.[124] This is illustrated by a lack of the dansyl emission peak in the control experiment that was conducted on the isolated C2 domain under the same set of conditions as C1B-C2 (inset of Figure III.13C). It is concluded that making loop regions of C2 more electropositive is not sufficient to drive membrane binding and speculated that Cd^{2+}, unlike Ca^{2+} and Pb^{2+}, cannot effectively coordinate lipid headgroups.[124] It was therefore surprising to find that Cd^{2+} supported the membrane association of C1B-C2 (Figure III.13C). This can be attributed this phenomenon to the increase in local concentration of C2 membrane binding functionalities provided by the formation of oligomeric species. The contribution of general electrostatics, which is too weak in the isolated domain, becomes significant enough in the oligomers to support their membrane interactions. Treatment with EGTA resulted in protein dissociation from the membrane and completely reversed the Trp fluorescence, consistent with the low micromolar affinity of Cd^{2+} to the loop regions of C2.

Linker region connecting the domains is involved in self-association

Having characterized the interactions of metal ions with C1B and C2, NMR experiments were conducted to determine the effect of Cd^{2+} and Pb^{2+} ions on the linker region. The ^{15}N-^{1}H HSQC spectra showed two signatures: (i) a decrease in cross-peaks intensities that affected the majority of N-H groups uniformly; and (ii) selective broadening of a subset of N-H cross-peaks (Figure III.14). Addition of EGTA reversed both the uniform and selective broadening (Figure III.14A). Furthermore, Cd^{2+}

occupying the Zn-sites on C1B was chelated by EGTA and replaced by the previously displaced Zn^{2+}. This indicates that both metal dependent self-association and Zn-displacement is reversible. Selective broadening occurred within the inter-domain linker region and the C-terminal α-helix. While this suggests that these regions undergo an additional process, it is not direct evidence that they mediate self-association. Therefore, a mutagenesis approach was developed to elucidate the mechanism of oligomerization.

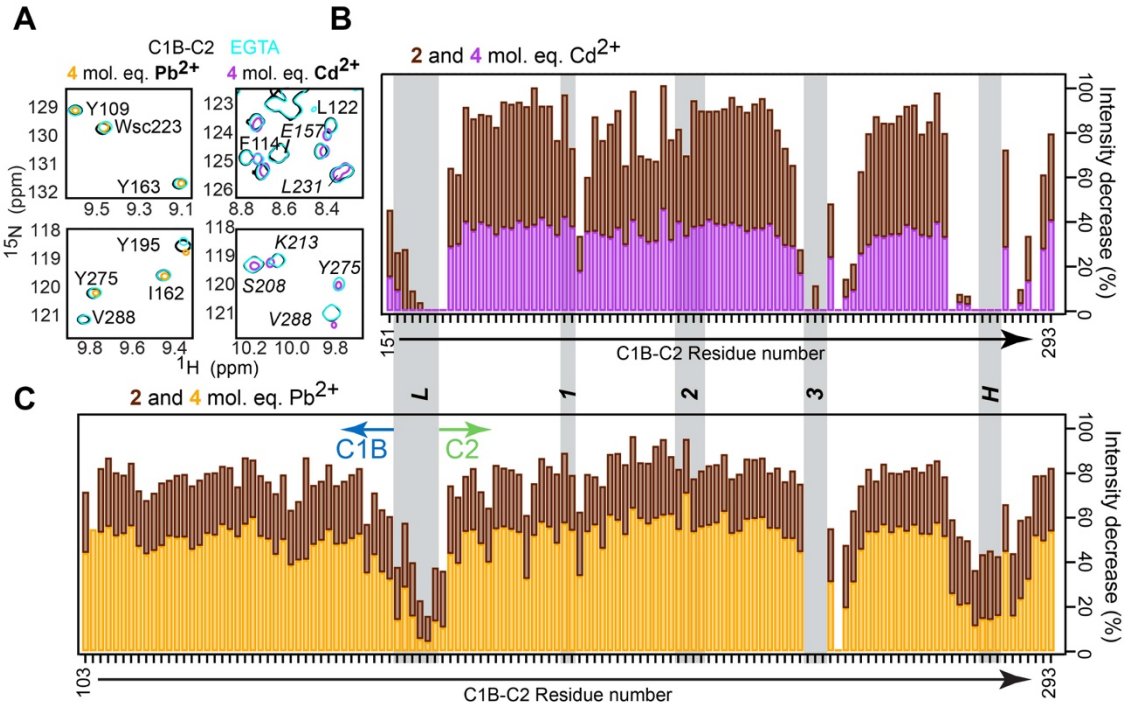

Figure III.14 Toxic heavy metals perturb the linker and c-terminal helix of C2. Peak intensity as a function of primary structure from ^{15}N-^{1}H HSQC spectra of C1B-C2 with 2-fold and 4-fold excess Pb^{2+} (A) and Cd^{2+} (B) normalized to peak intensity in the absence of Pb^{2+} and Cd^{2+}. Structural features are highlighted in grey on the plots. (C) Expansions of an overlay ^{15}N-^{1}H HSQC spectra of native (black), M^{2+}-treated C1B-C2 (gold and magenta), and after treatment with EGTA (cyan).

Known metal binding sites do not significantly contribute to self-association

Mutants were designed to disrupt Cd^{2+} and Pb^{2+} binding the CMBLs, linker region, and C-terminal α-helix (Table III-4, Figure III.15). The effect that these variants have on self-association was evaluated using size exclusion chromatography (Figure III.15A,C,D). Wild-type C1B-C2 in the presence of Ca^{2+} elutes in a single peak on an analytical gel filtration column (Figure III.15A). In the presence of Cd^{2+}, C1B-C2 elutes in two peaks, one corresponding to monomeric C1B-C2 and one corresponding to higher molecular weight oligomers (Figure III.15A). Interactions with the resin prevented exact determination of the molecular weight. Furthermore, resin interactions were stronger in the presence of Pb^{2+}. Therefore, the elution profiles of each variant compared with wild-type protein were used to qualitatively evaluate the relative amounts of monomer and oligomer (Figure III.15A-C).

Table III-4. Summary of the C1B-C2 variants.

Variant	Mutation	Location	Rationale
L3	D246N	C2 domain, loop 3	Disruption of M^{2+} binding to loop region
L1	D187N/D193N	C2 domain, loop 1	Disruption of M^{2+} binding to loop region
H1	E282K	C-terminal α-helix	Charge reversal of Cd3 ligand
tetraMut	D154K/H155G E157K/E282K	Linker and α-helix	Elimination of potential M^{2+} ligands in the linker/charge reversal of Cd3 ligands
GL	153-158→Gly_6	α-helix	Full linker replacement with Gly
LH	153-158→Gly_6 E281K/E282K/E284K	Linker and α-helix	Full linker replacement with Gly and charge reversal of α-helix

Variants that were previously shown to disrupt metal binding to the loops of C2, D246N (L3) and D187/193N (L1), had little effect on the amount of monomer that eluted from the analytical gel filtration column—although the L3 mutant had slightly

more monomer elute from the column than wild-type or the L1 mutant (Figure III.15B). From this it was concluded that Cd^{2+} and Pb^{2+} binding to the CMBLs does not contribute significantly to self-association. The charge reversal variant of Cd3 ligand, E282K, also had little effect on self-association (Figure III.15C). Collectively, this suggests that toxic metals binding to known metal binding sites doesn't significantly contribute to self-association. A variant was designed to eliminate residues that could potentially coordinate both Pb^{2+} and Cd^{2+} in the linker region combined with H1 mutation (tetraMut) (Table III-4). This variant had the largest effect on self-association, with significantly more monomer eluting from the column compared to wild-type (Figure III.15C). However, this still did not completely abolish oligomer formation, suggesting other ligands/regions that mediate self-association exist.

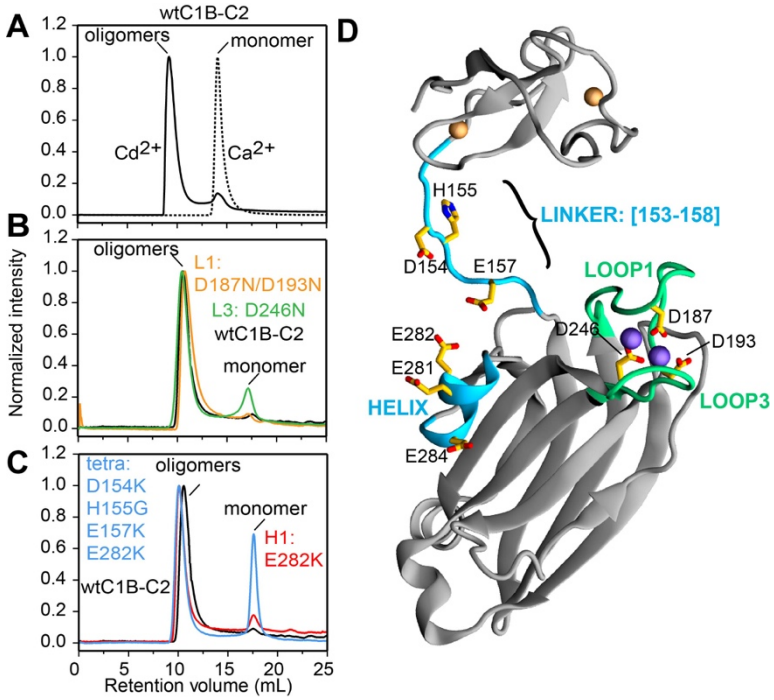

Figure III.15 Canonical metal binding sites do not contribute to Cd^{2+} mediated self-association. C1BC2 analytical gel filtration profiles for C1B-C2 variants compared with wt on (A) a Superdex 75 GL and (B-C) a Superdex 200 Increase 10/300 column at pH 7.4 in the presence of 1mM Cd^{2+}. (D) residues mutated are highlighted on ribbon diagrams of C1B (NMR structure, 2ELI) and C2 (crystal structure, 4L1L) with a modeled linker region.

Two, more extensive variants were designed that abolish all residues that could potentially coordinate Cd^{2+} and Pb^{2+} in the linker region and C-terminal helix. The GL variant targets the entire linker, replacing it with glycine (Table III-4). The LH variant combines the glycine linker with a charge reversal for all negatively charged residues in the C-terminal helix (Table III-4). A comparison of the ^{15}N-^{1}H HSQC spectra for wild-type C1B-C2 and the LH mutant assured that these mutations did not disrupt the fold of C1B-C2 (Figure III.16).

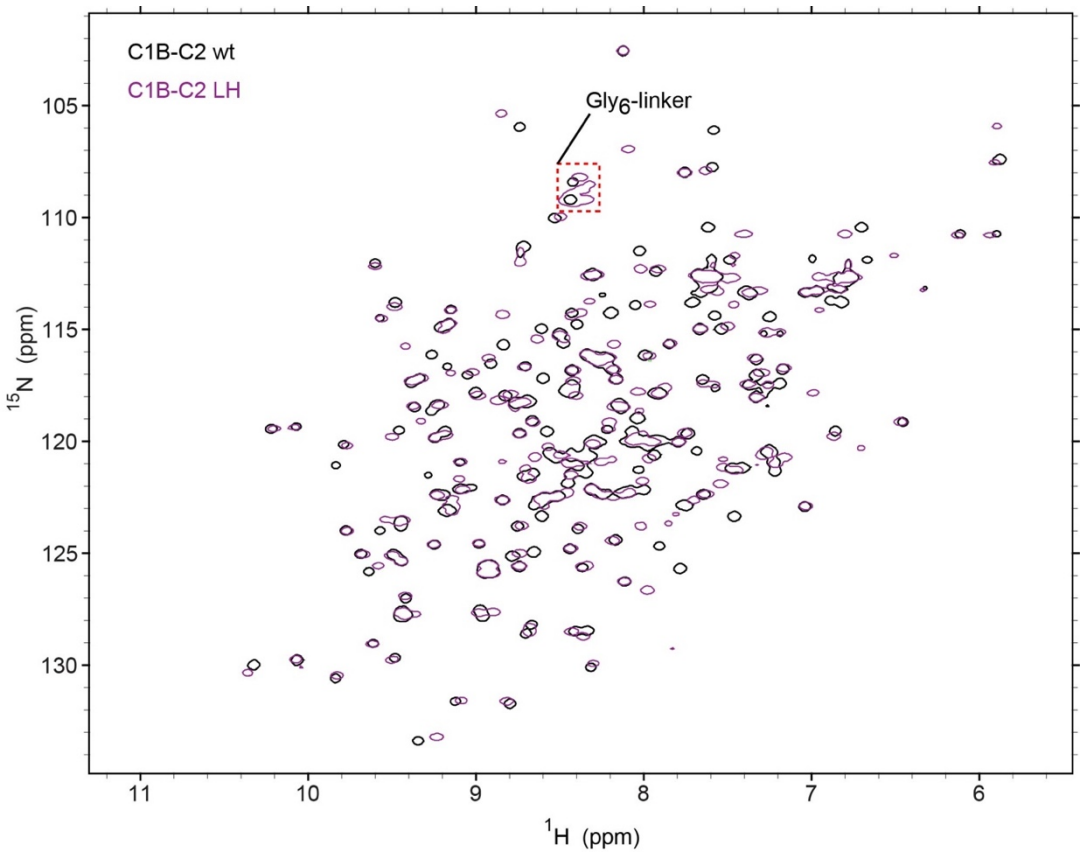

Figure III.16 LH variant does not perturb the structure of C1B-C2. Overlay of ^{15}N-^{1}H HSQC of 0.3 mM [U-^{15}N] C1B-C2 LH and wild-type in the metal-free state.

The relative extent of self-association was evaluated using ^{15}N-filtered ^{1}H-detected 1D NMR spectra in the presence of increasing amounts of Pb^{2+} and Cd^{2+} (Figure III.17A-B) for both variants. Wild-type C1B-C2 showed a 35% decrease in the integrated intensity in the presence of 4-molar equivalents of Pb^{2+} and 52% with the same ratio of Cd^{2+} as a result of oligomerization. The GL variant attenuated this intensity drop, with only an 18% decrease for the same concentration of Pb^{2+} and a 15% decrease for an equivalent concentration of Cd^{2+}. The largest attenuation of self-association was achieved by eliminating all potential coordinating residues in both the

linker region and C-terminal helix. The LH variant only had a 2-3% decrease in intensity in the presence of both Cd^{2+} and Pb^{2+}(Figure III.17A-B). The LH variants were visualized using negative stain EM in the presence of Pb^{2+} and Cd^{2+}. No oligomers were observed in the presence of Pb^{2+} although some oligomers (fewer than wild-type) were observed in the presence of Cd^{2+}. Despite this, there were no detectable oligomers that eluted from the analytical gel filtration column in the presence of either metal ion (Figure III.17C). It is worth noting that both of these regions are highly conserved in conventional PKC isozymes (Figure III.17E).

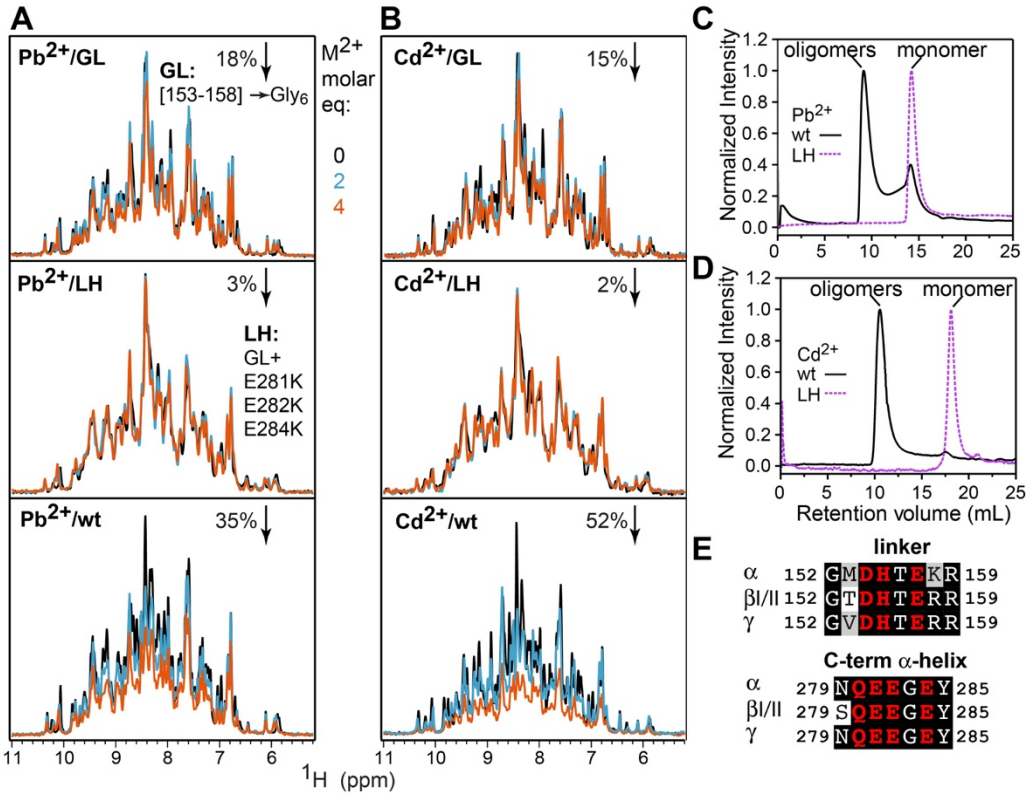

Figure III.17 Self-association is mediated by linker and C-terminal helix. ^{15}N-filtered ^{1}H-detected 1D NMR spectra in the presence of increasing amounts of (A) Pb^{2+} and (B) Cd^{2+} for Gly_6-linker mutant (GL), linker-helix mutant (LH), and wild-type C1B-C2. The decreases in the integrated intensity in the presence of 4-molar equivalents of metal relative to the metal-free spectra are indicated in orange.

Collectively, these data indicate that both the interdomain linker and C-terminal α-helix are crucial for Pb^{2+} and Cd^{2+} mediated self-association. This likely occurs through direct, shared coordination between ligands in these regions on opposite molecules. Since Ca^{2+} does not bind to these regions and regions known to bind Ca^{2+} do not contribute to self-association, it is clear that opportunistic binding and not ionic mimicry drives oligomerization. It is worth noting that these regions are highly

conserved within conventional isozymes (Figure III.17E). Therefore, it is plausible that this metal-induced self-association could occur in other conventional isozymes.

Discussion

The goal of this study was to investigate the interactions of toxic metal ions, Pb^{2+} and Cd^{2+}, with two, independently folded peripheral membrane binding modules from the regulatory region of PKCα. Cd^{2+} has been shown to activate nuclear PKC[17] and Pb^{2+} has been shown to have both activating[16] and inhibitory effects on PKC.[19,148] While both Pb^{2+} and Cd^{2+} have been previously shown to displace Ca^{2+} from the CMBLs of the C2 domain of PKCα[124,126], ionic mimicry alone is not enough to explain these toxic effects. The picture that emerges from this study reveals that Pb^{2+} and Cd^{2+} influence the regulatory region through by mimicking both Zn^{2+} and Ca^{2+} and opportunistic binding to regions outside of the known metal ion binding sites. Both metal ions had distinct influences on structure and function, unique from native metal ion cofactors, Zn^{2+} and Ca^{2+}. Cd^{2+} was able to spontaneously replace Zn^{2+} in the C1B domain, while Pb^{2+} was able to coordinate cysteines in structural Zn^{2+} sites without ejecting Zn^{2+}. Cd^{2+} and Pb^{2+} both bind opportunistically to other sites on C1B-C2 leading to self-association. Collectively, this work illustrates that the consequences of toxic metal ion encounters are complex and that even within proteins that are known to bind divalent native metal ions, the effects of toxic metals extend beyond ionic mimicry.

Toxic metal ions serve as ionic mimics for Zn^{2+} and Ca^{2+}

Pb^{2+} and Cd^{2+} had different abilities to serve as ionic mimics for Zn^{2+} and Ca^{2+}. Cd^{2+} is able to displace both Ca^{2+} and Zn^{2+}. While Cd^{2+} was able to support the fold and

function of the C1B domain it did not support the function of the isolated C2 domain. In contrast, Pb^{2+} was found only to serve as an ionic mimic for Ca^{2+} and was unable to replace Zn^{2+} or support the fold of the C1B domain. The proper folding of the C1B domain depends on two structural Zn^{2+} sites coordinated by the three cysteines and one histidine each with the motif, $HX_{12}CX_2CX_nCX_2CX_4HX_2CX_7C$ (where n is 13 or 14 and X is any amino acid), in a tetrahedral geometry.[149] Zn^{2+} and Cd^{2+} both have a preference for tetrahedral geometry when bound to cysteine/histidine ligands whereas Pb^{2+} has a preference for trigonal pyramidal geometry when bound to cysteines.[150] Despite this, Pb^{2+} is still able to displace Zn^{2+} in several Zn-binding proteins, often resulting in misfolding.[115,117,146] A study done by Godwin et al. using peptides that mimic Zn^{2+} coordination sites, found that the relative position of cysteines in the coordination sites governed the relative affinities of Zn^{2+} and Pb^{2+} to the sites.[150] Constructs with only two residues between the coordinating cysteines had insufficient separation of coordinating cysteines in the primary structure and disfavored the trigonal pyramidal geometry needed for Pb-S complexes, destabilizing the complex and resulting in a lower affinity of Pb^{2+} relative to Zn^{2+}. [150] In both Zn^{2+} sites of C1B, two of the coordinating cysteines are separated by only two amino acids in the primary structure (C115 and C118 in Zn(1) site and C132 and C135 in Zn(2) site) positioned to support a tetrahedral coordination geometry with Zn^{2+}. Therefore, it is concluded that Pb^{2+} has a lower affinity than Zn^{2+} due to the lack of three cysteines in favorable positions to coordinate Pb^{2+} in a trigonal pyramidal geometry. As a result, Pb^{2+} does not efficiently replace Zn^{2+}. Cd^{2+}, however, can adopt a tetrahedral geometry when coordinated by cysteines and histidines[151], which

is compatible with the geometry of both of the Zn^{2+} sites in C1Bα, allowing for efficient replacement.

Pb^{2+} and Cd^{2+} also differed in their abilities to mimic Ca^{2+}. Despite literature showing that Pb^{2+} enhances the aggregation of other proteins with inhibitory effects on function,[132,152] this study finds that, consistent with previous work, Pb^{2+} was able to both bind to the CMBLs in the C2 domain and drive membrane association.

Cd^{2+} was also able to bind to the CMBLs but was unable to drive membrane binding of isolated C2 domain, consistent with previous work. C1B-C2, in contrast, was able to bind to anionic membranes in the presence of Cd^{2+} due to the induced self-association. The avidity of the interactions of multiple membrane binding domains from the same oligomer associating with the membrane compensates for the weak interaction of Cd^{2+} bound C2 with phosphatidylserine. There is a precedence for this in FYVE domains[153] and Syt I.[154] FYVE domains rely on the avidity of multiple weak interactions with membranes through dimerization to efficiently bind membrane embedded ligands. Isolated C2A and C2B domains from SytI show extremely weak binding to anionic membranes in the presence of Cd^{2+}, but Cd^{2+} is able to drive membrane binding of the intact two-domain region. Thus the ability of Cd^{2+} to drive membrane binding is dependent on both ionic mimicry in the loops and opportunistic binding to other sites on C1B-C2. While it has been shown that Cd^{2+} stimulates activity of PKC, the mechanisms are unclear. This work illustrates the potential for Cd^{2+} to activate PKC through self-association and enhancement of the membrane binding properties of the regulatory region. Furthermore, it has been suggested that conventional

PKCs exist as multimers and oligomerization regulates and enhances activity.[63,155] This work shows that self-association of the regulatory region enhances interactions with membranes, suggesting one possible explanation for increased activity of PKC when present as an oligomer.

Opportunistic metal binding drives self-association of C1B-C2 region

Through analysis of existing structures, studies have shown that Pb^{2+} and Cd^{2+} can bind to protein regions not normally occupied by native metal ions because of more variability in coordination numbers and differences in ligand preferences.[151,156] This study found that, in addition to serving as ionic mimics for Zn^{2+} and Ca^{2+}, both Cd^{2+} and Pb^{2+} mediate self-association of the C1B-C2 regulatory region through opportunistic binding to sites outside of the physiological metal binding sites. Several studies have illustrated the propensity of PKCα to self-associate through the regulatory region in the presence of activators: Ca^{2+}, phorbol esters, or phosphatidylserine.[58,62-64,157] In the experiments in this chapter, significant self-association of C1B-C2 or C1C2c in the presence of Ca^{2+} only was not observed. However, at identical concentrations of Cd^{2+} and Pb^{2+}, both regions were found to self-assemble into higher order oligomers in the absence of other PKC activators. Variants that abolished metal binding to known Ca^{2+}-binding sites had very little effect on Cd-mediated self-association while multiple lines of evidence implicate the linker and C-terminal helix, regions where Ca^{2+} does not bind but contain multiple potential ligands that could coordinate Cd^{2+} and Pb^{2+}. Substituting these residues for residues that are unable to coordinate Cd^{2+} and Pb^{2+} significantly lowered the apparent affinity for self-association, indicating that opportunistic binding of

Pb^{2+} and Cd^{2+} to the linker and C-terminal helix of C2 mediate intermolecular contacts that stabilize the C1B-C2 oligomers. It is worth noting that while the C-terminal helix of C2 was found to be important for self-association, the isolated C2 domain does not self-associate. A study done on SytII found a similar phenomenon.[158] The isolated C2A and C2B domains were not found to self-associate. However, the intact C2A-C2B region was found to form dimers at low Pb^{2+} concentrations and oligomers at higher concentrations of Pb^{2+}. The multimers were thought to be mediated through either an intact linker or the combination of multiple weak interactions that were insufficient to drive self-association of the isolated domains. In C1B-C2 either the C2 domain does not associate with itself or that more than one type of interaction is needed to stabilize the oligomer and the avidity of multiple weak binding sites results in self-association.

CaM has been shown to interact with Pb^{2+} outside of the primary metal binding sites.[159] Pb^{2+} binding opportunistically to secondary sites on CaM resulted in a decreased flexibility of the linker. SAXS data in this study showed a decrease in flexibility of the linker region in response to Pb^{2+} and Cd^{2+}. Along with mutagenesis and NMR this highlights the importance of the linker in mediating self-association and the changes that occur in response to binding in this region. Variants that abolished ligands in the linker and C-terminal helix significantly lowered the apparent affinity of the oligomers, although some self-association was still observed in negative-stain EM images (although to a much lesser extent than wild-type). This indicates that at least one other site is intact and able to mediate self-association. There is evidence in the literature for a third Cd^{2+} binding site on C1B. Electrospray ionization mass spectrometry of a

C1Bη peptide with two native Zn-binding sites, after treatment with Cd^{2+} showed a significant population of peptide coordinated to three Cd^{2+} ions.[121] This was not observed after Zn-treatment. The third ion disappeared after treatment with EDTA, suggesting that the third site has a lower affinity than the two structural sites.[121]

Another potential interaction mode could be through intermolecular coordination of cysteines on C1B. UV-VIS data showed the potential for Pb^{2+} to externally coordinate cysteines on C1B. The propensity for Pb^{2+} to share coordination of cysteines with another metal is illustrated with homo-octomeric ALAD in the presence of Pb^{2+}.[156,160] In addition to Pb^{2+} replacement of Zn^{2+} in the binding pocket, a second Pb^{2+} ion shares coordination with one of the cysteine ligands already coordinated to the first Pb^{2+}. With C1B-C2, metal charge transfer bands appear at sub-saturating concentrations for the low affinity Pb^{2+} site on C2 with micromolar affinity indicating Pb^{2+} coordinates cysteines in C1B before the C2 loops are fully populated and cysteines in C1B can compete with CMBLs for Pb^{2+}. The most likely candidates for coordination are C132, C143, and C151 which have been shown to be the most solvent exposed.[147]

Including the potential of C1Bα to play an active role in self-association, there are five possible types of interactions that can be formed and it is likely that different combinations of these interactions exist in the oligomers. The different modes of interactions are likely favored by the flexibility of the C1B-C2 region that allows it to adopt different conformations.

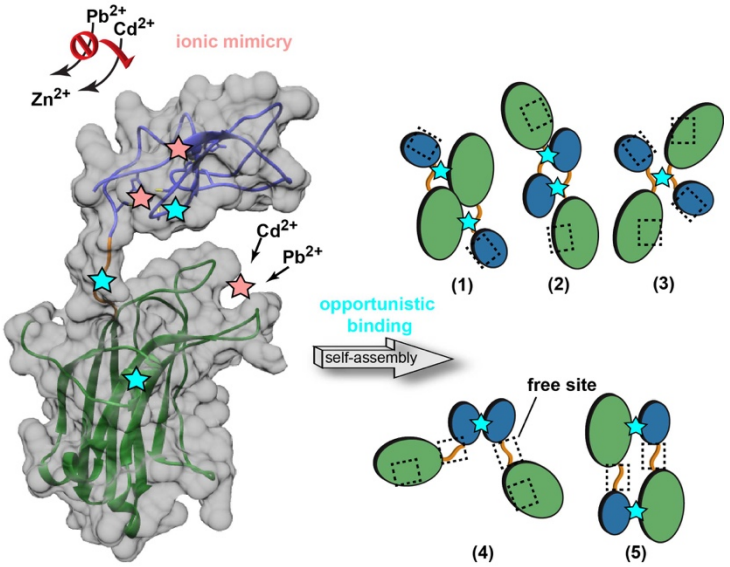

Figure III.18 Model describing the interactions of Pb^{2+} and Cd^{2+} with the C1B-C2 regulatory region. Pink stars indicate sites where native metal ions can be displaced by Pb^{2+} or Cd^{2+}. Cyan stars indicate opportunistic binding sites that promote self-association. Black boxes indicate sites within each possible dimer that are available to interact with Cd^{2+} or Pb^{2+} and facilitate interactions with neighboring dimers and the formation of higher order oligomers.

Based on the data presented in this chapter as well as previous work from the lab,[124,126] a model has been constructed to explain interactions of Pb^{2+} and Cd^{2+} with C1B-C2 regulatory region of PKCα (figure III.18). When Cd^{2+} encounters C1B-C2, it distributes between the loops of C2 and the structural Zn^{2+} sites in C1B, displacing and serving as an ionic mimic of Zn^{2+}. Pb^{2+}, however, populates the high affinity binding site in the loops of C2, and then targets cysteines without displacing Zn^{2+} at metal-to-protein ratios >1. With increasing concentrations, both Pb^{2+} and Cd^{2+} bind opportunistically to sites outside of known metal binding sites including the linker, C-terminal helix of C2, and an anionic patch near the bottom of C1B (cyan stars), mediating self-association and the formation of higher order oligomers. There are five

types of dimers that can be formed through interactions with Pb^{2+} and Cd^{2+} that stabilize the C1B-C2 oligomers: C2 to linker, C1B to linker, linker to linker, C1B to C1B, and C1B to C2. Each mode of interaction within C1B-C2 dimers leaves free sites (black boxes) that, along with additional Cd^{2+} or Pb^{2+} ions, bridge interactions with other dimers and mediate the formation of higher order oligomers.

CHAPTER IV

PARAMAGNETIC AGENTS REVEAL THE CONFORMATIONAL SPACE SAMPLED WITHIN THE C1B-C2 REGULATORY REGION

Background

Dynamic proteins and complexes play a role in all cellular processes and signal transduction cascades. It is essential to understand the dynamics and conformational landscapes of these systems in order to understand their functions. Therefore, an increasing amount of research is being dedicated to extracting protein ensembles from limited data sets [161-163] and even designing drugs to modulate them based on the resulting ensembles. [164-166]

Protein Kinase Cs (PKCs) are flexible isoenzymes that are integral components of cellular signaling processes that occur at the membrane surface.[167] Despite significant efforts aimed at gaining structural information on full-length PKC, this has eluded scientists for decades. This is in part due to its multi-modular structure, amphipathic nature, and inherent flexibility, that, while essential for function, provide significant challenges [97] for structural biologists.

The N-terminal regulatory region of PKCs is trafficked to anionic membranes upon sensing its ligands, which generates the necessary conformational rearrangements needed to pull the pseudosubstrate region from the active site of the kinase domain.

No information is available about the conformational changes that occur within the regulatory region during activation. Only one multi-domain crystal structure exists [61]

and most of the structural information for this region is primarily for the functionally autonomous isolated domains. This chapter details the steps taken towards assembling structural information on the full regulatory region by focusing on a multi-domain construct that comprises the C1B and C2 domains from the conventional isoform, α, representing the minimum machinery needed by PKC to bind both lipid and metal activators. To overcome the challenges presented by the flexibility of this region, paramagnetic lanthanides were used in combination with solution nuclear magnetic resonance (NMR) spectroscopy to obtain structural information that reports on the ensemble of conformations that C1B-C2 samples. Furthermore, a transient intermolecular interaction between C1B and C2 domains of neighboring molecules is identified.

Experimental Procedures

C1B-C2 Purification

The C1B-C2 region from 100-293 of PKCα (*M. musculus*) and isolated C2 domain of PKC*α* from *Rattus norvegicus* (residues 155–293) were cloned as described previously. [50,168] All proteins were expressed in *E. coli* BL21(DE3) cells. 5mL overnight cultures were grown from a fresh transformation of the appropriate plasmid and transferred to 1 L flasks of Luria-Bertani broth (FisherBioreagents) and grown to an OD_{600} of 0.6 and subsequently induced with 0.5 mM Isopropyl β-D-1-thiogalactopyranoside (FisherBioreagents) for 16 hours at 15 °C. For C1B-C2 which contains two structural-Zn^{2+} sites, 10 μM $ZnCl_2$ was added to the growth medium just prior to induction to ensure proper folding of the C1 domain. For the preparation of U-

^{15}N, [U-^{13}C,^{15}N, 55%-^{2}H], and [U-^{13}C,^{15}N] proteins, the re-suspension method of Marley et al [130] was used. The M9 minimal medium contained 1 g/L of ammonium chloride (^{15}N, 99%) (Cambridge Isotopes) and either 3 g/L d-glucose (Macron Chemicals) or 2 g/L d-glucose (^{13}C, 99%) (Cambridge Isotopes) as nitrogen and carbon sources, respectively. Induction of protein expression was conducted as described for the natural-abundance preparation. After induction cells were harvested by centrifugation at 4,000 g for 30 min at 4 °C and stored at −20 °C.

All C2 and C1B-C2 purification steps were carried out using an ÄKTA FPLC system (GE Healthcare Life Sciences). For C1B-C2, cells were lysed using B-PER™ Lysis reagent (Thermo-Scientific). The lysate was clarified by spinning down at 13,000 RPM for 30 minutes and passed over a HisTrap HP Ni affinity column (GE Healthcare Life Sciences) and eluted with a linear gradient of 1 M imidazole (ACROS Organics). C1B-C2 was cleaved from its SUMO fusion partner using SUMO protease for 1 hr. SDS-PAGE gel was used to assess the completion of the reaction. The cleavage solution was then passed back over the Ni affinity column. Tag-free C1B-C2 eluted in the flow through fractions while histidine-tagged SUMO and SUMO protease bound to the column. As a final polishing step, a cation exchange column (SOURCE 15S) was run in the presence of 0.1 mM $CaCl_2$. Purified C1B-C2 was then transferred to a 10 kDa VivaSpin 15R spin concentrator (Sartorius) for decalcification with three washes of 10 μM ethylene glycol-bis(β-aminoethyl ether)-N,N,N',N'-tetraacetic acid (EGTA) and buffer exchange into the final buffer. The isolated C2 domain was expressed and purified as previously described. [50]

Buffers/Metal ion solutions

All buffers were prepared using HPLC grade water (Macron) and trace amounts of metal ions were removed using Chelex® 100 resin (Sigma). For all C1B-C2 experiments the protein was exchanged into "MES buffer" containing 10 mM MES pH 6.0, 150 mM KCl, 1 mM Tris(2-carboxyethyl)phosphine hydrochloride (TCEP). For NMR experiments 8% D2O (Cambridge Isotopes) and 0.02% NaN_3 were added to the buffers. For SAXS experiments 2% glycerol was added to prevent radiation damage. Ln^{2+} stocks were prepared by dissolving Dysprosium (III) Chloride, Thullium (III) Chloride, Terbium (III) Chloride, and Lanthanum (III) Chloride (Sigma) in HPLC grade water.

Small-angle X-ray scattering (SAXS)

SAXS experiments were conducted on the SIBYLS [135] beamline at the Advanced Light Source synchrotron at the Lawrence Berkeley National Laboratory. Samples of 200-300 μM C1B-C2 were dialyzed against "MES buffer" for 48 hours in the presence or absence of 2 mM $CaCl_2$. Data was collected for a range of concentrations (1, 2.5, and 4.5 mg/mL) of C1B-C2 in a 96-well plate (Axygen). SAXS data were collected continuously with q ranging from 0.013 to 0.328 with exposures of 0.5, 1, 2, and 5 s. Buffer blanks taken before and after each sample exposure were subtracted from the sample signal for each concentration. Data sets free of signs of aggregation/radiation damage were merged using the median method in ScÅtter. For both apo and Ca^{2+}-bound

SAXS data this corresponded to 7 data sets. SAXS curves collected for both Ca^{2+}-bound C1B-C2 and apo C1B-C2 were almost super-imposable, indicating that there are no major metal-dependent conformational changes. Going forward the data for Ca^{2+}-bound C1B-C2 was used in the calculations to represent the metal bound state since lanthanides were used to extract PCS. SAXS data were re-binned to match the scattering angles calculated by RANCH for individual conformations using a set of scripts provided by Dr. Enrico Ravera.

UV-vis spectroscopy

UV-vis spectra were collected on a Beckman DU 640 spectrophotometer. 25 μM protein (C1B-C2, C2, or C1B) solution or "MES buffer" (for metal ion-only reference experiments) were placed in the sample cuvette; the reference cuvette contained metal ion-free MES buffer. Pb^{2+} was added stepwise from the corresponding stock solutions prepared in HPLC water to the sample and reference cuvettes. The samples were incubated for 5 minutes prior to the start of the measurements. The post-acquisition processing included the subtraction of the spectra of free Pb^{2+} from the spectra of protein-containing samples. The difference spectra were obtained by subtracting the spectrum of the apo protein from the spectra of the metal ion containing protein. All spectra were except for apo spectra that was not diluted were corrected for dilution prior to subtraction.

NMR spectroscopy

NMR experiments were carried out at 25 °C on a Bruker Avance III system equipped with a cryo-probe operating at ^{1}H Larmor frequency of 800 MHz (18.8 Tesla).

Temperature was calibrated using deuterated methanol (methanol- d4).[169] Sequence-specific assignments of the ^{1}H, $^{13}C\alpha$, $^{13}C\beta$, and ^{15}N resonances for the apo and Ca^{2+}-bound C1B-C2 were obtained using ^{2}H-decoupled three-dimensional HN(CA)CB, HNCA(CB), HN(COCA)CB, and HN(CO)CA experiments on a [U-^{13}C,^{15}N; 55%-^{2}H] C1B-C2 sample. [133] Assignments experiments were carried out in the presence of "MES buffer" with 50 mM KCl and transferred to 0, 100, and 150 mM KCl conditions.

For ^{1}H-^{15}N relaxation measurements, C1B-C2 was concentrated to 0.3 mM in "MES buffer" for NMR. Relaxation parameter sets were measured for all spectrally resolved ^{15}N-^{1}H backbone residues for C1B-C2 in the apo and Ca^{2+}-bound states containing 6 mM Ca^{2+} comprising the longitudinal relaxation rate constant (R_1), transverse relaxation rate constant (R_2-CPMG), and ^{1}H-^{15}N nuclear Overhauser enhancement (NOE).[170,171] The data were acquired in an interleaved manner. Delays used for R_1 were: 0.080 s, 0.23 s, 0.42 s, 0.65 s, 0.91 s, 1.19 s, and 1.5 s. Duplicates were collected for the 0.08 s, 1.5 s, and 0.65 s time points. Delays used for R_2 were: 0.006 s, 0.016 s, 0.028 s, 0.044 s, 0.08 s, and 0.100 with duplicates collected for the 0.006 s, 0.044 s, and 0.1 s time points. For ^{1}H-^{15}N NOE experiments, a recycle delay of 10 s was used for the reference experiment and the saturation period was 4 s. It has been shown that cross-correlated relaxation between ^{15}N chemical shift anisotropy and ^{15}N-^{1}H dipolar coupling becomes significant at high magnetic fields, leading to an incorrect steady state. [172,173] This was corrected for by using repetions of [τ/2-β-τ/2], where β is a hard 180º ^{1}H pulse and τ is set to 22 ms, during the saturation period as described in ref

[171]. Additionally, a water flip-back element was added to the reference experiment to suppress water.

Rotational correlation times were estimated for C1B and C2 as part of the C1B-C2 construct using ROTDIF [174] assuming an axially symmetric model. R1/R2/NOE values for all spectrally resolved residues were used, omitting residues with NOE values < 0.65 and exchange broadened residues [175], and the coordinates from the C1B-C2 crystal structure. Values were entered separately for the folded core of C1B and C2 to obtain rotational correlation times for each domain.

HYDRONMR [176] was used to predict the rotational correlation time of the C1B-C2 crystal structure using 0.0091 poise for the viscosity of water at 25 °C and 3.3 Å for the effective radius of the atomic elements. The value for the effective radius was chosen based on values used for similar sized multi-domain proteins. [177,178]

PCS Restraints

Lanthanide-induced pseudocontact shifts (PCSs) were used to determine the conformational preferences of C1B-C2 in solution. For fully paramagnetic samples, either 0.25 mM U-^{13}C,^{15}N C1B-C2 or U-^{15}N C1B-C2 was mixed with equimolar amounts of $LnCl_3$ (Ln = La, Tb, Tm, Dy) dissolved in HPLC water to generate a single Ln^{3+} bound to the C2 domain. PCS were measured using ^{15}N-HSQC at 298K at 800MHz for C1B-C2 bound to each paramagnetic Ln^{3+} (Tm^{3+}, Tb^{3+} and Dy^{3+}) in reference to diamagnetic La^{3+}. Assignment of C2 residues was carried out as described previously. [59] Assignment of C1B residues in C1B-C2 was done by comparison with the diamagnetic spectra. Mixed experiments were conducted with 0.125 mM U-^{15}N C1B-C2 D246N

mutant mixed with 0.125 mM of a 1:1 complex of natural abundance C1B-C2 wild-type protein bound to the appropriate Ln^{3+}.

PCSs from the isolated C2 domain were used to determine the axial and rhombic components of the magnetic susceptibility tensor anisotropies, metal position, and Euler angles for each metal (Table IV-1) using FANTEN [179] and the coordinates for the C2 domain were taken from the C1B-C2 crystal structure. PCS for Tm^{3+} and Tb^{3+} were collected previously. [59] PCS for isolated C2 with Dy^{3+} were collected as described above for C1B-C2. The correlation between the experimental and back calculated PCS is shown in figure IV.1.

Table IV-1. Magnetic Susceptibility Tensor parameters determined for C2.

Ln^{3+}	Ln^{3+} coord (x)	Ln^{3+} coord (y)	Ln^{3+} coord (z)	$\Delta\chi$axial ($12\pi \cdot 10^{-6} \cdot$ Å^3)	$\Delta\chi$rhombic ($12\pi \cdot 10^{-6} \cdot$ Å^3)	α (°)	β (°)	γ (°)
Tb^{3+}	-7.8	16.8	18.4	12572.62	-2206.43	-71.9	-80.3	-76.9
Dy^{3+}	-7.8	16.8	18.4	16355.03	-2793.516	-108.5	-76.9	-77.3
Tm^{3+}	-7.8	16.8	18.4	-7192.59	2569.155	-109.4	-103.2	100.8

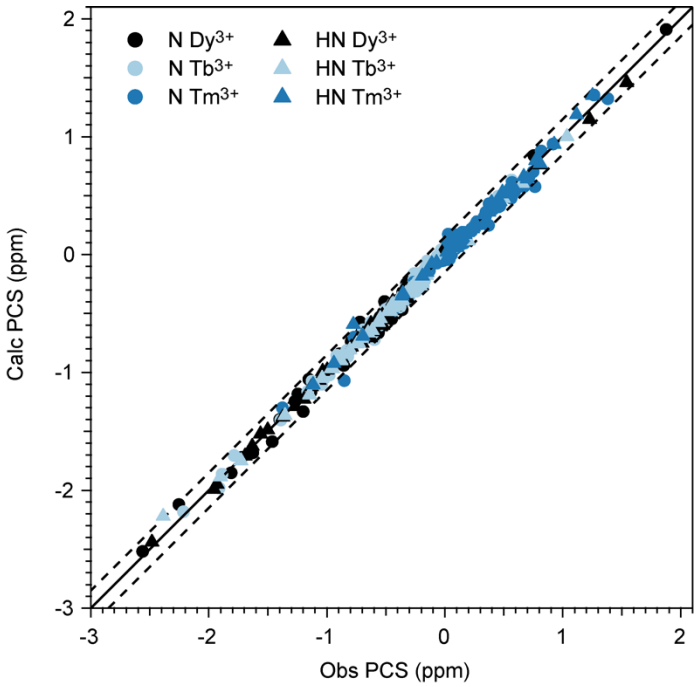

Figure IV.1 Agreement of PCS for tensor determination. Comparison between observed and back-calculated PCS from FANTEN tensor fitting.

Determining Intra-PCS

A transient intermolecular interaction that gives rise to PCS on C1B was detected for C1B-C2. To disentangle the contributions from intra- and intermolecular PCS, a pair of NMR experiments were conducted for each Ln^{3+} (Figure IV.2).

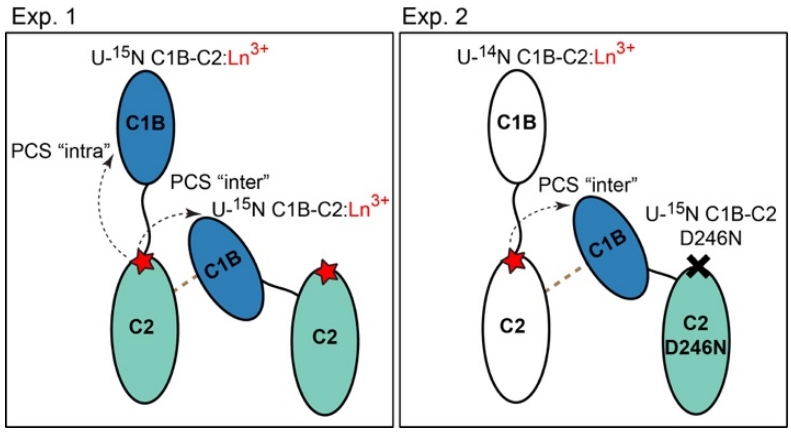

Figure IV.2 NMR experimental set up designed to separate intra- and inter-PCS.

Sample 1 contained 250 μM of U-^{15}N enriched C1B-C2 with a single lanthanide ion bound in the loops of C2 (prepared as described above). The PCS observed on C1B in ^{15}N-HSQC have two contributions: intramolecular PCS from its own C2 domain and intermolecular PCS from the interaction between neighboring C1B-C2 molecules. The equation for the observed residue specific PCSs is therefore:

Equation 13

$$PCS_{obs,1} = PCS_{intra} + f_D\, PCS_{inter}$$

where f_D is the fractional population of the C1B-C2 dimer.

Sample 2 contained 250 μM of equimolar amounts of natural abundance, "NMR-invisible" C1B-C2 bound to a lanthanide ion and U-^{15}N enriched C1B-C2 D246N mutant. This mutant disrupts a key metal binding residue in the loops of C2 and has been shown to abolish metal binding. Therefore, the observed PCS only has one contribution from the intermolecular interaction between C1B-C2 molecules. The equation for the residue specific observed PCSs is:

Equation 14

$$PCS_{obs,2} = 0.333\, f_D\, PCS_{inter}$$

There are three potential types of dimers in the mixed sample, only one of which gives rise to PCS. Therefore, the 0.333 scaling factor comes from the fraction of the productive dimer. Combining the above equations yields the equation for the intramolecular PCS:

Equation 15

$$PCS_{intra} = PCS_{obs,1} - \frac{PCS_{obs,2}}{0.333}$$

The above set of experiments were conducted with Dy^{3+}, Tm^{3+}, Tb^{3+}, and La^{3+} and used to extract intramolecular PCS. These PCS were then used for MaxOcc analysis.

Measurement of intermolecular ^1H PRE rates

3-(2-Iodoacetamido)-PROXYL was purchased from Sigma Aldrich. Cysteines were substituted for lysines on C1B-C2 at positions 181/268 and 181 for C2α using a QuikChange® Site-Directed Mutagenesis kit (Stratagene). All cysteine variants were prepared without isotope labeling. The cysteines were covalently modified with 3-(2-Iodoacetamido)-PROXYL under the following conditions: 75 μM protein, 6 x molar excess of PROXYL, and 20 mM TrisHCl buffer at pH 8.0 with 150mM KCl. The reaction was allowed to proceed for 18 hours, in the dark under nitrogen. Reducing reagent was removed just prior to modification with two rounds of desalting using PD-10 desalting columns (GE). The completeness of the reaction was assessed using mass-spectrometry. Excess of the labeling reagent was removed using VivaSpin® 2 centrifugal concentrators (Viva Products) with a molecular weight cutoff of 5 kDa for

C2a and 10 kDa for C1B-C2. The modified proteins were exchanged into NMR buffer and used for the preparation of the paramagnetic and diamagnetic NMR samples. The "paramagnetic" samples were generated by mixing equimolar amount of PROXYL-tagged natural abundance K181C/K268C C1B-C2 and [U-^{15}N] enriched wild-type protein. A diamagnetic variant of PROXYL was not commercially available so therefore the unmodified protein was used as a diamagnetic reference in the case of C1B-C2. The total protein concentration was 0.3 mM in the C1B-C2 samples.

The ^{1}H paramagnetic relaxation enhancement (PRE) rates Γ_2 are defined as the difference in the ^{1}H transverse relaxation rate constants obtained for the diamagnetic and paramagnetic samples, $R_{2,dia}$ and $R_{2,para}$:

Equation 16

$$\Gamma_2 = R_{2,para} - R_{2,dia}$$

The measurements of the ^{1}H R_2 values were conducted on an 18.8 Tesla NMR instrument using the two-point acquisition scheme.[180] The uncertainties in Γ_2 values were estimated from the root-mean-square noise of the spectral planes, as described in ref [180].

Maximum Occurrence Calculations

Maximum occurrence (MO) calculations were employed to characterize the conformational space sampled by C1B-C2 using the MaxOcc software [181] kindly provided by Drs. Enrico Ravera and Witold Andralojc. Calculations were conducted on the Ada and Terra clusters of the Texas A&M High Performance Research Computing facility. For these calculations, a large pool of conformations is needed to represent the

conformational space that C1B-C2 can sample. 50,000 random conformations of C1B-C2 as well as their scattering profiles were generated using RANCH 2.1 (from the Ensemble Optimization Method software suit developed by the European Molecular Biology Laboratory) [163] taking the starting coordinates from the C1B-C2 crystal structure. The coordinates of C2 were held fixed and the coordinates of C1B were randomized by varying the dihedral angles of the linker residues (M153-K159) using angles typically found in intrinsically disordered proteins. Pseudocontact shifts were then calculated for each of the 50,000 conformations using the program CALCALL (also provided by Drs. Enrico Ravera and Witold Andralojc [182]) and the tensor parameters determined from isolated C2. The MO values are determined individually for randomly selected conformations and represent the maximum population that each conformation can have in solution as part of an ensemble and still be compatible with experimental observables. Conformations with high MO values are therefore more likely to be sampled. The MO values were calculated for 600 randomly selected structures, using the experimental SAXS data and PCS as restraints (weighted 0.05 and 1 respectively). To determine the MO value, MaxOcc increases the weight of the selected conformation (and therefore its calculated PCS and SAXS) in combination with all other conformations in the pool until there is no longer agreement with the experimental observables. The top scoring structures with MO values above 0.4 as well as the bottom structures with MO values less than 0.1 were chosen for further analysis. This resulted in 49 and 38 structures, respectively.

Results

C1B-C2 crystallizes in a compact conformation

The crystal structure for C1B-C2 was previously determined by Dr. Krystal Morales in collaboration with Drs. Anup Aggarwal, Joseph Mire, and James Sacchettini (Figure IV.3). While crystallization of both the apo and Ca^{2+}-bound states were attempted, only the Pb^{2+}-bound form of C1B-C2 would crystallize. In the conformation that crystallized, there is an interaction between C1B and C2 mediated by a fourth Pb^{2+} ion that coordinates D254 in C2 and two cysteines, C118 and C143, that also coordinate a structural Zn^{2+} ion in the C1B domain. A citrate molecule completes the coordination sphere of the fourth Pb^{2+} ion. This interaction sequesters an area of 565 $Å^2$ and forces C1B-C2 to adopt a compact conformation. Electron density is completely missing for residues 154-156 and most of the side chain electron density is missing for 157-158, which suggests that despite the fixed orientation of C1B-C2 mediated by Pb^{2+}, the linker region is flexible. Compared to the isolated domains (C1B NMR structure, 2ELI and C2 Pb^{2+}-bound X-ray structure, 3TWY) the pairwise root-mean-square deviations for backbone atoms were 0.848 Å and 0.466 Å for C1B and C2 respectfully. This indicates that connecting the two domains using their native linker does not significantly perturb their backbone conformations. The conformation that crystallized is not compatible with the simultaneous membrane binding of C1B and C2. As a result of Pb^{2+} serving as a cross linker, the C1B and C2 membrane binding loops point in different directions and a portion of CMBL1 is sequestered. This mode of crosslinking comes from the unique properties of Pb^{2+}. As an intermediate Lewis acid, it can coordinate both oxygen and

sulfur ligands. PKCs native ligand, Ca^{2+}, is a hard Lewis acid that prefers all oxygen coordination spheres and could not coordinate both C1B and C2 in this manner. Therefore, while this structure provides information about domain structure of C1B-C2, it is unlikely that this is a major conformation in solution in the absence of Pb^{2+}. It was clear that crystallography is not a viable approach to structurally characterizing this region. Therefore, going forward, a solution NMR approach was pursued.

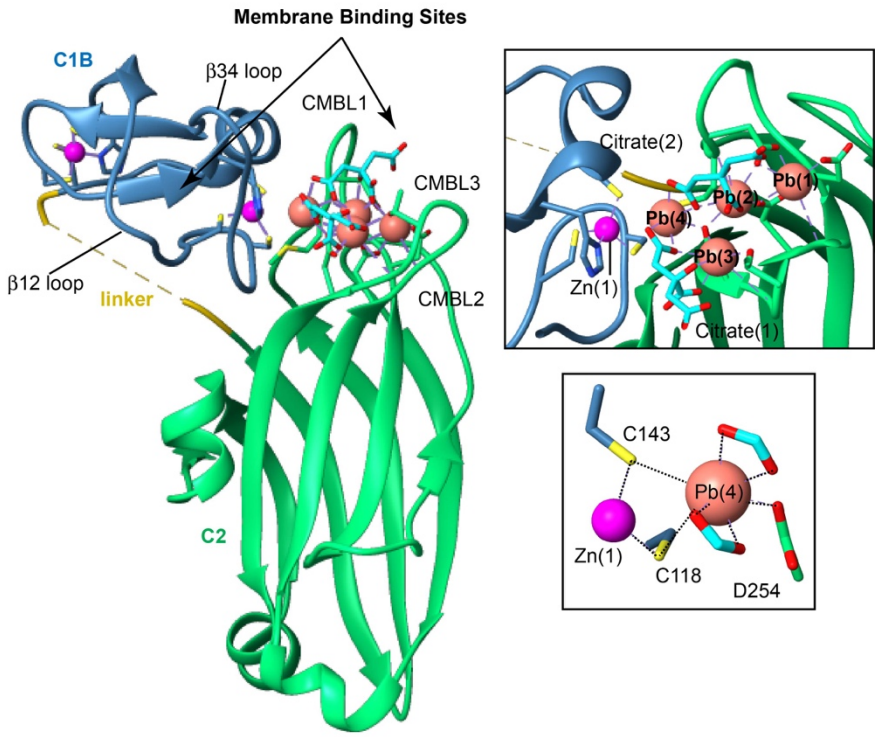

Figure IV.3 C1B-C2 crystallizes in a compact conformation. Crystal structure of C1B-C2 showing the domain structure of C1B and C2 along with the details of Pb-coordination and crosslinking between C1 and C2.

C1B-C2 is partially flexible in solution

As a first step to probing the behavior of C1B-C2 in solution, the rotational diffusion properties of C1B-C2 were evaluated. R_1, R_2, and $\{^1H\}$-^{15}N nOe relaxation parameters were collected for the C1B-C2 backbone N-H groups in two metal-ligated states: apo and Ca^{2+}-bound (Figure IV.4). The objective of these experiments was two-fold: to characterize the C1B-C2 backbone sub-nanosecond motions and to determine if these motions are altered by Ca^{2+} binding. Residues with a poor signal-to-noise ratio and poor resolution were omitted from the analysis. This resulted in 134 backbone amide groups that were suitable for analysis of apo C1B-C2 and 135 residues that were suitable for analysis of Ca^{2+}-bound C1B-C2. Detailed inspection of the relaxation data indicated that the crystallized compact conformation of C1B-C2 is likely not a major conformation in solution. The average R_1 values of each of the three regions (C1B, linker, and C2) were different, which indicates that each region has a different mobility on the sub-nanosecond timescale. Interestingly, there were also no differences in the average R_1 values of each region upon the addition of Ca^{2+} consistent with no change in the picosecond to nanosecond motions of the C1B-C2 region upon Ca^{2+}-binding. The median R_2 values, which are additionally sensitive to the overall molecular tumbling rate, were lower for C1B than C2 in both metal-bound states (Table IV-2), which indicates that the motions of the domains are at least partially uncoupled from one another. This is echoed by the rotational correlation times that were estimated from the R_1, R_2, and NOE values (Table IV-3). In the context of the two domain region, C1B and C2 have different correlation times compared to their isolated counterparts.

Furthermore, C1B's rotational correlation time is lower than that predicted from the crystal structure using HYDRONMR. This is consistent with an intermediate case of the domains neither tumbling completely dependent nor completely independent of one another. There was a uniform elevation in the R_2 rates (Figure IV.4) of the Ca^{2+}-bound C1B-C2 compared to the apo. Again, this was reflected in a uniform increase of the rotational correlation times for C1B and C2 in the Ca^{2+}-bound state. The most likely explanation for this is an increase in the apparent size due to either a small amount of aggregation in the presence of Ca^{2+} or transient self-association between neighboring C1B-C2 molecules. Self-association has been observed previously in the isolated C2 domain in the presence of Ca^{2+}. [183] It is possible that C1B-C2 self-associates in the same manner upon addition of Ca^{2+}. Another explanation is that there is a transient interaction between neighboring C1B and C2 domains that mimics the proposed interaction between C1A and C2.

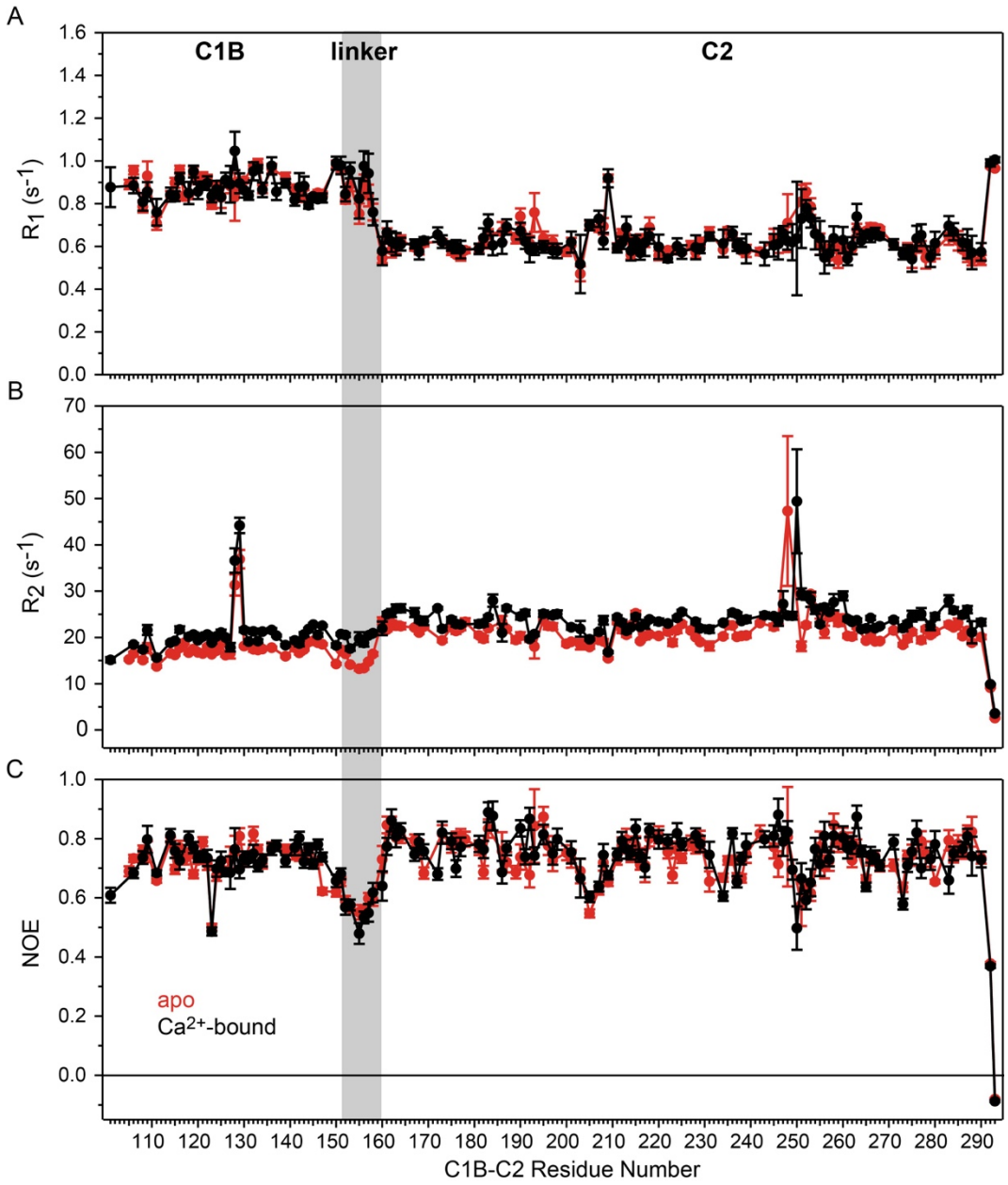

Figure IV.4 C1B-C2 is partially flexible. (A-C) ^{15}N C1B-C2 relaxation data comprising R_1, R_2, and NOE at 800 MHz.

Several signatures indicate that the linker region between the C1B and C2 domains is at least partially flexible. The median R_2 values of the linker region are lower in the apo form relative to C1B and C2, and the R_1 values are elevated for the

linker region in both the apo and Ca^{2+} bound forms (Figure IV.4). The NOE values of the linker region in both the apo and Ca^{2+}-bound C1B-C2 are lower than the folded domains' NOE values, indicating greater flexibility in this region.

The detailed inspection of the properties of the individual residues revealed that the dynamic "QG" motif (Q128 and G129) in the C1B domain has elevated R_2 values consistent with conformational exchange on the microsecond to millisecond times scales, which was observed with previous studies. [103] Therefore, the dynamics of the isolated C1B domain are preserved in the context of the two-domain construct. In addition, elevated R_2 values are observed for CMBL3 residues, D248 in the apo state, and T250 in the Ca^{2+}-bound state. The NOE values are also lower for this region (246-253) in both the apo and Ca^{2+}-bound states, which is again consistent with the behavior observed of the isolated C2 domain. [183]

Collectively, these data show that each domain retains its properties in the context of its neighbor and behaves as a flexible protein in solution, mediated by its dynamic inter-domain linker. However, two things suggest that the domains are not tumbling randomly and independently of one another. First, the NOE values for the linker region are higher than one would expect for a completely flexible or disordered region which would typically have very low or even negative NOE values. Additionally, both domains have elevated rotational correlation times relative to their isolated counterparts. Therefore, it is likely that the linker region is not completely unrestricted and that C1B-C2 may adopt preferred orientations in solution. To investigate this, an approach was developed with paramagnetic lanthanides to characterize the

conformational space sampled by C1B-C2. The ultimate goal is to assess the position of the membrane binding loops prior to membrane insertion.

Table IV-2. Median R_1, R_2, and NOE values for C1B-C2 in the different metal-ligated states.

	R_1 (s^{-1})	R_2 (s^{-1})	NOE
Apo			
C1B	0.89	17.4	0.73
C2	0.61	21.3	0.74
linker	0.83	14.5	0.58
Ca^{2+}			
C1B	0.87	20.3	0.73
C2	0.61	23.9	0.76
linker	0.89	20.1	0.56

Table IV-3. Rotational correlation times predicted from ROTDIF 3.1 (C1B-C2) and from ref [103] and [183] for isolated C1B and C2 respectively. *Predicted values from HYDRONMR and the crystal structure.

	Apo (ns)	Ca^{2+}-bound (ns)	Predicted* (ns)	Isolated apo (ns)	Isolated Ca^{2+}(ns)
C1B	10.5±0.03	11.5±0.1	13.6	3.28	-
C2	13.7±0.2	14.9±0.1	13.6	9.0±0.1	9.3±0.1

Conformationally averaged restraints

The high magnetic moment of unpaired electrons results in profound effects in an NMR spectra. All paramagnetic substances give rise to paramagnetic relaxation enhancement (PRE) that results in broadening of the observed resonances in proximity

to the paramagnetic center. In paramagnetic substances with anisotropic magnetic susceptibility tensors, meaning the magnitude of the magnetic susceptibility changes with direction, there are two additional effects: pseudocontact shifts (PCSs) and residual dipolar couplings (RDCs). PCS depend on the distance and orientation of the nuclei being observed with respect to the paramagnetic center. RDCs are distance independent and depend on the orientation of the bond vector of the J-coupled nuclei with respect to the metal center. The distance and orientation dependence of these effects can be exploited to gain structural information. In the case of flexible, multidomain proteins, these restraints are conformationally averaged, with largely populated conformations making a larger contribution to the measured restraint. Here the Maximum Occurrence method is used with PCS and small angle X-ray scattering (SAXS) as restraints to determine the maximum weight that sterically allowed conformations in solution can be and still be compatible with the experimental restraints. This gives information on which conformations are the most likely to be sampled by C1B-C2 in solution as well as on which areas are less populated.

Paramagnetic lanthanide ions are useful for gaining structural information for biological macromolecules due to their varied paramagnetic properties. A single lanthanide ion can be bound in the loops of the C2 domain [59] and from this 162 intramolecular PCS were collected on the C1B domain from three different paramagnetic lanthanide ions bound to the C2 domain: Tm^{3+}, Tb^{3+}, and Dy^{3+} (Figure IV.5). All three metal ions have anisotropic magnetic susceptibility tensors. La^{3+} was used as a diamagnetic reference.

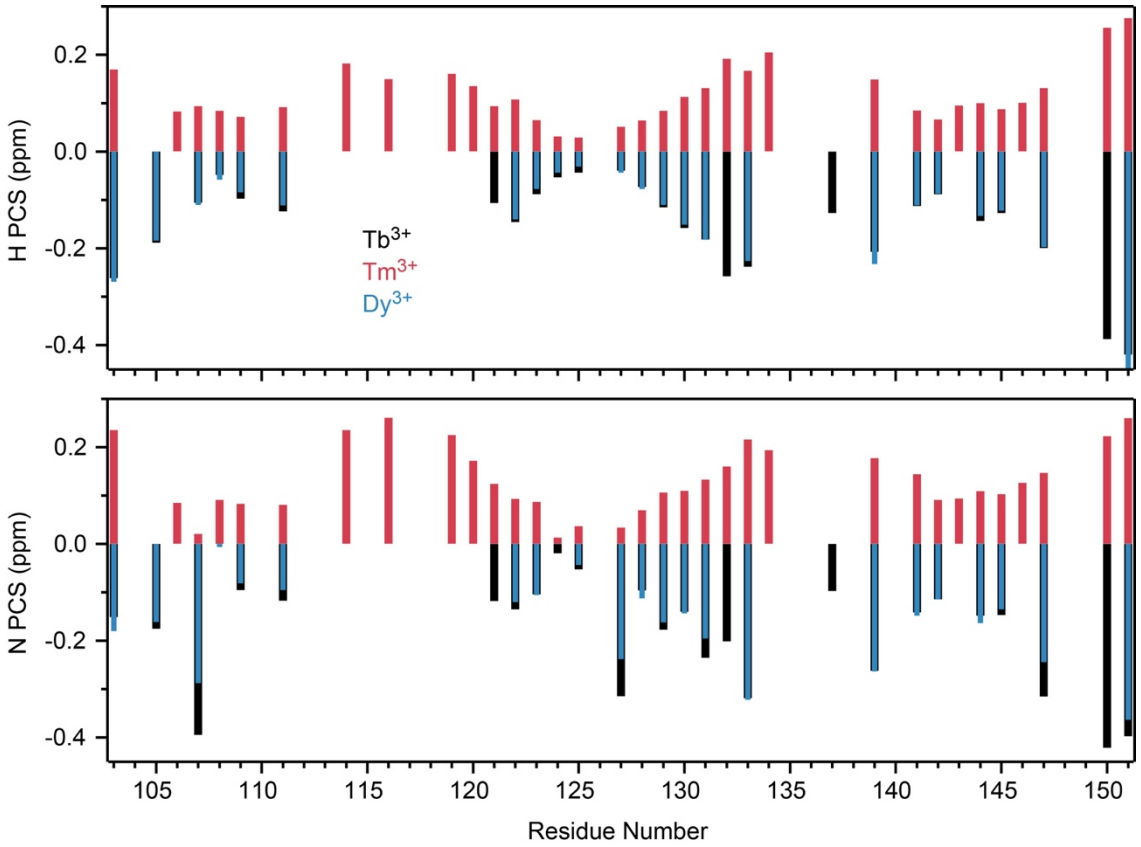

Figure IV.5 Intramolecular PCS for C1B-C2 bound to Ln^{3+} at 800 MHz.

In order to gain structural information from PCS, the coordinates of the metal center, the magnitudes of the axial and rhombic components of the magnetic susceptibility tensors, and the Euler angles relating the tensor to the molecular frame of the protein must be determined. These parameters were determined from the PCS on the isolated C2 domain. [59] Due to a transient self-association detected between neighboring molecules, the C1B intramolecular PCS had to be extracted according to the protocol outlined in the methods section above. The calculated PCS from the best fit ensemble are in good agreement with the experimental PCS

. The Maximum Occurrence value (MO value) was calculated for each randomly selected conformation using a target function set such that the q-factor at the given weight of any conformer taken with the rest of the possible conformations could not exceed 20% greater than the q-factor of the best fit ensemble. In addition to PCS, SAXS data were collected for both Ca^{2+}-bound C1B-C2 and apo C1B-C2 (Figure IV.6).

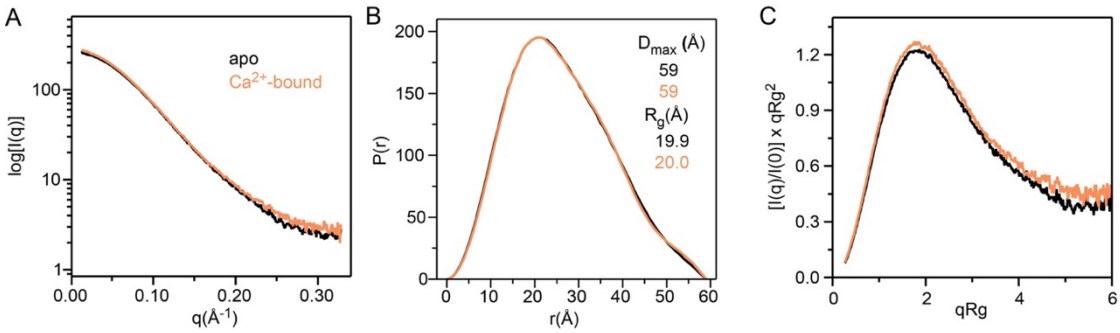

Figure IV.6 SAXS data for C1B-C2 in the apo and Ca^{2+}- bound forms. Lack of changes are observed in comparisons of the raw scattering curves (A), P(r) (B), and the dimensionless Kratky plot (C).

The SAXS data were consistent with the NMR dynamics data. The SAXS curves for both metal bound states were almost super-imposable, which indicates that there are no major Ca^{2+}-dependent conformational changes (Figure IV.6). Furthermore, the dimensionless Kratky plot displayed the characteristics of a flexible, multidomain protein: a plateau-like region at larger qRg values and lack of a maximum of 1.1 at qRg = √3. Since there were no metal dependent changes in the scattering data, the Ca^{2+}-bound C1B-C2 data was used. The agreement between the experimental and calculated

scattering intensity and PCS are good for the best fit ensemble (Figure IV.7B). Overall, the data were sufficient to determine the conformational preferences of C1B-C2.

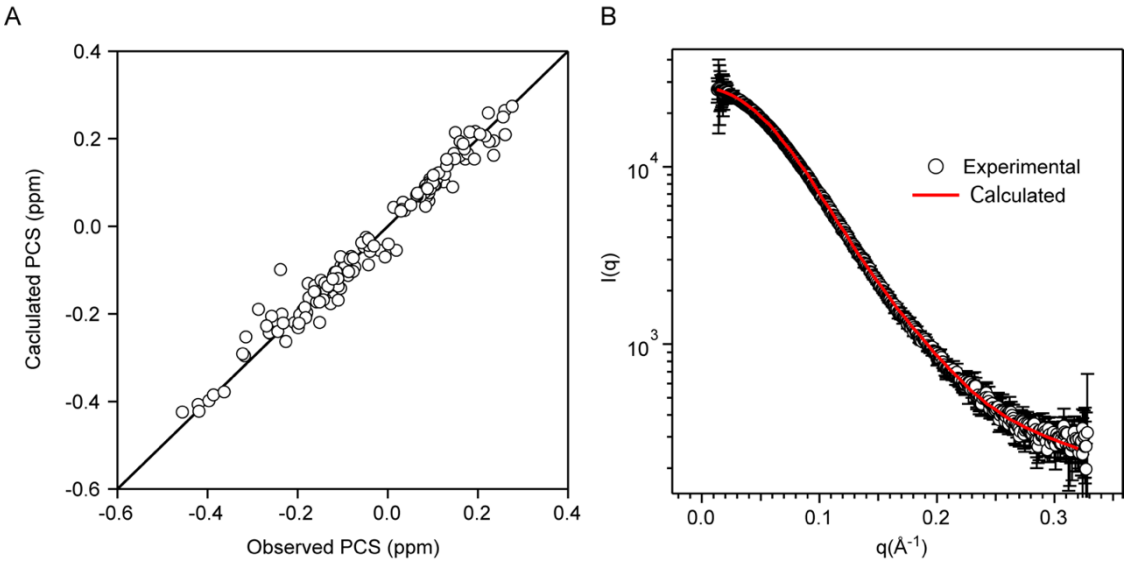

Figure IV.7 Comparison of the experimental PCS and SAXS curves with the averaged data from the best fit ensemble chosen by MaxOcc. (A) Comparison of experimental and calculated PCS. (C) Comparison of the full experimental SAXS data with calculated SAXS data.

C1B-C2 samples primarily open conformations

The MO values were determined for 600 structures that were randomly selected from a pool of 50,000 conformations, representing the allowed conformational space of C1B-C2. The distribution of MO values ranged from 0.03 to 0.68, and only 8% of the total structures had MO values greater than 0.4 (Figure IV.8A). 6% of the structures had MO values below 0.1, which indicated that a portion of the theoretically allowed conformational space cannot be appreciably populated and still be consistent with the data. The conformation of C1B-C2 in solution isn't random and the experimental

restraints are sufficient to distinguish between the areas that C1B-C2 can and cannot sample.

To characterize the structures that were the most consistent with the experimental data and therefore the most representative of the conformations sampled by C1B-C2, a set of angles, θ and ϕ, were defined to determine the relative position of the C1B loops to the C2 loops (Figure IV.8B). The parameter, R, was defined as the distance between the Cα atom of L125 and T251 on the loop tips of C1B and C2, respectively (Figure IV.8B). θ was defined as the angle between R and the Z-axis of the C2 inertia tensor and ranges from 0° to 180° (Figure IV.8B). ϕ is defined as the angle between R and the X-axis of the C2 inertia tensor and ranges from -180° to 180°.

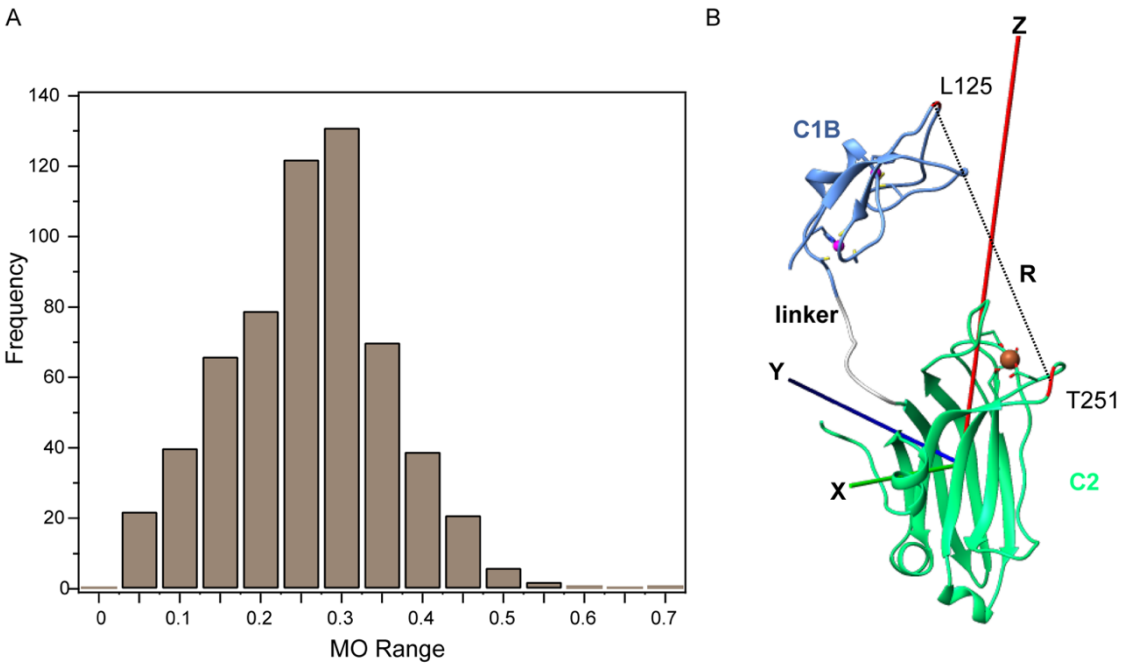

Figure IV.8 Conformational analysis of C1B-C2. (A) Distribution of MO values for 600 structures from MaxOcc analysis. (B) Random C1B-C2 conformation from the

MaxOcc analysis with the parameters used to characterize the conformational space sampled by C1B-C2.

The distributions of R, θ, and ϕ for the top-scoring structures with MO values above 0.4 as well as the bottom structures with MO values less than 0.1 (Figure IV.9) were evaluated. The top-scoring structures are on average more extended than the low-scoring structures, with smaller R values correlating with lower MO scores (Figure IV.9A). The distance between the tips of the C1B and C2 loops varies from 39 to 67 Å for the top structures. For the low-scoring structures, the distances are between 16 and 41 Å, which indicates that these structures are more compact. The ranges of both θ and ϕ are also slightly more narrow for the top-scoring structures versus the low-scoring structures (Figure IV.9B,C). The conformations with high MO values have θ values that range from 38 to 136° whereas the low-scoring conformations range from 16 to 134°. The range of ϕ values is even narrower for the top-scoring conformations (Figure IV.9C). Collectively, this indicates that the motion of C1B relative to C2 is somewhat restricted and that all conformations cannot be sampled equally. This is consistent with C1B-C2 relaxation data that show that the linker region isn't fully flexible.

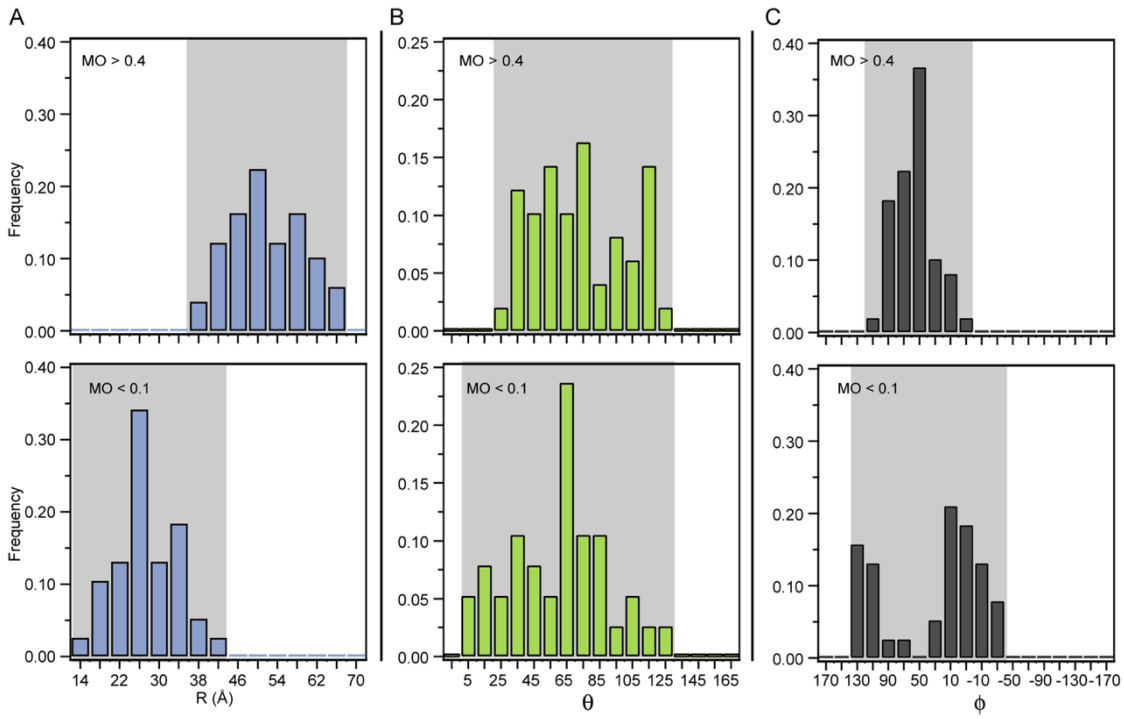

Figure IV.9 C1B-C2 samples a narrow region of the allowed conformation space. Distributions of R (A), θ (B), and ϕ (C) for the top and bottom conformations from the MaxOcc analysis.

C1B-C2 samples "open" conformations, poised for membrane insertion

The top and bottom structures from the MaxOcc analysis were inspected and overall, the low-scoring structures were more compact than top-scoring structures. There were 6 structures with MO values above 0.5 (Figure IV.10).

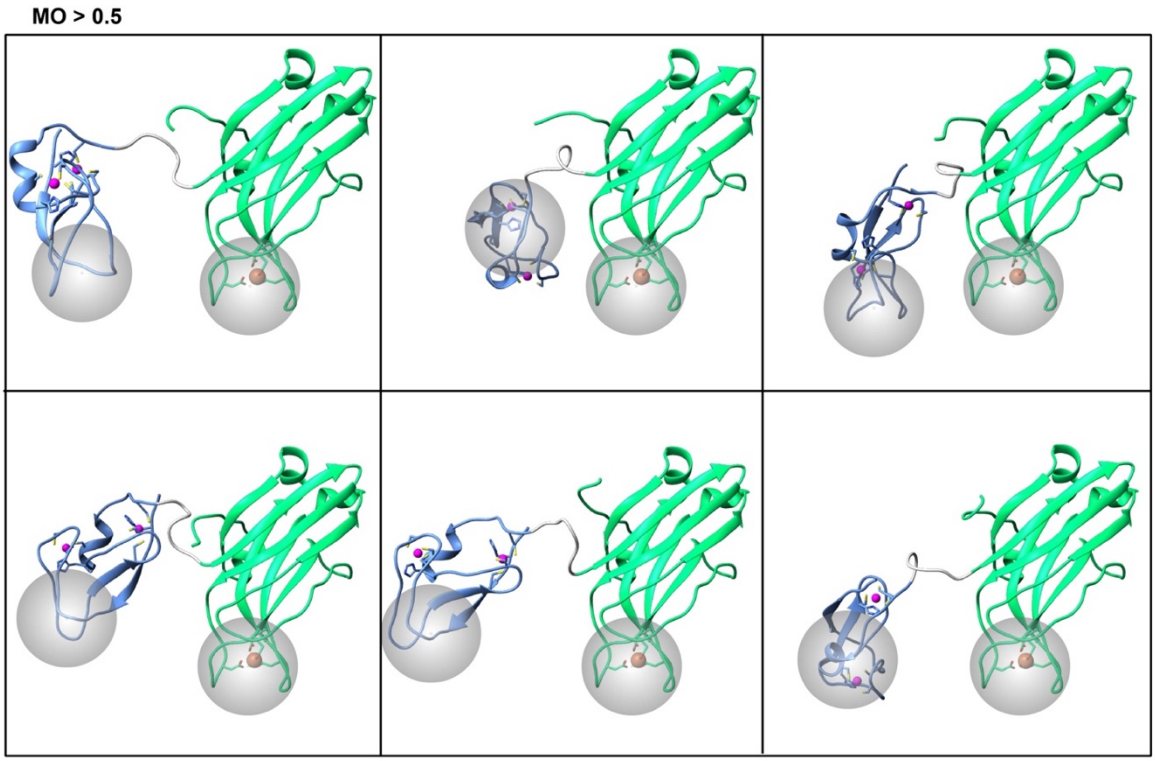

Figure IV.10 C1B-C2 samples mostly "open" conformations. Top-scoring conformers from C1B-C2 MaxOcc analysis. The membrane-binding loops are indicated with grey circles.

These structures can be more than 50% populated in solution and still be compatible with the experimental observables. In all structures in this category C1B-C2 is in an "open" conformation, with both membrane binding sites exposed and C1B pushed away from C2. While in the entire pool of conformations C1B can sample many orientations near the bottom and top of C2, in all of the top structures C1B is found to the left of the C2 loops. The membrane binding sites for C1B and C2 have varied relative orientations. However, in all structures both sites are free to bind their respective membrane-embedded ligands. Most of the top scoring conformations have loop positions

that would be compatible with the loops of both domains binding the membrane simultaneously. However, for two of the six top scoring conformations, the C1B domain's position relative to the C2 domain would need to change significantly in order for the simultaneous binding to membranes to take place.

Compact conformations, like the conformation found in the crystal structure, scored consistently lower in the MaxOcc analysis, which indicates that they cannot be highly populated in solution. All but one of the low-scoring conformations have relative positions in the C1 and C2 membrane binding sites that would require significant rearrangements to allow for simultaneous membrane insertion (Figure IV.11). Furthermore, in some structures, the C2 loops are partially occluded. In all structures, C1B is packed up against C2 loops. This is true for the Pb-crosslinked crystal structure as well.

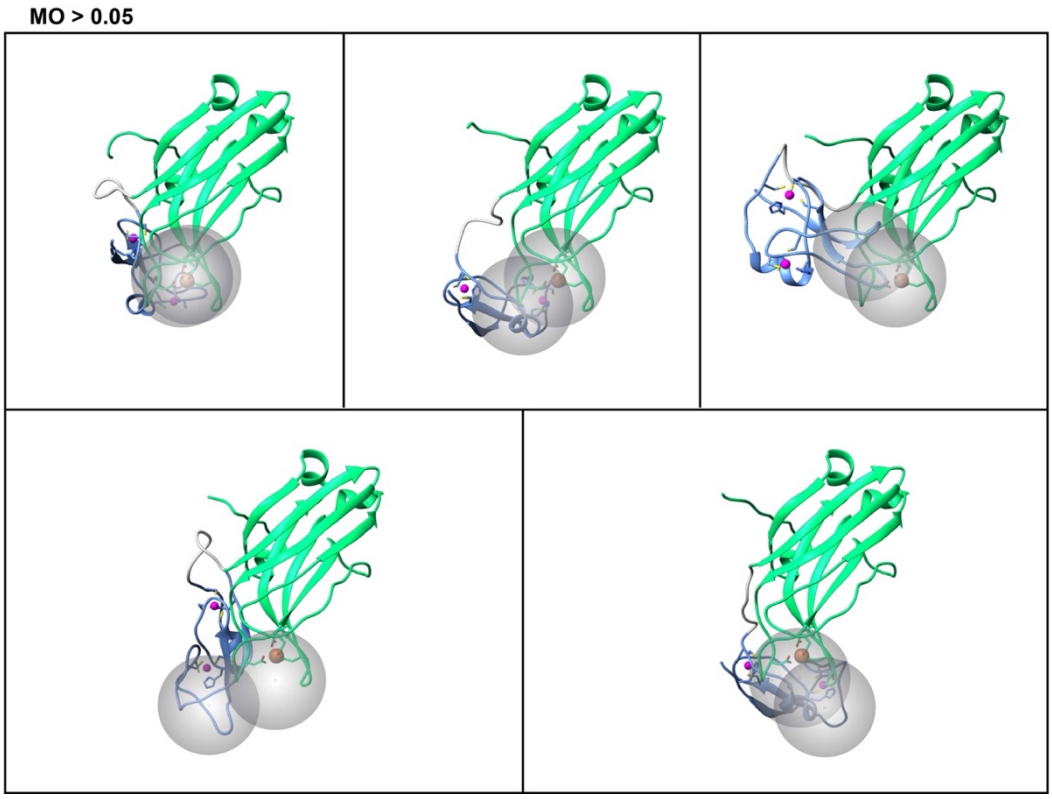

Figure IV.11 Compact conformations score low in MaxOcc analysis. Bottom scoring structures from MaxOcc analysis. The membrane binding loops are indicated with grey circles.

Using Naccess with a probe size of 1.4 Å, the solvent accessibility of the top and bottom scoring conformers (Figure IV.12A-B) was calculated. For the top-scoring conformation there was no change in the solvent accessibility relative to the isolated domains for the C1B or C2 loop regions. However, the bottom-scoring conformation had a decreased solvent accessibility of CMBL1 and CMBL3 (sequestering 81.4 and 98.9 $Å^2$, respectively). Collectively, this suggests that C1B-C2 samples states that are poised for the simultaneous membrane insertion of the C1 and C2 domains and that the C1B domain does not occlude the membrane binding of the C2 domain to membranes.

This is in sharp contrast to the C1B-C2 crystal structure that shows the C1B-C2 region in a compact conformation.

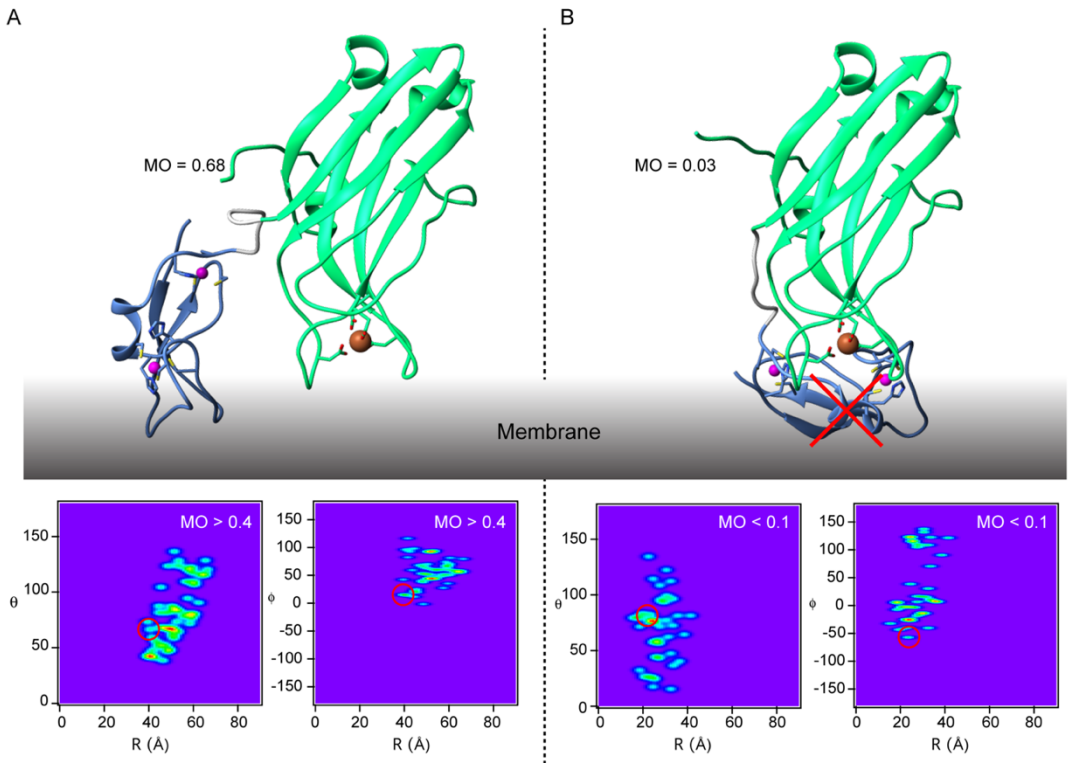

Figure IV.12 C1B-C2 samples "open" conformation in solution. (A) Top structure from MaxOcc analysis of C1B-C2 with θ, ϕ, and R indicated on heat maps. (B) Bottom structure from MaxOcc analysis of C1B-C2 with θ, ϕ, and R indicated on heat maps.

C1B-C2 transiently self-associates

It was surprising to find that C1B-C2 gave rise to PCS on neighboring molecules through transient self-association. The PCS detected on C1B-C2 were primarily in the C1B loops, which suggested that there was an interaction between neighboring C1B and

C2. To determine if this was mediated by lanthanide ions, it was investigated if this dimer was detectable in the apo form of the protein. To gain access to the apo form of C1B-C2, paramagnetic relaxation enhancement (PRE) was used. PRE is an excellent tool for detecting transient protein-protein interactions. By attaching a paramagnetic tag to the C2 domain PRE in the apo state can be measured without the need for paramagnetic metal ions. Two C1B-C2 cysteine variants (K181C and K268C on the C2 domain) were constructed in order to measure intermolecular PRE in C1B-C2 and modified them with a PROXYL tag harboring a stable nitroxide group bearing an unpaired electron. PROXYL-tagged, natural abundance C1B-C2 cysteine mutant was mixed with U-^{15}N C1B-C2wt with no paramagnetic tag (Figure IV.13B). PRE was collected for backbone amide groups (Figure IV.13D) as described in the methods section and was observed again primarily on C1B loop residues. There was a smaller elevation of PRE values for the C2 loop region and the interdomain linker region.

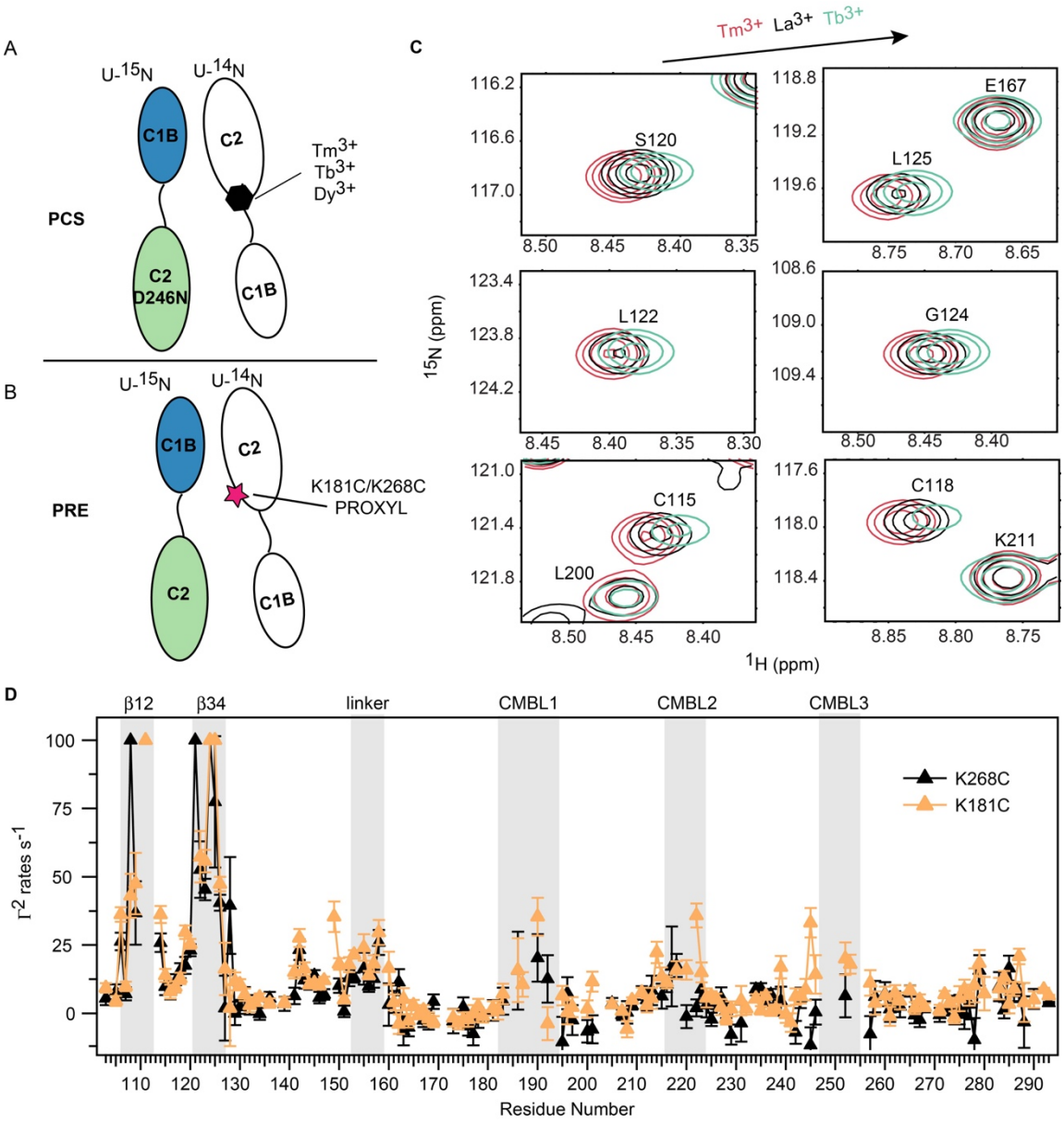

Figure IV.13 C1B-C2 has propensity to self-associate in a manner that is unique from the isolated C2 domain. (A-B) Experimental design for paramagnetic intermolecular experiments. (C) Detected intermolecular PCS on C1B-C2 at 800 MHz. (D) Intermolecular ^{1}H Γ_2 values plotted against the residue number in C1B-C2. Residues that were broadened beyond detection are assigned a ^{1}H Γ_2 rate of 100 s^{-1}.

Collectively, this indicates that a transient intermolecular interaction exists between neighboring C1B-C2 molecules, likely between the C1B and C2 domains.

Discussion

In the activation pathway, PKCα starts out in a compact, latent form where the membrane binding sites of the regulatory region are masked by at least two proposed intermolecular interactions: C1A/C2[57,58] and C2/V5.[59] Prior to membrane binding, the C1 domains must be unmasked in order to bind their respective ligands. There is no structural information about the regulatory region during any of phase of the activation pathway. The data presented in this chapter takes the first steps to understanding the structure and dynamics of this region during activation by characterizing the conformations sampled by the C1B-C2 domains. By omitting the C1A domain that has been proposed to interact with the C2 domain in the full length enzyme, insight into the conformational preferences of the C1B-C2 region after unmasking of the C1 domains but prior to membrane insertion can be gained. Despite the large area of allowed conformational space that can theoretically be sampled by C1B-C2, only a narrow range of space can be appreciably populated and still be consistent with the data. This analysis found that C1B-C2 samples more extended, "open" conformations, with both sets of loops exposed. In a majority of the top scoring conformers, the membrane binding loops of C1B and C2 face the same plane in orientations that would be compatible with simultaneous membrane binding. While the flexible linker allows C1B-C2 to sample many conformations, this raises the possibility that membrane binding proceeds through conformational selection, where the membrane-bound conformation of C1-C2 pre-exists and facilitates ligand recognition.

It is proposed that Ca^{2+} binding serves multiple purposes in modulating C2 affinity for membranes: contributing to the change of electrostatic potential in C2, coordinating the head groups of anionic lipids such as phosphatidylserine (PS), and contributing to interdomain rearrangements in the regulatory region that primes the enzyme for membrane association.[44] The former two have been studied extensively in the context of isolated C2 domains.[184] Although Ca^{2+} binding does not have a profound effect on the structure of the C2 domain[50], it has a large effect on the conformational dynamics of the loop regions and the dynamics and stability of the N- and C-termini. [183] The latter is thought to give rise to the conformational rearrangements that lead to the solvent exposure and ligand recognition of the membrane binding sites of C1 and C2 domains. However, the impact of calcium binding on the structure and dynamics of the full regulatory region of PKC remains uncharacterized.

Due to the changes in the N-terminus of C2 upon Ca^{2+} binding, the work in this chapter investigated if Ca^{2+}-binding propagated these changes to the C1B domain due to their proximity in the primary structure of PKC. No changes were observed in the sub-nanosecond dynamics upon Ca^{2+} binding. Furthermore, according to the SAXS data, there are no major perturbations in the conformations sampled by C1B-C2 upon Ca^{2+} binding. Propagation of the Ca^{2+}-binding event to the parent enzyme therefore likely requires the involvement of the C1A domain and the kinase domain[185] or a change in dynamics on a different time scale. Further studies on the full regulatory region are needed to understand the structural impact of Ca^{2+} binding.

One surprising finding of these studies is that C1B-C2 transiently self-associates through an interaction between C1B and C2. Several studies have highlighted the ability of PKC to self-associate through interactions within the regulatory domains.[57,58,186] While there are no proposed interactions between C1B and C2 domains that have been shown to be important for function, several studies focus on the importance of C1A/C2 interactions for maintaining the latent enzyme. Despite this, there is no structural information about this interaction. A high sequence identity between C1A and C1B domains raises the possibility that the C1A/C2 mode of interaction is being probed. C1A domains are notoriously instable and insoluble. The intermolecular experiments with C1B and C2 could open the door to future studies to use C1B as a surrogate to gain structural information about the C1A/C2 interaction. Mutations can then be designed on the C1A domain in the full length enzyme to study their impact on function and to validate the resulting structural model.

Collectively, the work presented in this chapter highlights the importance of flexibility in the structure and function of the PKC regulatory region and opens the door to new ways of targeting PKC, as well as study the intermolecular interactions that stabilize the latent enzyme.

CHAPTER V

MULTIVALENT INTERACTIONS OF THE C1B-C2 REGULATORY REGION WITH MEMBRANE MIMETICS AND FUTURE DIRECTIONS

Background

In this chapter, the objective is to elucidate how the PKCα regulatory domains interact with membranes in the presence of their native ligands and how these interactions differ when C1B is bound to tumor-promoting phorbol esters. Membrane binding of the C2 domain from the regulatory region of conventional PKCs and the subsequent membrane insertion of one or both C1 domains is required for full activation of conventional PKCs.[167,187] This process is modulated by metal ions [3,188], anionic lipids [189], and membrane-embedded diacylglycerol. However, the mechanistic details of the membrane association process are poorly understood. These studies focused on obtaining structural information about the interactions of the PKC regulatory domains with membrane mimetics and how these interactions modulate the Ca^{2+} requirements of membrane association.

Conventional isoforms contain tandem C1 domains preceding a Ca^{2+}-dependent C2 domain. The C2 domain binds both phosphatidylserine (PS) and phosphatidyl-inositol 4,5-bisphosphate (PIP2) in a Ca^{2+}-dependent manner. The native agonist for C1 domains is diacylglycerol, made available by the hydrolysis of PIP2. Like diacylglycerol, plant-derived phorbol esters can also facilitate the membrane association process of PKC but C1 domains have a much higher affinity for phorbol esters compared

to diacylglycerol. Activation of PKC by phorbol esters leads to prolonged activation, faster downregulation of PKC [190] and tumorigenesis.[4,79,191] Researchers are limited in their design of potential PKC activators because of their phorbol ester-like tumor promoting activities. Therefore, understanding the structural differences in phorbol ester- and diacylglycerol-induced activation of PKC is extremely important for designing better modulators of PKC that lack tumor-promoting activity. Despite the importance of PKC activators, existing information about C1 domain/membrane interactions is limited. This is, in part, largely due to the challenges of working with peripheral membrane binding proteins and selecting membrane mimetics that are both suitable for biophysical studies and physiologically relevant.

Upon binding C1 ligands hydrophilic residues in the binding cleft are masked, increasing the hydrophobicity of the domain and facilitating membrane insertion. [30] The membrane interactions of C1B domain from PKCδ has been explored in micelles with and without a short chain diacylglycerol analog, DOG. [167] The addition of DOG was found to change the depth of insertion. However, the lose packing and curvature of micelles does not always faithfully reproduce the conditions of a planar bilayer. Additional studies are needed in membrane mimetics containing a bilayer.

This chapter describes efforts towards obtaining structural information of the regulatory domains in complex with isotropically-tumbling bicelles in the presence of different C1 domain targeting cofactors, specifically diacylglycerol and phorbol 12,13-dibutyrate. Bicelles are composed of long chain lipids that form a bilayer with

hydrophobic edges capped by short chain lipids. Bicelles have the advantage of a physiologically relevant bilayer packaged in a small NMR-friendly form.

In addition, conventional and novel PKCs have complex, multivalent interactions with membranes that require coordination of multiple domains and multiple ligands. To examine the multivalent nature of PKC, the interplay between metal ions and lipid-ligands in the membrane binding process will also be probed.

Experimental Procedures

C1Bα Purification

C1Bα was purified according to Stewart et. al. [103] PKCα cDNA from Mus Musculus was purchased from Open Biosystems and residues S100-G152 were cloned into a pET-SUMO expression vector (Invitrogen) bearing kanamycin resistance as a C-terminal fusion with histidine-tagged SUMO. Plasmids were transformed into BL21(DE3) E. coli cells and colonies were inoculated into 5 mL Luria Bertani (LB) broth supplemented with 50 μg/mL Kanamycin. Cell cultures were grown to an optical density (OD) of 1 and used to inoculate 4- 1 L cultures of LB. At OD 0.6, the cultures were spun down at 3,500 RPM for 25 minutes and washed with M9 salts. The pellets were resuspended in 1 L of 85% D_2O minimal media supplemented with 0.5 g of ^{13}C, ^{15}N, D Isogro ® powdered growth medium (Sigma) with 2 g/L ^{13}C-glucose (Cambridge Isotopes) and 1 g/L ^{15}N-ammonium chloride (Cambridge Isotopes) as carbon and nitrogen sources, respectively. Protein production was induced with 0.5 mM isopropyl β-D-1-thiogalactopyranoside (IPTG) at 15 ºC for 16 hours. 10 μM $ZnSO_4$ was added to the cultures just prior to induction to ensure proper folding. Cells were harvested at

4,000 RPM for 30 minutes. For NMR experiments, the proteins were concentrated to 0.3–0.5 mM, and exchanged in the buffer containing 20 mM [^{2}H-4]-imidazole at pH 6.5 (Cambridge Isotopes), 50 mM KCl, 8% ^2H_2O, 1 mM tris(2-carboxyethyl)phosphine (TCEP), and 0.02% NaN_3.

C1B-C2 Purification and sample preparation

C1B-C2 linker variants were created using a QuikChange Site-directed mutagenesis kit (Stratagene). C1B-C2 and its variants were purified as described in Chapter 4. For NMR experiments, [U-^{15}N, 75%-^{2}H] C1B-C2 was concentrated to 0.3 mM in 10 mM MES pH 6.0, 150 mM KCl, 1 mM TCEP, 8% ^2H_2O, and 0.02% NaN_3.

Preparation of bicelles

Isotropic tumbling bicelles with a q of 0.5 were used as membrane mimetics for C1B-C2 and isolated C1Bα experiments. The composition of bicelles for C1B-C2 experiments was: 6.7 mol % 1,2-dimyristoyl-sn-glycero-3-phospho-L-serine (DMPS), 26 mol %, 1,2-dimyristoyl-sn-glycero-3-phosphocholine (DMPC), 60.0 mol % 1,2-dihexanoyl-sn-glycero-3-phosphocholine (DHPC), 6.6 mol % 1,2-dihexanoyl-sn-glycero-3-phospho-L-serine (DHPS), and 0.7 mol % L-α-phosphatidylinositol-4,5-bisphosphate (PIP2) (Brain, Porcine). This resulted in 17.2 DMPS and 1.7 molecules of PIP2 per bicelle. For isolated C1Bα, bicelles were prepared with 33.3% DMPC and 66.6% DHPC. The short chain and long chain lipids dissolved in chloroform were measured out separately and dried under a stream of N_2 (g). The dried lipids were placed under vacuum for two hours. The lipids were rehydrated with buffer, mixed, and subjected to freeze/thaw cycles with vortexing in between until the solution remained

clear at room temperature. Phosphate quantification assay was used to measure the concentration of the bicelle stocks. For diacylglycerol (DAG) experiments, the short chain diacylglycerol analogue, 1,2-dioctanoyl-sn-glycerol (DOG), was mixed with the long chain lipids before mixing to ensure that DOG was trafficked to the bilayer.

Measurement of ^{1}H Paramagnetic Relaxation Enhancement

Transverse ^{1}H paramagnetic relaxation enhancement (PRE) rates were collected for C1Bα in complex with bicelles on a Bruker AVANCE III instrument operating at a ^{1}H Larmor frequency of 800 MHz equipped with a cryogenically cooled probe. D4-methanol was used to calibrate temperature. For paramagnetic samples, 1-palmitoyl-2-stearoyl-(5-doxyl)-sn-glycero-3-phosphocholine (Avanti) was incorporated into the bicelles with two molecules per bicelle. This was done by drying down the appropriate amount of paramagnetic lipids and incubating it with the diamagnetic sample. PRE rates were measured and calculated as described in Chapter 4 with the exception that the pulse program was modified with a Transverse Relaxation-Optimized Spectroscopy (TROSY) [192] selection scheme.

Measurement of PCSs and RDCs

Pseudocontact shifts (PCSs) for linker variants were collected as described in Chapter 4 on a Bruker AVANCE III instrument operating at a ^{1}H Larmor frequency of 600 MHz. In addition, residual dipolar couplings (RDCs) were measured for native, Ln^{3+}-bound C1B-C2 as well as the proline and glycine linker variants by measuring the J_{HN} splitting for C1B-C2 bound to isotropic La^{3+} and anisotropic Tb^{3+} using in-phase and antiphase (IPAP) J-coupled HSQC spectra. [193] The splittings for La^{3+} bound C1B-C2

were subtracted from Tb^{3+} bound C1B-C2 to obtain RDCs. Chemical shift perturbations were calculated as described in Chapter 3.

Assignment of C1B methyl region

For the assignment of the methyl region of C1Bα, U-^{15}N, ^{13}C-C1Bα was concentrated to 0.286 mM in 10 mM MES pH 6.0, 150 mM KCl, 1 mM TCEP, 0.02% NaN_3, and 8% D_2O. The following experiments were collected on the apo protein, ^{13}C CT-HSQC, H(CCO)NH [194,195], and CC(CO)NH [194]at a field strength of 500 MHz. ^{13}C-HMQC was collected for C1Bα in the presence of 200 mM PS/PIP2-containing bicelles with 2 mol. Eq. PDBu.

Protein-to-membrane FRET

Protein and membrane interactions driven by Ca^{2+} were monitored by protein-membrane-FRET between C1B-C2 variants labeled with an Alexa Fluor™ 488 C5 Maleimide (ThermoFisher Scientific) fluorophore and Rhodamine-doped large unilamellar vesicles (LUVs). LUVs were prepared as previously described [50] using 1-Palmitoyl-2-oleoyl-sn-glycero-3-phosphocholine (POPC), 1-palmitoyl-2-oleoyl-sn-glycero-3-phospho-L-serine (POPS), and 1,2-dioleoyl-sn-glycero-3-phosphoethanolamine-N-(lissamine rhodamine B sulfonyl) (Liss Rhod-PE), all from Avanti Polar Lipids. The composition of LUVs was POPC:POPS:Rh-PE=79:20:1 molar % for "C1B-ligand-free" liposomes and experiments where phorbol 12,13-dibutyrate (PDBu) as a C1 ligand was added externally. For experiments with native activator, diacyclglycerol, 10% 1-2-dioleoyl-sn-glycerol was added and the amount of POPC was reduced at the liposome preparation stage. For PIP2 experiments, 2% L-α-

phosphatidylinositol-4,5-bisphosphate (Brain, Porcine) was added and the concentration of POPC was adjusted accordingly. To label C1B-C2 variants with the donor fluorophore, a cysteine was substituted for a lysine residue at position 181. The protein was reduced with 2 mM dithiothreitol (Sigma) for 2 hours prior to the labeling reaction. To remove reducing reagent, the protein was exchanged into extensively degassed reaction buffer (20 mM Tris HCl pH 8.0, 150 mM KCl) using two successive PD-10 desalting columns (GE Healthcare). The protein was immediately placed under a constant stream of N_2(g). Four molar equivalents of Alexa Fluor™ 488 C5 Maleimide (ThermoFisher Scientific) fluorophore were added to the protein and the solution was incubated for the appropriate amount of time determined individually for each variant. The success of the reaction was verified by MALDI-TOF mass spectrometry and excess reagent was then removed using a PD-10 desalting column. Any unlabeled protein was removed using a cation exchange column (SOURCE 15S) and the protein was buffer exchanged into MES buffer.

All FRET experiments were carried out on an ISS PC1 fluorometer (ISS, Champaign, IL) at 25 °C by exciting at 484 nm and following the decrease in emission of the donor molecule at 517 nm upon addition of increasing amounts of Ca^{2+} from a concentrated stock solution added to 50 nM protein pre-incubated with 600 μM LUVs. Experiments were conducted in 20 mM HEPES pH 7.4 and 100 mM KCl ("FRET-buffer"). The fluorescence of a "blank" sample containing all components except for C1B-C2 was recorded and subtracted from the fluorescence of the sample cuvette. The fluorescence was corrected for dilution where Ca^{2+} was added. Buffering with 0.5 mM

ethylene glycol-bis(β-aminoethyl ether)-N,N,N′,N′-tetraacetic acid (EGTA) was used to control trace amounts of residual Ca^{2+}. The amount of free Ca^{2+} in solution was calculated according to ref [196]. Three repeats were done for each experiment. To ensure that protein binding to LUVs and not the cuvette walls was being monitored, the cuvettes were coated overnight with a 1 mg/mL solution of IgG® (Sigma Aldrich) dissolved in FRET-buffer to prevent protein adsorption. The cuvettes were rinsed with water and buffer and allowed to dry before use. The donor emission was monitored over time with Ca^{2+} addition in the absence of LUVs to ensure that the decrease in emission was not due to protein sticking to the walls. In all cases the decrease in Alexa fluorescence in the absence of LUVs was < 10% at the maximum concentration of Ca^{2+} added during the experiments.

The change in Alexa fluorescence upon Ca^{2+}-addition was normalized to the maximum change in fluorescence and plotted as a function of the free-Ca^{2+} concentration. The resulting curves were then fit with the Hill Equation:

Equation 17

$$\Delta F = \Delta Fmax \left(\frac{[Ca^{2+}]^H}{[Ca^{2+}]_{\frac{1}{2}}^H + [Ca^{2+}]^H}\right)$$

Where ΔFmax is the maximum change in fluorescence observed, $[Ca^{2+}]_{1/2}$ amount of Ca^{2+} needed to reach half-maximal binding, and H is the Hill coefficient.

C1B binding to DAG probed by ultracentrifugation

Large unilamellar vesicles (LUVs) were prepared containing sucrose according to the protocol outlined in Giorgione and Newton [197] with 10 mM HEPES pH 7.4, 100 mM KCl, and 170 mM sucrose. The pelleting efficiency of the sucrose loaded LUVs

was determined to be >98% for all experiments by measuring phosphate concentration before and after centrifuging the samples. The composition of LUVs was POPC/POPS/DAG 70:20:10 mol %. 50 nM native-linker C1B-C2 K181C Alexa 488 was incubated with 0.6 mM LUVs for five minutes. LUVs were centrifuged in an Optima MAX-XP tabletop ultracentrifuge for 30 min at 50 000 rpm and 25 °C. The amount of C1B-C2 in the supernatant was quantified using the fluorescence of Alexa 488 normalized to the Alexa 488 fluorescence in the absence of LUVs. 0.5 mM EGTA was added to all samples to control trace amounts of Ca^{2+}. All experiments were conducted in FRET buffer.

Turbidity Assay

To assess tethering in C1B-C2 liposome samples, the absorbance at 405 nm was monitored using a SpectraMax Plus 384 microplate reader. FRET-buffer with 0.5 mM EGTA was used for all samples. The blank, which was subtracted from the absorbance of the samples, contained FRET-buffer and all components of the reaction except for liposomes. The absorbance of solutions with all reactants except for protein were subtracted from each condition. Each sample was 100 μL. Liposome concentration used was 0.9 mM. Concentration of native C1B-C2 added was 2 μM. 0.3 mM free Ca^{2+} was added from a concentrated stock solution.

Diffusion-ordered spectroscopy

The translational diffusion coefficients, D_t, for bicelles were measured under different sample conditions using NMR. Bipolar-gradient based diffusion-ordered spectroscopy (DOSY) with convection compensation was carried out on an Avance III

Bruker instrument operating at the ^{1}H Larmor frequency of 800 MHz and equipped with a cryogenically cooled probe for C1B-C2 samples and an Avance III Bruker instrument operating at the ^{1}H Larmor frequency of 500 MHz for C1B samples. The diffusion time interval and gradient pulse lengths were optimized for each sample. Diffusion time intervals were set to 300 ms for all bicelle measurements, with gradient pulse durations being set to 1.0-1.5 ms. Water diffusion coefficient measurements were carried out for each condition using a 30 ms diffusion time and a 0.75 ms gradient pulse duration and used to estimate the solvent viscosity. The pulsed gradient field strength was incremented linearly from 2% to 95% in 16 steps. The well resolved DMPC methyl peak was chosen for D_t determination due to the low solubility of free DMPC in solution. Temperatures were calibrated with [$^{2}H4$]-methanol. The data were analyzed using the TopSpin3.2 software (Bruker Biospin). Shigemi tubes were used to minimize the contribution of convection to the diffusion measurements for all C1B-C2 samples. Shigemi tubes and convection compensation were not needed for C1B samples as they were all done at 298 K and convection was minimal.

Results

Ligands do not perturb isotropic bicelles

Isotropically tumbling DMPC/DHPC bicelles with a q of 0.5 were employed as a membrane mimetic to gain structural information on C1Bα membrane interactions. Prior to characterizing C1Bα interactions with ligands in bicelles, the bicelles were characterized to ensure that their morphology was not disturbed by the ligands or by protein binding. Diffusion ordered spectroscopy (DOSY) was used to measure the

translational diffusion coefficients of the bicelles in the presence of different ligands/protein (Table V-1). A population of DHPC exists as free monomer in solution. [198] Therefore, to avoid underestimation, the diffusion coefficient was determined using the acyl-CH_3 moiety of DMPC, which exists primarily in the bilayer. [198] The translational diffusion coefficient for water was also determined for each sample and the ratios, $D_{t,bicelle}/D_{t,water}$, were considered as part of the changes in viscosity.

The translational diffusion coefficient (D_t) of bicelles in the absence of protein and externally added ligands is 6.14×10^{-11} m^2s^{-1} (Table V-1). This is close to the published value for q = 0.5 DMPC/DHPC bicelles with 100 mM total lipid concentration ($5.6 \pm 0.01 \times 10^{-11}$ m^2s^{-1}). [198] The addition of protein and ligand does not significantly decrease the diffusion coefficients or ratios. This indicates that protein binding and ligand incorporation doesn't perturb bicellar morphology or significantly increase the size.

Table V-1. Ligands do not perturb bicelle morphology. Translational diffusion coefficients (D_t) determined from DOSY experiments at 500 MHz.

Conditions	**D_t DMPC m^2/s**	**D_t water m^2/s**	**D_t DMPC/D_t water**
100 mM Bicelles	6.14×10^{-11}	2.13×10^{-9}	2.88×10^{-2}
+0.4 mM C1Bα + 0.8 mM PDBu	5.97×10^{-11}	2.07×10^{-9}	2.89×10^{-2}
+0.4 mM C1Bα + 8 mM DOG	5.71×10^{-11}	2.16×10^{-9}	2.64×10^{-2}
+0.4 mM C1Bα + 0.8 mM PMA	6.31×10^{-11}	2.08×10^{-9}	3.04×10^{-2}

PKCα has also been shown to interact with PS [81,143,199] and PIP2. [200,201] To study these interactions and eventually extend these studies to the entire regulatory region of PKC, bicelles were designed with PS and PIP2. A stable bicelle was created with all of the components necessary for both C1 and C2 domains to bind. DHPS and DMPS were added at 10% and 20%, respectively as well as 2% brain PIP2. DOSY was again used to measure the diffusion coefficients of the bicelles by themselves and in the presence of externally added ligands (Table V-2). The $D_{t,bicelle}/D_{t,water}$ for bicelles only (Table V-2) was comparable to that of DMPC/DHPC bicelles (Table V-1), which indicates that incorporating anionic components did not change the bicellar morphology. In addition, both C1 and C2 ligands were added and the temperature of the experiments was varied. In all cases, the $D_{t,bicelle}/D_{t,water}$ doesn't change. It was concluded that the bicelles are stable and suitable for the experiments.

Table V-2. Ligands do not perturb bicelle morphology. Translational diffusion coefficients (D_t) determined from DOSY experiments at 800 MHz.

Condition	Temperature (K)	D_t DMPC (m^2/s)	D_t water (m^2/s)	D_t DMPC/D_t water
200 mM Bicelles	298.15	4.97E-11	1.72E-09	2.81E-02
200 mM Bicelles	303.15	5.49E-11	1.94E-09	2.84E-02
200 mM Bicelles	308.15	6.08E-11	2.14E-09	2.87E-02
200 mM Bicelles	313.15	6.78E-11	2.40E-09	2.91E-02
200 mM Bicelles	318.15	8.17E-11	2.69E-09	2.85E-02
+ 1.2 mM Ca^{2+}	298.15	4.85E-11	1.69E-09	2.89E-02
+ 1.2 mM Ca^{2+}	303.15	5.51E-11	1.91E-09	2.92E-02
+ 1.2 mM Ca^{2+}	308.15	6.38E-11	2.15E-09	2.95E-02
+ 1.2 mM Ca^{2+}	313.15	7.21E-11	2.41E-09	2.98E-02
+ 1.2 mM Ca^{2+}	318.15	9.32E-11	2.77E-09	2.94E-02
+ 0.6 mM PDBu	298.15	4.51E-11	1.58E-09	2.84E-02
+ 0.6 mM PDBu	303.15	5.20E-11	1.79E-09	2.86E-02
+ 0.6 mM PDBu	308.15	5.91E-11	2.01E-09	2.89E-02
+ 0.6 mM PDBu	313.15	6.58E-11	2.26E-09	2.90E-02
+ 0.6 mM PDBu	318.15	7.34E-11	2.52E-09	2.92E-02
+ 1.2 mM Ca^{2+}/0.6 mM PDBu	298.15	4.52E-11	1.58E-09	2.83E-02
+ 1.2 mM Ca^{2+}/0.6 mM PDBu	313.15	6.80E-11	2.26E-09	2.95E-02

C1B transiently associates with bicelles in the absence of ligands

It has been proposed that C1 domains pre-associate with bilayers in the absence of ligands. [81] C1B has also been shown to have a propensity to associate with detergent micelles, even in the absence of C1 ligands.[103,167] However, their loose packing and curvature renders experiments with micelles prone to artifacts and the molecular details of membrane interactions in the absence of ligands are uncharacterized. As a first step

to characterizing interactions of C1B with membranes, isotropic tumbling, q = 0.5 DMPC/DHPC bicelles were added in the absence of C1 ligands. Upon the addition of bicelles to C1Bα, the backbone chemical shifts of residues in both C1B loops are perturbed (Figure V.1) while Y123, L125, and G129 in the β34 loop are broadened due to the chemical exchange. This is consistent with C1B pre-associating with bicelles in the absence of ligands and suggests that both loops participate in this association.

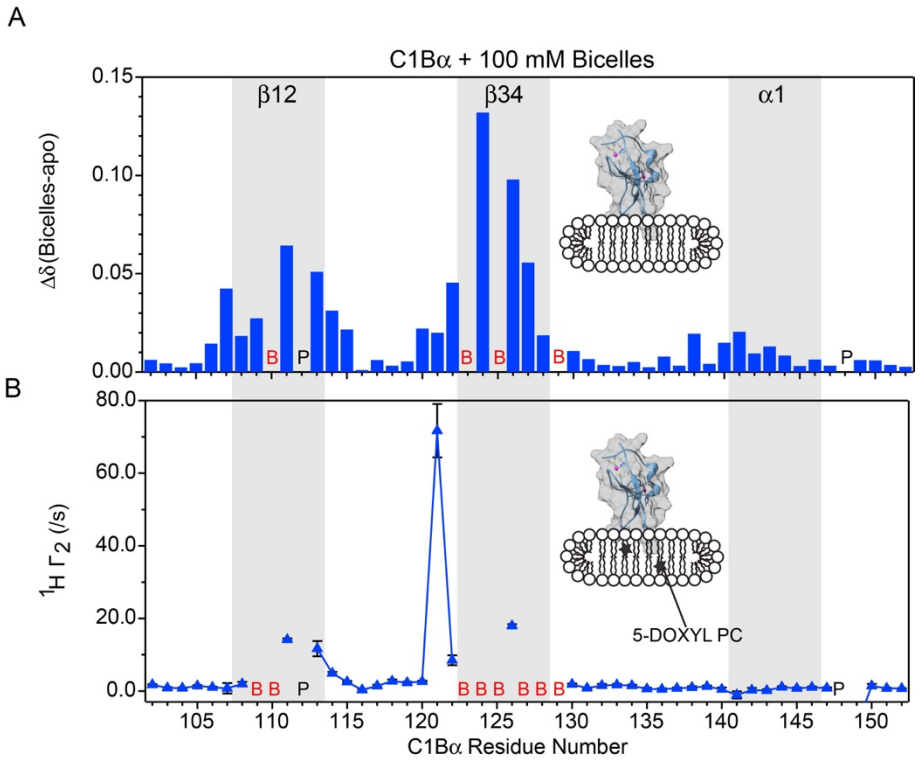

Figure V.1 C1Bα transiently associates with isotropically tumbling bicelles. (A) Chemical shift perturbations upon addition of 100 mM bicelles to C1Bα. (B) ^{1}H Γ_2 rates for 0.4 mM C1Bα in the presence of 100 mM bicelles. Rates were determined by subtracting ^{1}H R_2 values for the diamagnetic sample from ^{1}H R_2 values from samples with 2 molecules of 16:0-5 Doxyl PC per bicelle. Residues that are broadened due to chemical exchange are indicated with a "B". Prolines are indicated with a "P".

While CSPs are a useful tool in detecting protein interactions, they cannot by themselves unambiguously identify the interaction interface. This is because changes in structure or dynamics upon binding can give rise to CSPs away from the binding site. Therefore, paramagnetic relaxation enhancement (PRE) rates were collected for C1B in the presence of bicelles. Transverse ^{1}H PRE rates were obtained by incorporating 16:0-5-doxyl PC, bearing a stable nitroxide at position 5 on the acyl chain. The magnitude of the observed PRE observed depends on the distance with respect to the paramagnetic center. Despite the exchange broadening, elevated PRE rates were observed for three reporters in the loops--S111 and T113 in the β12 loop and I126 in the β34 loop. This is direct evidence that both loops are inserted into the bilayer. In addition to loop residues, PRE was observed for L121 preceding the β34 loop. This indicates that this residue was inserted deeply into the bilayer and in closer proximity to the doxyl group.

β34 loop of C1B partitions deeper into the bilayer in the presence of phorbol esters

Two molar equivalents of phorbol 12,13 dibutyrate (PDBu) added to the C1B/bicelle mixture was enough to saturate C1B. Residues broadened beyond detection in the presence of bicelles could only be recovered upon PDBu addition. CSPs were again only observed for residues in both ligand binding loops (Figure V.2).

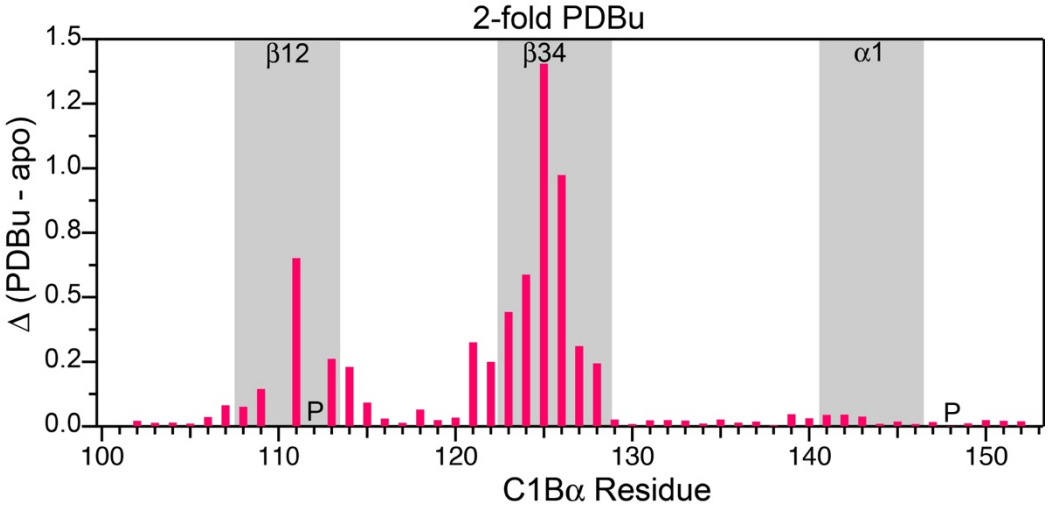

Figure V.2 PDBu binding recovers exchange broadened C1B residues in the presence of bicelles. Chemical shift perturbations upon addition of 2-fold phorbol 12,13-dibutyrate (PDBu) and 100 mM bicelles to C1Bα. Prolines are indicated with a "P". G110 is exchange broadened in the apo spectra but is recovered upon addition of PDBu.

Upon addition of bicelles and then PDBu, the ^{1}H R_2 rates for the diamagnetic samples increase relative to the apo protein, due to the larger apparent molecular weight when associated with bicelles (Figure V.3). Two-fold PDBu saturates C1B. The assumption is made that 100% of C1B is bound to bicelles in the presence of PDBu and used the average ^{1}H R_2 rates to estimate the population of C1B bound to bicelles in the absence of ligands to be ~27%.

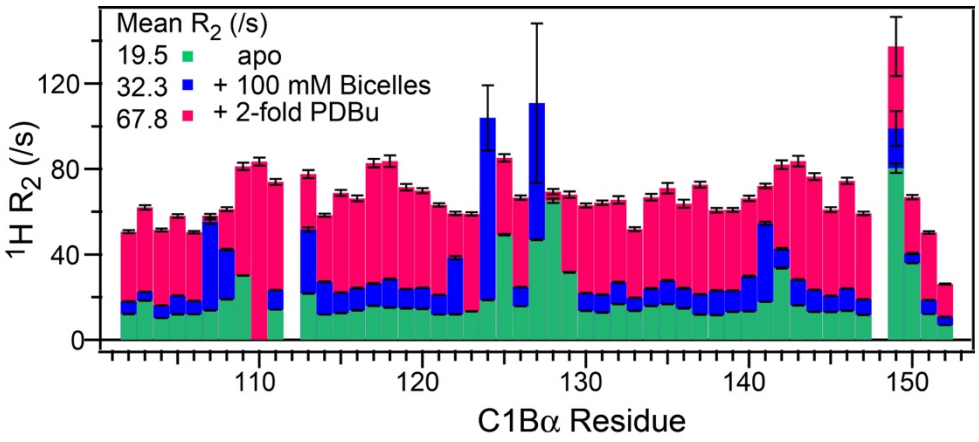

Figure V.3 ^{1}H R_2 increases upon bicelle and PDBu addition. Rates are shown for 0.4 mM C1Bα in different ligand complexed states (diamagnetic sample). The average R_2 values for each state are indicated. From these values the population of bound species was estimated to be 26.5% in the presence of bicelles only.

Transverse ^{1}H PRE for C1Bα backbone N-H groups in the presence of PDBu and bicelles were then collected. This revealed that the β34 loop penetrates deeper into the bilayer. PRE values were larger for residues in the β34 loop than in the β12 loop (Figure V.4). L121 also has a large PRE indicating that this residue penetrates deeper into the bilayer.

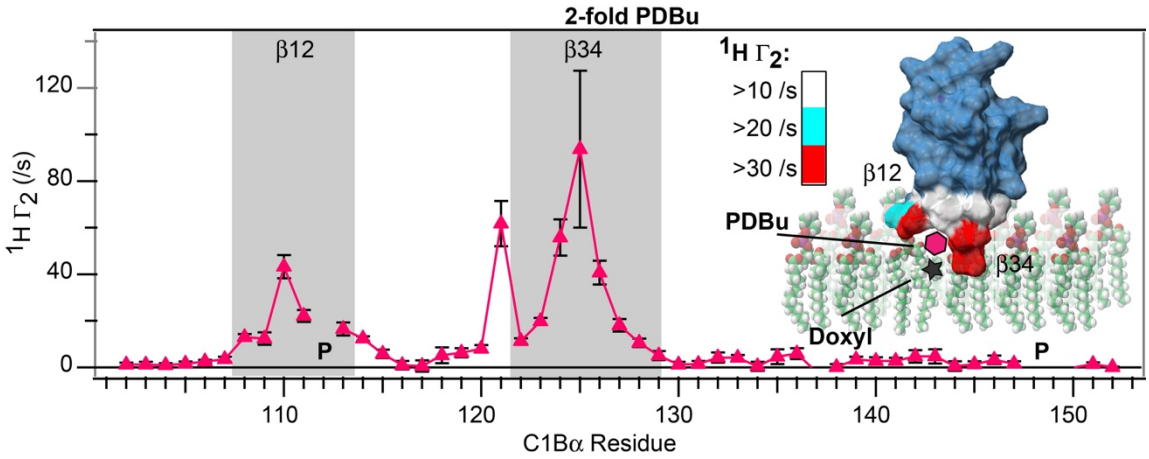

Figure V.4 The β34 loop of C1B is inserted deeper into the membrane with PDBu. ^{1}H Γ_2 rates for 0.4 mM C1Bα in the presence of 2-fold PDBu and 100 mM 16:0-5-Doxyl PC doped bicelles. Prolines are indicated with a "P".

Although there are not enough reporters on the loops in the absence of ligands due to exchange broadening, PRE is only observed in the loop regions in the presence and absence of ligands, which indicates that the same regions of the protein are responsible for binding in both cases. To see if PDBu is incorporating into the bilayer and not into the less densely packed short chain lipids that cap the bilayer, since PDBu is added externally, bicelles with phorbol 12-myristate 13-acetate (PMA) were made. The PRE pattern, ^{1}H R_2 of the diamagnetic sample, and the chemical shift perturbations were compared and found to be virtually identical (Figure V.5) to that of PDBu. This is consistent with C1B inserting into the bilayer in the presence of PDBu.

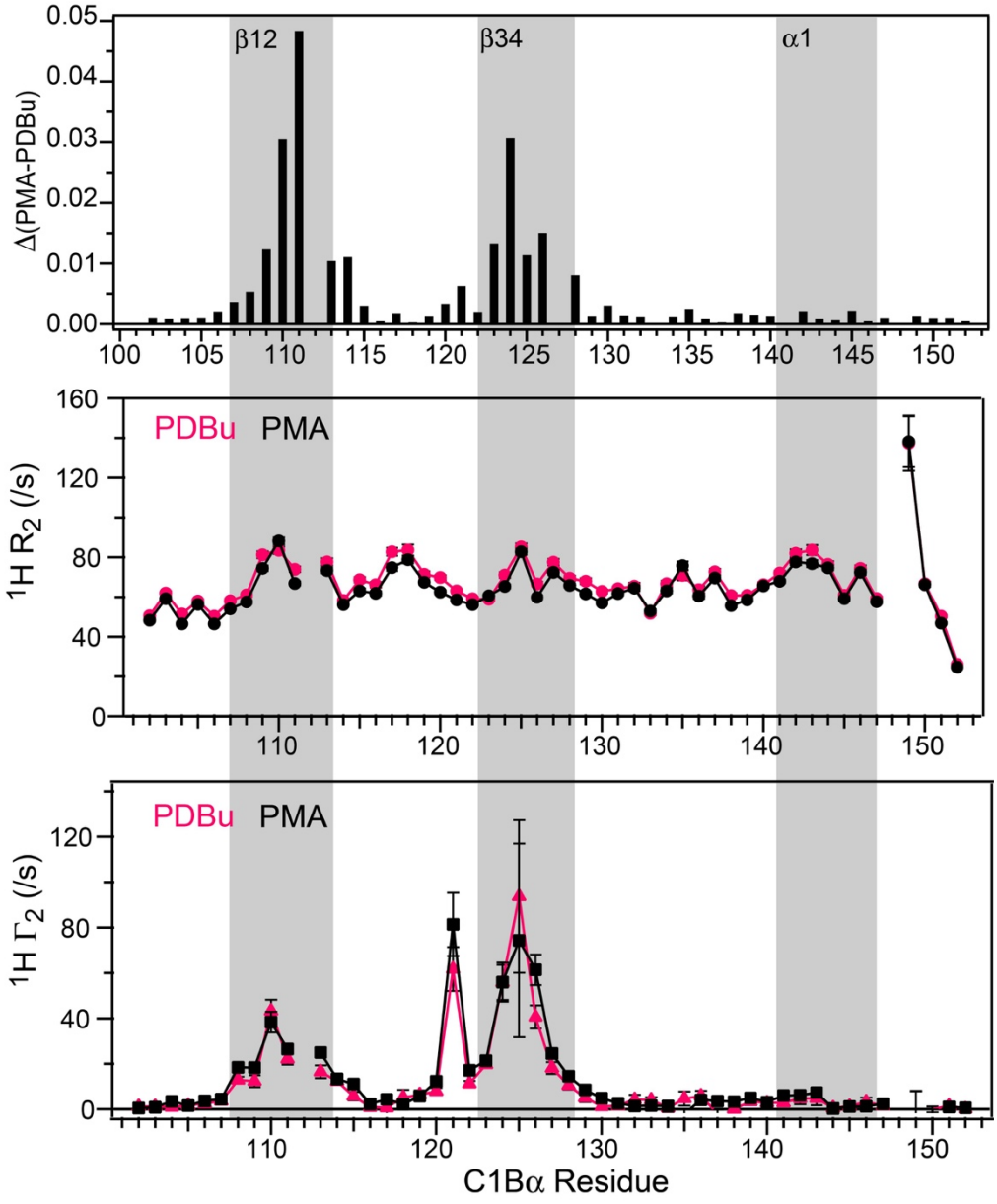

Figure V.5 PDBu and PMA generate identical PRE profiles on C1B. Chemical shift perturbations, ^{1}H R_2 rates, and ^{1}H Γ_2 rates for C1Bα in the presence of 100 mM DMPC/DHPC bicelles with either phorbol 12-myristate 13-acetate (PMA) or the short chain phorbol, PDBu.

Next, interactions of C1Bα with bilayers in the presence of its native ligand, diacylglycerol, were investigated. Bicelles were made with a short-chain diacylglycerol, 1,2-dioctanoyl-sn-glycerol (DOG) incorporated into the bilayer. The final concentration of DOG in the samples was 8 mM for a 20-fold excess of DOG:C1Bα. Elevated ^{1}H R_2 and chemical shift perturbations indicate that C1Bα is bound to the bicelles under these conditions (Figure V.6). The magnitude and pattern of the diamagnetic ^{1}H R_2 rates for DOG-bound C1Bα are comparable to PDBu-bound C1Bα. There is a slight elevation in the rates for DOG compared with PDBu that suggests that the ternary complex is larger. This can be attributed to the high concentration of DOG incorporated into the bilayer and increasing the effective size. DOG was not considered in the calculations for the q of the bicelle because the chain length of 8 carbons is between the chain lengths of DMPC (14:0) and DHPC (06:0). Although the bicelles were made by mixing DOG with DMPC to "trap" DOG in the bilayer, some DOG could be incorporated into the sides of the bicelle. The exchange behavior in the loops, observed in the absence of ligands with bicelles (Figure V.3), is presented as elevated ^{1}H R_2 rates for loop residues and was not observed with DOG-bound C1Bα. From this it is concluded that all of C1Bα is bound to the bicelles. G110 is the only residue in the loop region with elevated ^{1}H R_2 rates. G110 is a dynamic residue, completely broadened beyond detection in the apo protein. The dynamics of this residue are quenched upon PDBu binding but not upon DOG binding (Figure V.6). The PRE for DOG was larger in the loop regions than with the PDBu with three residues (L121, G124, and L125) completely broadened by doxyl (Figure V.6). While docking and restrained molecular dynamics studies need to be

completed to understand the membrane binding geometry, this suggests that C1Bα penetrates deeper into the bilayer in the presence of DOG than with PDBu.

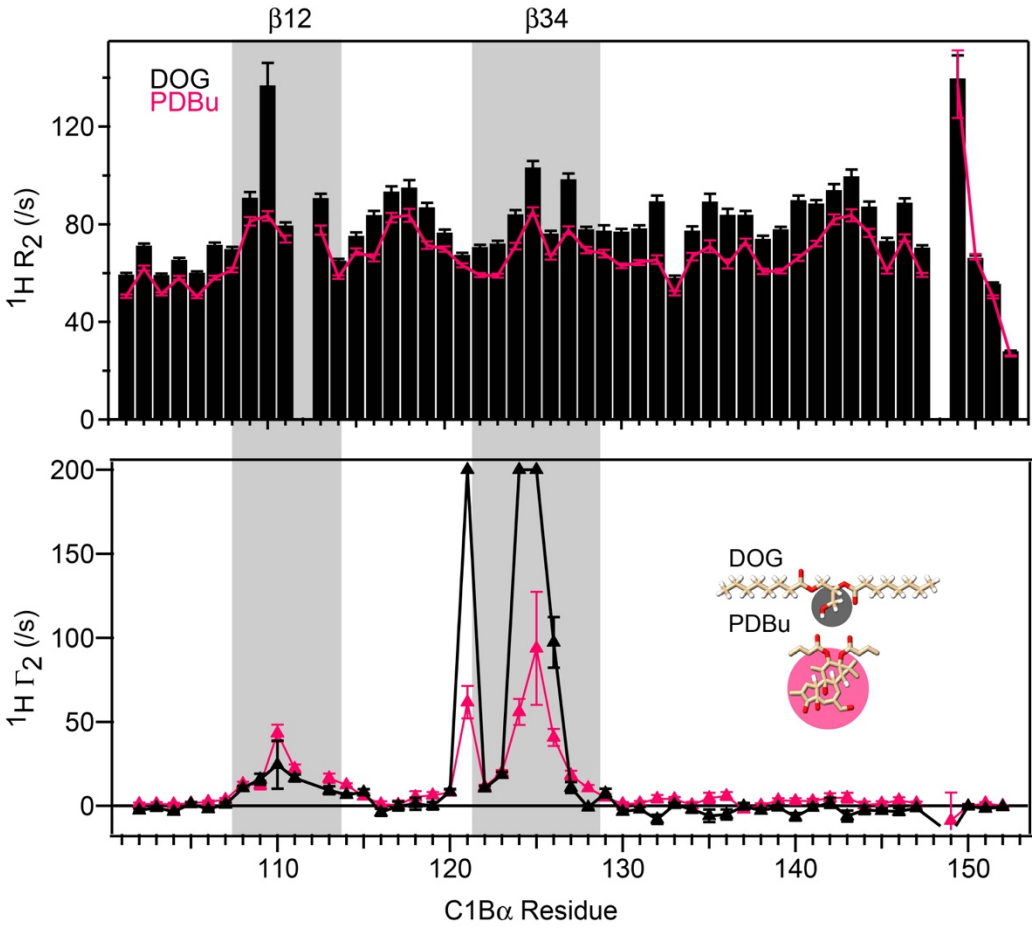

Figure V.6 DOG drives C1Bα deeper into the membrane. ^{1}H R_2 rates, and ^{1}H Γ_2 rates for C1Bα in the presence of 100 mM DMPC/DHPC bicelles with either PDBu or DOG. Residues broadened beyond detection were assigned a ^{1}H Γ_2 rate of 200 s^{-1}.

Proline-linker variant decreases conformational variability of C1B-C2

Having characterized the interactions of C1B with bicelles in the presence of different ligands, experiments were conducted to determine how different C1 ligands

affected the coupling between C1 and C2 domain membrane insertion. Additionally, in Chapter 4 it was shown that C1B-C2 has a great deal of conformational variability mediated by its flexible linker. The objective was to determine how changing the conformational entropy of C1B-C2 by changing the flexibility of the linker region changes the interplay between C1 and C2 in their interactions with membranes.

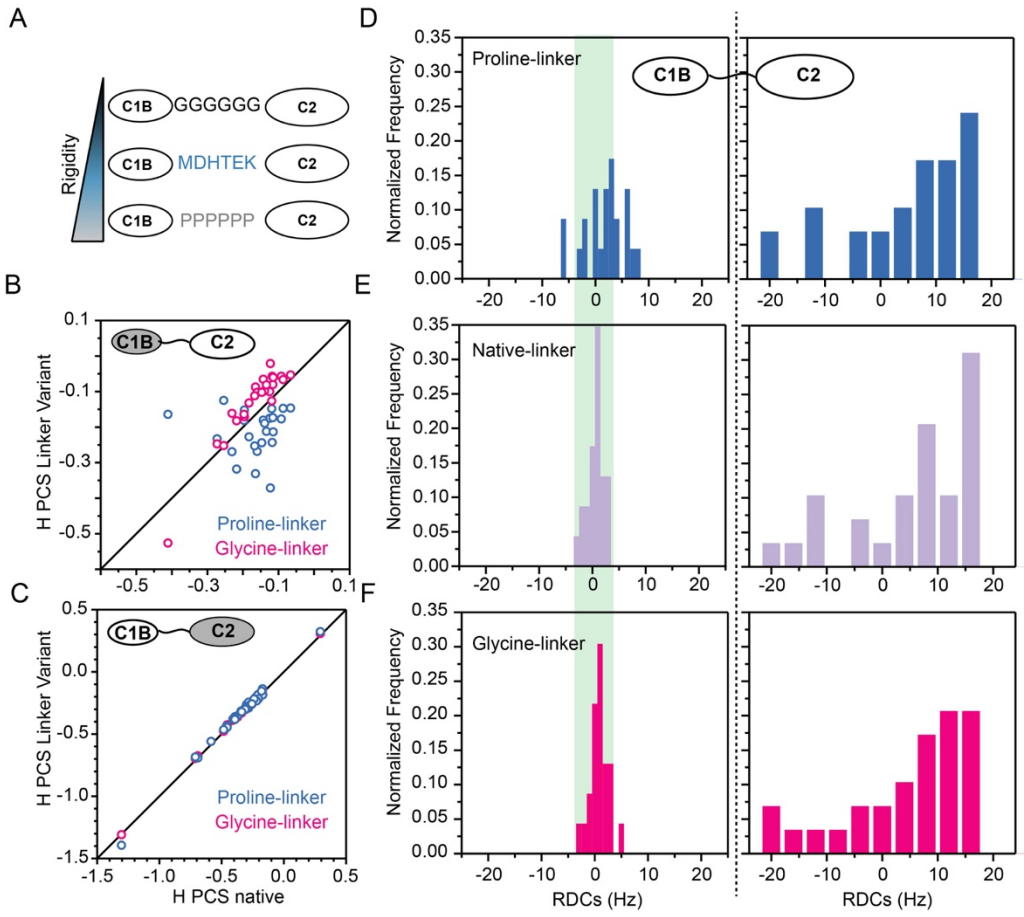

Figure V.7 Proline-linker rigidifies C1B-C2. (A) Distribution of residual dipolar couplings (RDCs) for C1B and C2 from C1B-C2 complexed to Tb^{3+} at 600 MHz. (B) Comparison of ^{1}H pseudocontact shifts (PCS) from backbone N-H groups for native-linker and glycine/proline linker variants separated by domain.

Two inter-domain linker variants for C1B-C2 were designed, replacing six residues between the folded cores with glycines or prolines to create a more flexible and more rigid interdomain linker, respectively (Figure V.7A). As a control, to evaluate if these modifications had the desired effects on C1B-C2, pseudocontact shifts (PCS) and residual dipolar couplings (RDCs) were collected for all variants from the paramagnetic Tb^{3+} bound in the C2 domain. These report on the structural ensemble (RDCs and PCS) and flexibility (RDCs) of C1B-C2 (Figure V.7). By evaluating the RDC distributions of C1B and C2 (aligned domain) information can be gained on the extent of conformational averaging of C1B relative to C2 which qualitatively reports on the flexibility of the linker.

For the native-linker, the aligned domain (C2) has a larger distribution of RDCs compared to the unaligned domain C1B (Figure V.7D-F). The distribution of RDCs is similar for C2 complexed to Tb^{3+} in all variants which is a good indication that the structure of C2 with the linker variants is not perturbed. The distribution of RDCs for C1B was much like the glycine-linker variant and native-linker, consistent with maintaining the flexibility of the linker while changing the identity (Figure V.7E-F). However, the proline-linker variant had a larger distribution of RDCs for C1B than the native-linker or glycine linker, consistent with the restriction of C1B and with less conformational averaging (Figure V.7D). These findings were echoed by the PCSs (Figure V.7B,C). Thus, good agreement was found between the PCS for C2 from the native-linker with both linker variants (Figure V.7C). The C1B PCSs for the glycine-linker variant were smaller than that of the native C1B-C2 linker variant (Figure V.7B).

The magnitude of PCSs on the C1B domain depend on the distance and orientation of the C1B relative to C2 as well as the extent of conformational averaging. Therefore, the smaller PCS observed in the glycine-linker variant were most likely due to an increase in flexibility relative to the native C1B-C2 linker and more extensive conformational averaging. It could also be due to C1B-C2 adopting more extended conformations. On the other hand, the proline linker variant on the other hand had larger C1B PCSs and a worse correlation with the native linker variant. This is consistent with a more rigid protein and a perturbation of the native conformational ensemble. From these experiments it can be concluded that substituting the linker region for prolines decreased the conformational variability of C1B-C2 while substituting for glycines maintained the variability while serving as a control for changing the identity of the linker.

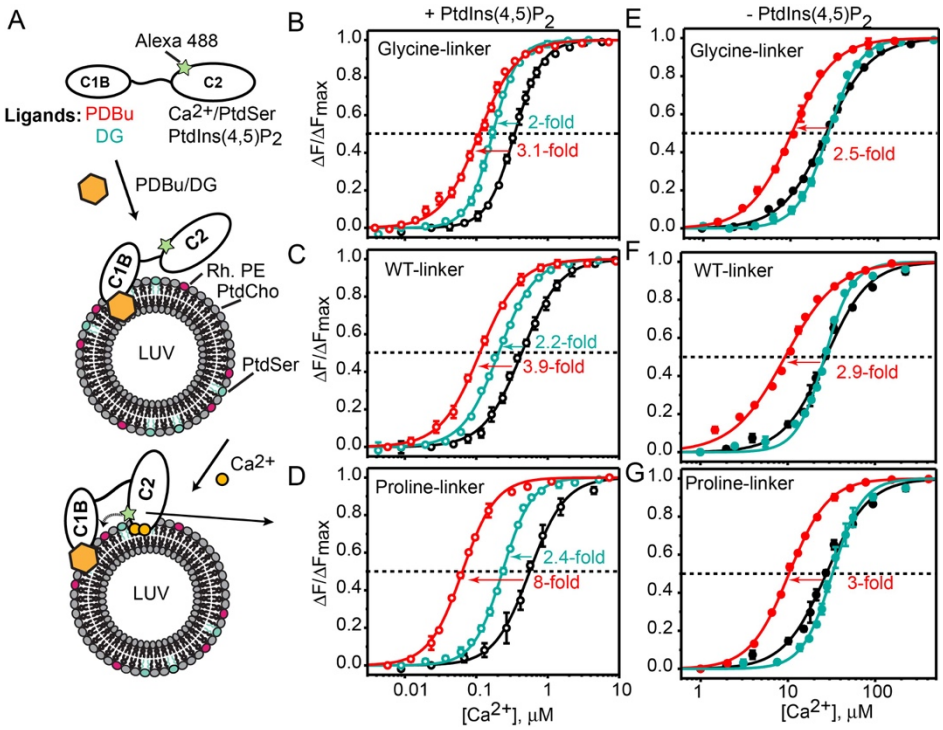

Figure V.8 The C1B-C2 linker region tunes avidity. A) Linker variants used in this study. Residues 153-158 (native linker in blue) were replaced with glycines or prolines to make the linker more flexible or more rigid, respectively. B) Experimental design for protein-to-membrane FRET experiments. Ca^{2+} drives C1B-C2 Alexa 488 to Rhodamine PE and PS/PIP2 doped liposomes resulting in FRET between Alexa 488 and Rh. PE. C) Normalized protein-to-membrane FRET as a function of Ca^{2+} concentration in the presence (red) or absence (black) of PDBu. The fold-decrease in Ca^{2+} needed to achieve half-maximal membrane binding as indicated on the graph.

PIP2 is required to achieve maximum coupling between C1 and C2 ligands

Next, how these variants altered the Ca^{2+} concentrations needed to drive the C2 domain to the membrane in the presence of C1 ligands was probed. For the assay rhodamine-PE doped liposomes (acceptor) and C1B-C2 linker variants tagged with an Alexa 488 fluorophore (donor) at position 181 on the C2 domain (Figure V.8A) were used. When Ca^{2+} is added, C1B-C2 is trafficked to anionic liposomes and Alexa 488

fluorescence is quenched by rhodamine. There is only FRET when binding of C2 domain to the membrane with the addition of Ca^{2+}. As a measure of the "coupling" between C1 and C2 ligands, the Ca^{2+} concentrations needed to drive membrane binding in the presence and absence of C1 ligands for each variant (Figure V.8B-G; Table V-3) were compared.

Table V-3. PIP2 is required to maximize interactions of C1B-C2 with membranes. $[Ca^{2+}]_{1/2}$ values from protein-to-membrane FRET experiments with C1B-C2.

	$[Ca^{2+}]_{1/2}$ +PtdIns(4,5)P_2			**$[Ca^{2+}]_{1/2}$** -PtdIns(4,5)P_2		
Linker	Ligand-free	DAG	PDBu	Ligand-free	DAG	PDBu
Glycine	0.34±0.01	0.17±0.01	0.11±0.01	25.6±0.5	27.0±0.5	10.3±0.1
Native	0.43±0.04	0.2±0.01	0.11±0.01	27.4±0.6	26.6±0.2	9.3±0.2
Proline	0.56±0.02	0.23±0.01	0.07±0.01	31.0±0.2	32.5±2.0	10.3±0.2

First, liposomes bearing both phosphatidylserine and phosphatidylinositol 4,5-bisphosphate were used. The high local concentration created by tethering C1B-C2 to the membrane through C1/ligand interactions decreases the amount of Ca^{2+} needed for C2 to bind to the membrane (Figure V.8B-D). For wild-type C1B-C2 with the native linker, the $[Ca^{2+}]$ needed to achieve half-maximal binding ($[Ca^{2+}]_{1/2}$) was 0.43±0.04 μM. Upon incorporation of 10% DAG into the liposomes, the $[Ca^{2+}]_{1/2}$ was lowered 2.2-fold. External addition of PDBu lowered the $[Ca^{2+}]_{1/2}$ even more by 3.9-fold relative to C1B ligand-free.

Omitting PIP_2 from the membrane attenuated this effect, suggesting a synergy between PIP_2 and C1 ligands. Omitting PIP2 significantly increased the concentration of Ca^{2+} needed to drive membrane binding. For the native-linker variant, this resulted in a 64-fold increase in the $[Ca^{2+}]_{1/2}$. In the absence of PIP2 the overall avidity from incorporating PDBu was decreased for all variants (Figure V.8E-G). Furthermore, the effect of rigidifying the linker disappears with similar avidities for all variants (Figure V.8E-G).

The most striking finding is that while in the absence of PIP2 there is only a 20% decrease in avidity for native C1B-C2 and there is no avidity upon incorporation of DAG for any of the variants. One possible explanation for this is that C1B-C2 is not binding to DAG in the absence of PIP2. To test this, ultracentrifugation assays were conducted with sucrose-loaded vesicles containing 20% PtdSer and 10% DAG under the same conditions set forth in the fluorescence experiments. For all experiments, >98% of the vesicles were pelleted. The emission of 50 nM Alexa 488 labeled C1B-C2 in the presence and absence of 0.6 mM vesicles was measured. In the absence of Ca^{2+}, ~35% of the total protein was pelleted with the liposomes (Figure V.9A). In the absence of Ca^{2+}, this can only be due to C1B binding to the membrane. As a control to make sure that all of the protein could be pulled down saturating Ca^{2+} was added and ~90% of the protein was pelleted. This indicates that despite the lack of avidity, C1B-C2 is still able to bind to DAG in the absence of PIP2.

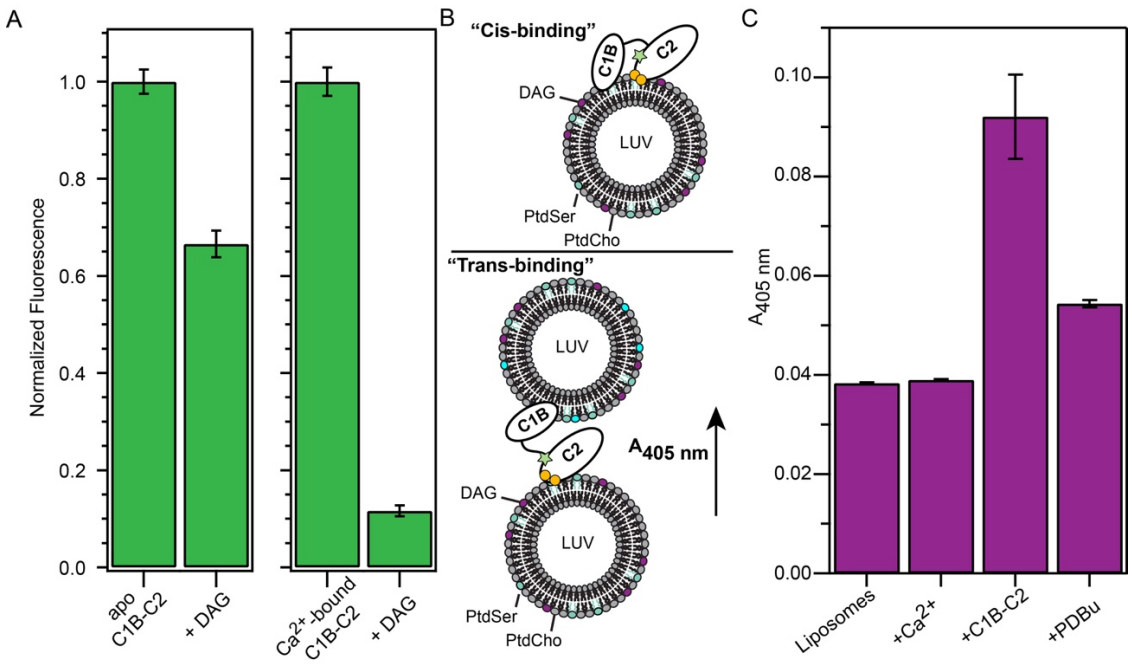

Figure V.9 C1B-C2 binds DAG and has the potential to tether liposomes. (A) Fluorescence of C1B-C2 K181C conjugated to Alexa 488 in the presence of sucrose-loaded vesicles containing 20% PS and 10% DAG normalized to the fluorescence in the absence of vesicles. (B) Schematic showing the two possible binding modes when both C1B and C2 interact with liposomes. (C) Absorbance of liposome solutions at 405 nm. Increases are caused by tethering of liposomes due to "trans" binding.

Another possibility is that in the absence of PIP2, C1B and C2 are not binding to the same liposome ("cis-binding") and are instead binding to neighboring liposomes ("trans-binding") as shown in Figure V.9B. The trans-binding mechanism causes turbidity in the samples due to the increase in apparent size of the liposomes. To distinguish between these two binding modes, the absorbance of the samples at 405 nm[202] (assay used by Liu et. al.[203]) was monitored, which increases when the solution becomes turbid. The addition of 0.3 mM free Ca^{2+} did not increase the turbidity of the sample (Figure V.9C). However, the addition of C1B-C2 in the presence of Ca^{2+}

doubled the absorbance, consistent with the trans-binding mechanism bridging the liposomes together. This was reversed upon addition of a 4-fold excess of PDBu (Figure V.9C). This is consistent with PDBu driving cis-binding and reversing the tethering. A higher concentration of protein (2 μM) was needed to achieve a measureable turbidity, leading to the possibility that trans binding is due to saturation of the available "cis" binding sites on the surface of the liposome. However, the decrease in absorbance upon the addition of PDBu suggests that the trans binding was disrupted, most likely through a switch to cis binding, consistent with the presence of enough space on the liposomes to bind in cis. Collectively, these experiments show that the lack of avidity with PS liposomes is not due to a lack of DAG binding and could be due to an inability of C1B and C2 to bind to the same bilayer surface. This also indicates that PIP2 in the membrane is essential for achieving the maximum coupling between C1 and C2 ligands.

Discussion and future directions

This work showed that C1Bα transiently pre-associates with bicelles in the absence of C1 ligands, and this occurs through the ligand-binding loops. This has been observed previously for C1 domains in micelles [103,204], but the details of the interaction have not been characterized for the C1Bα domain in a bilayer. The chemical shift perturbations and PRE patterns for C1Bα with bicelles were similar to those in the presence of ligands. This suggests that the insertion and membrane binding geometry of C1B is largely driven by the interactions with the membrane and are not fully dependent on the ligands. The bilayer interaction is weak in the absence of ligands, although it is likely to be stronger in the context of the full regulatory region due to membrane

interactions with C1A and C2 when Ca^{2+} is present. Residues in the loops β34 loop (L125, H127, Q128) had elevated ^{1}H R_2 values in the apo protein that are quenched upon ligand binding. G110 in the β12 loop was completely broadened due to exchange. These dynamics are quenched upon binding ligands although G110 has elevated R_2 values when C1Bα is bound to DOG.

There were subtle differences in the NMR signatures of C1B ligand binding. The PRE values were larger for C1Bα in the presence of DOG, which suggests that C1B inserts deeper into the membrane in the presence of DOG compared to PDBu. This is likely due to the bulkier head group of PDBu (Figure V.6). The shallower insertion in the presence of PDBu leaves the C1 domains more exposed and could contribute to this instability. Although PDBu is a higher affinity ligand for C1Ba, the membrane insertion is shallower. This indicates that the membrane insertion depth does not correlate with affinity.

Future directions with these data involve using restrained molecular dynamics simulations to obtain a structural model of C1Bα in complex with membranes. With the model for the C1Bα membrane complex in mind, backbone PRE and CSP that have already been collected as well as additional restraints collected for methyl groups will be used. There are several methyl groups in the membrane binding region. Triple resonance assignment experiments have already been collected and methyl groups for the C1Bα domain (Figure V.10) have been assigned. Several residues shift in response to PDBu/bicelle binding (Figure V.10).

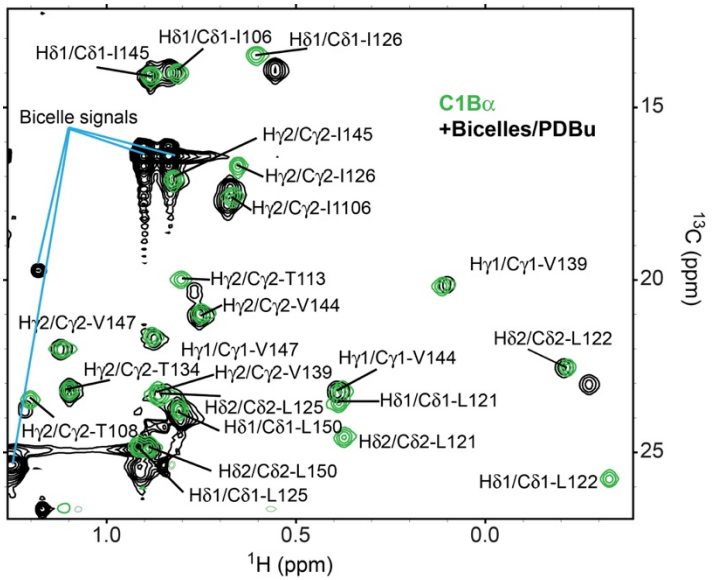

Figure V.10 Assigned methyl spectra of C1B. Overlay of ^{13}C-HMQC of apo U-^{15}N, ^{13}C C1Bα (green) and bound to PDBu in the presence of bicelles containing a PS and PIP2 component (black).

Additional work involves extending these studies to multi-domain regulatory regions from PKCα. Towards this goal, the feasibility of collecting restraints for C1B-C2 in complex with bicelles and PDBu has already been established. C1B-C2 bound to bicelles containing PS, PIP2 and PDBu. Notably, despite the large apparent molecular weight of the complex (~150 kDa), high quality spectra were obtained as shown in Figure V.11. Furthermore, chemical shift perturbations show that both C1 and C2 bind to the bicelle (Figure V.11).

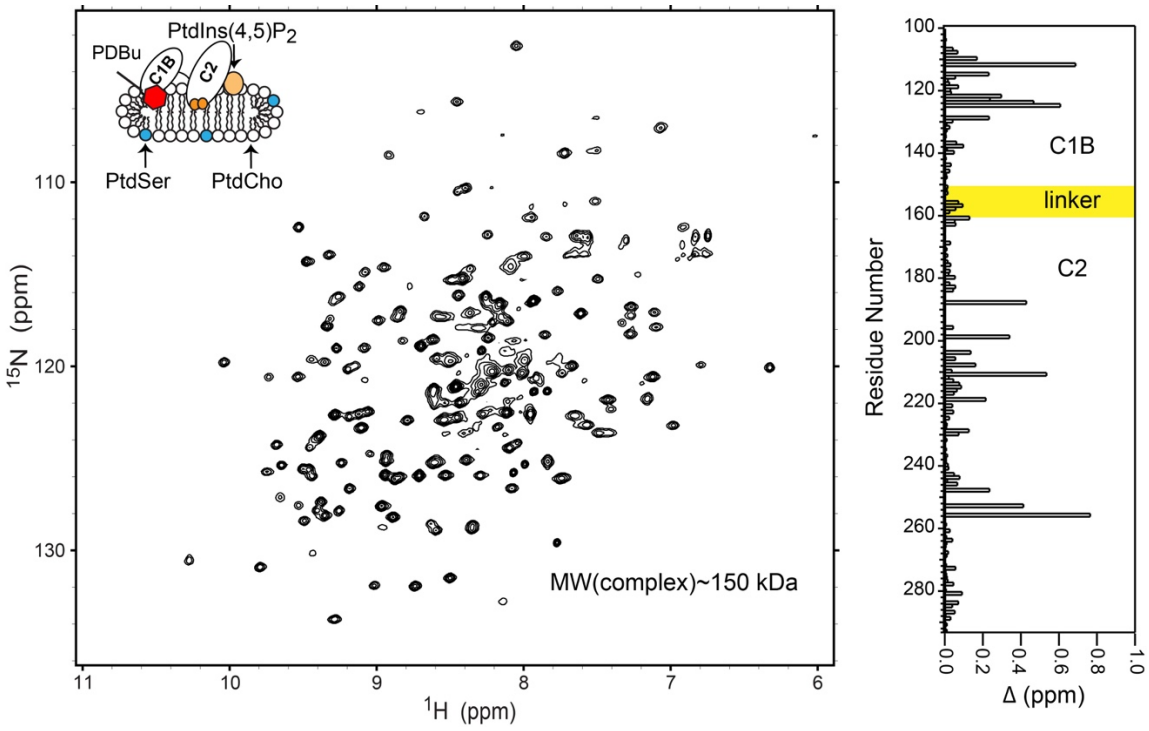

Figure V.11 Multi-component isotropic bicelle enables acquisition of high quality NMR spectra in the presence of Ca^{2+} and PDBu. (A) ^{15}N –TROSY spectra of C1B-C2 bound to bicelles. (B) Chemical shift perturbation analysis of C1B-C2 bound to isotropic bicelles indicates that both domains bind the bicelle in the presence of their ligands.

Our functional studies identify the linker region between C1 and C2 domains as a potential target to modulate the Ca^{2+} dependence of PKC in the presence of C1 ligands. By rigidifying the linker region with prolines a factor of 2-fold greater avidity was achieved between C1 and C2 ligands. The most plausible explanation for this is that by rigidifying the linker, the conformational space sampled by C1B and C2 decreased, lowering the entropic penalty for simultaneous membrane binding. In contrast, by maintaining the flexibility of the linker but changing its identity by substituting it with

glycines, the native coupling between the C1 and C2 membrane binding was preserved. This highlights the importance of the conformational heterogeneity and linker region in maintaining the balance in the activating power between C1 and C2 ligands.

Many of the existing drugs target C1 domains of PKC. [205,206] Modulating the flexibility of the linker could serve as a way to tune the activity of PKC in the presence of C1 activators. Furthermore, dynamic and transient interactions are crucial for cell signaling cascades. These data suggest that the flexible nature of the linker plays a role in maintaining the right balance of the PKC response to Ca^{2+} in the presence of PDBu. The Ca^{2+} response of C1B-C2 in the presence of diacylglycerol was less dependent on the flexibility of the linker region. This could be due to the fact that C1B/DAG's much weaker interactions than those of C1B/PDBu; conversely, independence gained could also be due to a difference in the membrane binding geometry.

Additionally, these studies revealed an additional role for PIP2 in regulating PKC. PIP_2 was essential to the enhancement of membrane interactions of C1B-C2 with DAG. Upon sensing Ca^{2+}, the C2 domain of conventional isoforms associates with PS molecules in the plasma membrane. One PS molecule is replaced by PIP2. Due to the bulky head group of PIP2, there is a change in the membrane binding geometry of the C2 domain.[52] These results suggest that the orientation change upon binding PIP2 may mediate simultaneous DAG binding to the C1B domain and to achieve full activation.

In this chapter, the objective is to elucidate how the PKCα regulatory domains interact with membranes in the presence of their native ligands and how these interactions differ when C1B is bound to tumor-promoting phorbol esters. Membrane binding of the C2 domain from the regulatory region of conventional PKCs and the subsequent membrane insertion of one or both C1 domains is required for full activation of conventional PKCs.[167,187] This process is modulated by metal ions [3,188], anionic lipids [189], and membrane-embedded diacylglycerol. However, the mechanistic details of the membrane association process are poorly understood. These studies focused on obtaining structural information about the interactions of the PKC regulatory domains with membrane mimetics and how these interactions modulate the Ca^{2+} requirements of membrane association.

Conventional isoforms contain tandem C1 domains preceding a Ca^{2+}-dependent C2 domain. The C2 domain binds both phosphatidylserine (PS) and phosphatidyl-inositol 4,5-bisphosphate (PIP2) in a Ca^{2+}-dependent manner. The native agonist for C1 domains is diacylglycerol, made available by the hydrolysis of PIP2. Like diacylglycerol, plant-derived phorbol esters can also facilitate the membrane association process of PKC but C1 domains have a much higher affinity for phorbol esters compared to diacylglycerol. Activation of PKC by phorbol esters leads to prolonged activation, faster downregulation of PKC [190] and tumorigenesis.[4,79,191] Researchers are limited in their design of potential PKC activators because of their phorbol ester-like tumor promoting activities. Therefore, understanding the structural differences in phorbol ester- and diacylglycerol-induced activation of PKC is extremely important for

designing better modulators of PKC that lack tumor-promoting activity. Despite the importance of PKC activators, existing information about C1 domain/membrane interactions is limited. This is, in part, largely due to the challenges of working with peripheral membrane binding proteins and selecting membrane mimetics that are both suitable for biophysical studies and physiologically relevant.

Upon binding C1 ligands hydrophilic residues in the binding cleft are masked, increasing the hydrophobicity of the domain and facilitating membrane insertion. [30] The membrane interactions of C1B domain from PKCδ has been explored in micelles with and without a short chain diacylglycerol analog, DOG. [167] The addition of DOG was found to change the depth of insertion. However, the lose packing and curvature of micelles does not always faithfully reproduce the conditions of a planar bilayer. Additional studies are needed in membrane mimetics containing a bilayer.

This chapter describes efforts towards obtaining structural information of the regulatory domains in complex with isotropically-tumbling bicelles in the presence of different C1 domain targeting cofactors, specifically diacylglycerol and phorbol 12,13-dibutyrate. Bicelles are composed of long chain lipids that form a bilayer with hydrophobic edges capped by short chain lipids. Bicelles have the advantage of a physiologically relevant bilayer packaged in a small NMR-friendly form.

In addition, conventional and novel PKCs have complex, multivalent interactions with membranes that require coordination of multiple domains and multiple ligands. To examine the multivalent nature of PKC, the interplay between metal ions and lipid-ligands in the membrane binding process will also be probed.

In this chapter, the objective is to elucidate how the PKCα regulatory domains interact with membranes in the presence of their native ligands and how these interactions differ when C1B is bound to tumor-promoting phorbol esters. Membrane binding of the C2 domain from the regulatory region of conventional PKCs and the subsequent membrane insertion of one or both C1 domains is required for full activation of conventional PKCs.[167,187] This process is modulated by metal ions [3,188], anionic lipids [189], and membrane-embedded diacylglycerol. However, the mechanistic details of the membrane association process are poorly understood. These studies focused on obtaining structural information about the interactions of the PKC regulatory domains with membrane mimetics and how these interactions modulate the Ca^{2+} requirements of membrane association.

Conventional isoforms contain tandem C1 domains preceding a Ca^{2+}-dependent C2 domain. The C2 domain binds both phosphatidylserine (PS) and phosphatidyl-inositol 4,5-bisphosphate (PIP2) in a Ca^{2+}-dependent manner. The native agonist for C1 domains is diacylglycerol, made available by the hydrolysis of PIP2. Like diacylglycerol, plant-derived phorbol esters can also facilitate the membrane association process of PKC but C1 domains have a much higher affinity for phorbol esters compared to diacylglycerol. Activation of PKC by phorbol esters leads to prolonged activation, faster downregulation of PKC [190] and tumorigenesis.[4,79,191] Researchers are limited in their design of potential PKC activators because of their phorbol ester-like tumor promoting activities. Therefore, understanding the structural differences in phorbol ester- and diacylglycerol-induced activation of PKC is extremely important for

designing better modulators of PKC that lack tumor-promoting activity. Despite the importance of PKC activators, existing information about C1 domain/membrane interactions is limited. This is, in part, largely due to the challenges of working with peripheral membrane binding proteins and selecting membrane mimetics that are both suitable for biophysical studies and physiologically relevant.

Upon binding C1 ligands hydrophilic residues in the binding cleft are masked, increasing the hydrophobicity of the domain and facilitating membrane insertion. [30] The membrane interactions of C1B domain from PKCδ has been explored in micelles with and without a short chain diacylglycerol analog, DOG. [167] The addition of DOG was found to change the depth of insertion. However, the lose packing and curvature of micelles does not always faithfully reproduce the conditions of a planar bilayer. Additional studies are needed in membrane mimetics containing a bilayer.

This chapter describes efforts towards obtaining structural information of the regulatory domains in complex with isotropically-tumbling bicelles in the presence of different C1 domain targeting cofactors, specifically diacylglycerol and phorbol 12,13-dibutyrate. Bicelles are composed of long chain lipids that form a bilayer with hydrophobic edges capped by short chain lipids. Bicelles have the advantage of a physiologically relevant bilayer packaged in a small NMR-friendly form.

In addition, conventional and novel PKCs have complex, multivalent interactions with membranes that require coordination of multiple domains and multiple ligands. To examine the multivalent nature of PKC, the interplay between metal ions and lipid-ligands in the membrane binding process will also be probed.

CHAPTER VI

SUMMARY AND FUTURE DIRECTIONS

The findings presented in this dissertation take the first steps towards assembling the trajectory of the full regulatory region of PKC during activation, by focusing on a multidomain construct containing both C1 and C2 domains.

Chapters II and IV provide methods to overcome the challenges associated with studying flexible, membrane-associated proteins. In Chapter II, the groundwork was laid for experiments for structural studies on the regulatory region of PKC by producing full-length regulatory regions from PKCδ and PKCα free of large, bulky solubility tags. The key findings of this chapter are (1) the development of robust expression and purification protocols that enables the production of both regulatory regions in quantities sufficient for biophysical studies and (2) design of mutants and incorporation of osmolytes that stabilize the fold and decrease the aggregation behavior of the regulatory regions. These optimizations facilitated the collected of the first, high-quality NMR spectra of each region, demonstrating the feasibility of structural studies on these regions.

In Chapter IV the challenges associated with the flexibility of the regulatory region of PKCα are overcome by using paramagnetic lanthanides to characterize the conformational space sampled by C1B-C2. This was made possible by the development of a protocol to separate the contributions from a transient intermolecular interaction to structural restraints. The use of the C1B-C2 regulatory region allowed access to the structure of the untethered state of the regulatory region prior to membrane insertion,

free from the intramolecular interaction between C1A and C2. There was a clear distinction between conformations that could and could not be sampled by C1B-C2. This study suggests that C1B-C2 samples orientations that are highly compatible with simultaneous membrane insertion. These findings add to the existing knowledge about the activation pathway of PKC. Despite its importance and despite the fact that PKC was discovered over 40 years ago, there is no structural information about this region during any stage of activation. This is important because understanding the structure is essential for understanding its function and how to modulate it. Gaps in our understanding are largely due to the ill behavior of the regulatory domains. They are amphiphilic, aggregation prone, and the flexibility of this region that is essential for its function, poses a challenge to structural biologists. This work overcomes these challenges to provide one of the first missing pieces to this puzzle. In the context of the activation pathway, it is shown that when autoinhibitory interactions of the parent enzyme are relieved, C1 and C2 domains adopt orientations with both membrane binding sites in the same plane in the absence of any activating ligands. This provides mechanistic information of how C1 and C2 domains coordinate interactions with membranes, through a preorganized membrane binding site. Functional studies using protein-to-membrane FRET were consistent with this. C1 ligands lowered the concentration of Ca^{2+} needed to drive C1B-C2 to PIP2 and PS doped LUVs.

An intermolecular association between neighboring C1B-C2 molecules was identified. Data indicates that the interface is between the C1B and C2 domains. Although there are no functional studies that indicate interactions between the C1B and

C2 domains, the high sequence identity with C1A (54% sequence similarity) and similarity in structure opens the possibility that the C1A-C2 mode of interaction is being probed. The C1A-C2 interaction is proposed to be one of the most important interactions for maintaining the latent for of the enzyme but the details are still unknown due to the notoriously ill behavior of C1Aα. However, the C1B domain is well behaved. The C1B and C2 interaction could be a means to probe the C1A/C2 interaction by using C1B as a surrogate. The feasibility of such studies has already been outlined in this dissertation. Both paramagnetic lanthanides bound to the C2 domain and PRE from tags bearing an unpaired electron can be used to get complementary structural information. Future studies should be aimed at obtaining a structural model of the C1B/C2 complex using paramagnetic agents and the knowledge from this can be applied to the C1A/C2 interaction. While the details remain elusive, Ca^{2+}-binding to the C2 domain is proposed to propagate to other regions of the protein through a change in the dynamics at the N- and C-termini to facilitate activation.[183] We did not observe any effect of Ca^{2+} binding on the sub-nanosecond dynamics of C1B-C2. However, an experiment reported here suggests a different possible mechanism for the propagation of the Ca^{2+} binding event. When U-^{15}N labeled C1B "NMR-visible" was mixed with ^{14}N-C2 K181C-MTSL "NMR-invisible", PRE was observed on C1B (Figure VI.1). This is consistent with an intermolecular interaction between C1B and C2. Interestingly, Ca^{2+} addition decreased the PRE observed on C1B. This suggests two things: (1) the site for C1B and C2 interaction is near the loop region of C2 and (2) Ca^{2+} binding to the loops of C2 breaks up the interaction. It is assumed that these experiments are probing the C1A-C2

interaction due to the similarities between C1B and C1A. Therefore, it is likely that Ca^{2+} binding to the loops provides electrostatic repulsion necessary to relieve this autoinhibitory interaction, leading to activation.

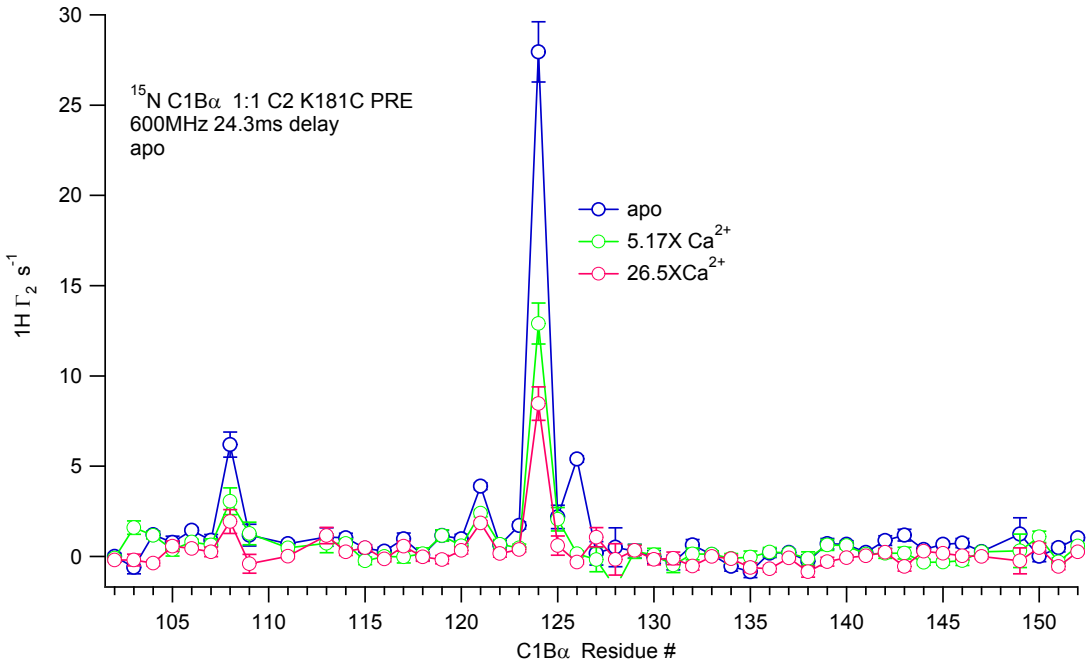

Figure VI.12 Ca^{2+} breaks up an intermolecular interaction between C1B and C2. Intermolecular $^{1}H\ \Gamma_2$ values plotted against the residue number for ^{15}N-C1B mixed with ^{14}N C2 K181C labeled with MTSL in the presence of increasing amounts of Ca^{2+}.

Chapter V details preliminary work on interactions of the regulatory domains with membrane mimics. Although it is known that C1 domains associate with membrane mimics in the absence of ligands, this work found that this interaction proceeds through the ligand binding loops in the presence of a bilayer and the interaction mode is similar in the presence of ligands. Although a structural model has not been

obtained yet, PRE data is consistent with the C1B domain being tilted with respect to the membrane, with the β34 loop penetrating deeper into the bilayer. Ligand identity did not change the overall PRE patterns, although in the presence of 1,2-dioctanoyl sn-glycerol (DOG), a short chain diacylglycerol (DAG) analogue, the magnitude of the PRE was larger, which indicates that DOG causes deeper penetration. The deeper penetration of C1B in the presence of DOG versus PDBu could potentially explain the increased down regulation of PKC mediated by PDBu. The large headgroup of PDBu could push C1B out, leaving its reactive cysteine more exposed and therefore PKC more vulnerable to reactive oxygen species. As a future direction, this can be tested by investigating the reactivity of this cysteine in the presence of PDBu/DOG doped membrane mimics. Future directions involve combining the restraints gathered and presented in this thesis with molecular dynamics simulations to obtain a structural model of the interactions of C1B with bilayers. This will shed light on the molecular mechanism of membrane interactions and the differences between PDBu and DOG.

Membrane studies were also extended to the C1B-C2 region. An NMR-friendly bicelle with all ligands necessary to bind both C1B and C2 domains was developed and characterized. These bicelles enabled high-quality $^{1}H,^{15}N$-TROSY spectra to be obtained and will facilitate the extension of structural studies to the C1-C2 membrane binding region. Finally, functional studies in this chapter found that the flexibility of the inter-domain linker region tunes the coordination between C1 and C2 membrane interactions in the presence of a strong C1 ligand. This could be an important tool for

designing drugs to target the regulatory region. The potency can be tuned by altering the rigidity of the linker region.

Membrane insertion of both C1 and C2 domains is required for full activation of conventional PKCs. Studies from Chapter V found that the low-abundance lipid, phosphatidylinositol 4,5-bisphosphate (PIP2), was absolutely essential for achieving the maximum thermodynamic benefits of bivalent binding in the presence of DAG. This is despite the finding that C1B-C2 is bound to DAG in the absence of PIP2 under the conditions in these experiments. Experiments show tethering of large unilamellar vesicles, which indicates that C1B-C2 can bind to neighboring liposomes. Therefore, the lack of avidity could be the result of simultaneous membrane insertion of C1B and C2 being disfavored. PIP2 is known to cause a change in the membrane binding of the C2 domain. These results suggest that this change in orientation could facilitate the ability of both domains to insert into the membrane. The small differences in the magnitude of PRE patterns with C1B in the presence of bicelles and C1 ligands could explain why. The deeper insertion of the C1 domain into the membrane in the presence of DAG could cause conformational strain relieved by tilting the C2 domain more perpendicular to the bilayer surface. PDBu abolished the need for PIP2 to achieve bivalency in membrane interactions. Another study hinted at the PIP2-dependence of combined C1-C2 membrane interactions.[81] In this study, the diffusion of the regulatory region was only decreased in the presence of PIP2/DAG containing membranes. DAG/PS/Ca^{2+} alone was insufficient to increase the drag afforded by two membrane interacting modules. However, the constructs used in this study had bulky MBP tags on

the proteins that complicate the analysis. Consistent with their findings, this work shows that PIP2 is essential for the multivalent interactions of C1 and C2 domains with membrane mimics and provides a direct measurement of avidity using tag-free proteins. Furthermore, while it is known that both C1 and C2 domain interactions with membranes are absolutely essential to achieving full activation, it is currently unknown if both domains, C1A, or C1B bind to the membranes in addition to C2. Collectively, our work suggests that at least in the case of the native ligand, DAG, C1B cannot be the sole C1 domain responsible for inserting into the membrane to facilitate interaction, unless PIP2 is available. One potential model is that in the absence of PIP2, C1A is the primary C1 domain responsible for membrane insertion. However, in the presence of PIP2 either the C1B domain or both the C1A and C1B domain insert into the membrane. This presents a previously unexplored, additional layer of regulation afforded by PIP2.

Finally, Chapter III details interactions of the regulatory region with xenobiotic metal ions, Pb^{2+} and Cd^{2+}. Two divalent ions are essential for the fold and function of the regulatory region of PKCs. C1 domains cannot fold properly without two Zn(II) ions. While the C2 domain does not need Ca^{2+} to fold properly, Ca^{2+} is essential to its function. This work finds that toxic metal ions interact with the regulatory region using two different modes: ionic mimicry and opportunistic binding. It was already known that both Pb^{2+} and Cd^{2+} can bind to the loops of the C2 domain. Here another mode of ionic mimicry is presented for Cd^{2+}: spontaneously replacing Zn^{2+} in the C1B domain. Solution NMR showed that Cd^{2+} was able to support the fold and function of isolated C1B. Furthermore, replacement started before the high-affinity sites on the C2 loops

were completely populated, indicating that the structural Zn-sites on C1B can compete with the C2 domain for Cd^{2+}. Pb^{2+}, in contrast, was not able to replace Zn^{2+} due to geometry preferences with an all sulfur coordination sphere. A unique property of the C1B domain in PKC is the presence of a reactive cysteine in the second Zn-site.[31] This is proposed to be the entry point for reactive oxygen species that activate PKC. Cd^{2+} has a larger ionic radius and is more polarizable than Zn^{2+}. Therefore, in proteins this often results in stronger bonds. Consistent with this, both sites had higher affinities to Cd^{2+} than to Zn^{2+}. The broad implication for replacement at this site is that Cd^{2+} could potentially protect C1B and, therefore, the parent enzyme from activation by reactive oxygen species. A future direction is to test this by comparing the reactivity of the C1B domain as a Cd-finger and a Zn-finger. This can be achieved by refolding C1B in the presence of Cd^{2+} and monitoring the reaction of the domain with a cysteine reactive tag. Opportunistic binding of both Pb^{2+} and Cd^{2+} was found to mediate self-association of C1B-C2. The regions identified, the interdomain linker and C-terminal helix of C2 have not been shown to bind Ca^{2+}. These regions of the protein are highly conserved in conventional enzymes. Therefore, it is plausible that other conventional enzymes could self-associate in the presence of Cd^{2+} and Pb^{2+}. In particular, PKCγ has been shown to have unmasked regulatory domains in the latent form and therefore would be the most susceptible to self-association driven by toxic metal ions. Very interestingly, there were no single nucleotide polymorphisms (SNPs) within these regions. Along with the high conservation of these regions, this indicates that these regions are likely extremely important for PKC function.

The most surprising finding of this study was that self-association enhanced interactions of the regulatory region with membranes. While previous studies showed that Cd^{2+} is unable to support binding of the isolated C2 domain to anionic membranes, both Pb^{2+} and Cd^{2+} supported the membrane binding of C1B-C2. This was attributed to the avidity of multiple weak interactions of C1B-C2 with membranes. Self-association, like Zn-replacement, starts to occur before the loops are fully populated with either metal ion, which indicates that both opportunistic binding and ionic mimicry are important for interactions of PKC with Pb^{2+} and Cd^{2+}. Several studies have shown that the self-association through the regulatory region is another mode of PKC regulation.[58,62-64] This has been shown to be mediated primarily by Ca^{2+}, the C1A domain, and the C2 domain. One proposed mechanism for regulation is sequestration of intramolecular interaction sites by intermolecular interactions.[57] Our studies show that self-association increases the affinity of the regulatory domains for membranes, suggesting an additional role for self-association in regulation. The exact mechanism of Ca^{2+} in driving self-association is unknown. Although we did not observe Ca^{2+} binding to the linker and the C-terminal helix, it is interesting to speculate that in the full length enzyme where both C1A and C2 are present to strengthen the intermolecular interactions, Ca^{2+} binding to these regions could stabilize the multimers. Support for this comes from two pieces of evidence: (1) there were minor chemical shift perturbations observed in the linker region between C1B-C2 upon Ca^{2+} addition (data not shown), (2) Ca^{2+} addition to isolated C2 gave rise to intermolecular PRE, indicating a transient intermolecular interaction mediated by Ca^{2+}.[183] The PRE pattern observed in the

isolated C2 domain resembles the predicted PRE from the conformation found in the PKC βII crystal structure.[61] In this structure, ligands from both the linker and the C-terminal helix mediate the dimerization of C2. Pb^{2+} and Cd^{2+} bind with much higher affinities to this region as the same concentrations of Ca^{2+} in our studies could not drive self-assembly. However, Ca^{2+} could be using a similar mechanism to mediate self-association but the C1A-C2 interaction is additionally needed because of the relatively weaker ability of Ca^{2+} to drive self-association. This can be explored using the conventional, full length regulatory domain construct from Chapter II.

The work presented in this dissertation sheds light on the interactions of xenobiotic metal ions with the regulatory region, but these ions can also potentially exert their toxic effects by acting on the kinase domain. The function of the kinase domain relies on the divalent metal ion, Mg^{2+}, to aid in catalysis. Other studies have investigated the ability of toxic metal ions to substitute for Mg^{2+} in kinase domains. One study was done on PKA, which is also a member of the AGC family of kinases and very similar to PKC. Cd^{2+} was found to bind to the kinase domain but was unable to fully support the function.[207] Cd^{2+} was able to support phosphoryl transfer to substrates but was unable to support substrate turnover. Additionally, functional studies have shown that both Cd^{2+} and Pb^{2+} can activate PKC at low concentrations and Pb^{2+} inhibits PKC at higher concentrations, revealing the complexity of PKC interactions with toxic metal ions.[17,18,118,121] Murakami et. al. found that high concentrations of Pb^{2+} inhibited both PKC and PKM, a proteolytically generated kinase domain fragment.[71] This effect was found to be reversible upon chelation of Pb^{2+} and suggests that the ability of Pb^{2+} to

inhibit PKC is, at least in part, a result of interactions with the kinase domain as Pb^{2+} was able to inhibit the isolated kinase domain. Mg^{2+} is present in the cell in millimolar quantities and therefore both Pb^{2+} and Cd^{2+} would both need to bind with high affinity to the kinase domain in order to substitute for Mg^{2+}. Currently, there is no information on the affinities of Cd^{2+} nor Pb^{2+} to the kinase domain. Binding affinities for the isolated kinase domain and structural studies on full length PKC in the presence of Pb^{2+} and Cd^{2+} are needed to understand the interplay between the interactions of Pb^{2+} and Cd^{2+} with kinase domain and the regulatory domain to understand which interactions are important for modulating activity. Collectively, the work outlined in this dissertation adds a mechanistic understanding of the behavior of the regulatory region before and after membrane insertion. Furthermore, it lays the foundation for structural studies extending to full-length regulatory regions. Finally, this work changes our understanding of the way that PKC interacts with toxic metal ions.

REFERENCES

(1) Takai, Y., Kishimoto, A., et al. (1977) Studies on a cyclic nucleotide-independent protein kinase and its proenzyme in mammalian tissues. I. Purification and characterization of an active enzyme from bovine cerebellum, *J Biol Chem 252*, 7603-7609.

(2) Inoue, M., Kishimoto, A., et al. (1977) Studies on a cyclic nucleotide-independent protein kinase and its proenzyme in mammalian tissues. II. Proenzyme and its activation by calcium-dependent protease from rat brain, *J Biol Chem 252*, 7610-7616.

(3) Takai, Y., Kishimoto, A., et al. (1979) Calcium-dependent activation of a multifunctional protein kinase by membrane phospholipids, *J Biol Chem 254*, 3692-3695.

(4) Arcoleo, J.P., and Weinstein, I.B. (1985) Activation of protein kinase C by tumor promoting phorbol esters, teleocidin and aplysiatoxin in the absence of added calcium, *Carcinogenesis 6*, 213-217.

(5) Kikkawa, U., Takai, Y., et al. (1983) Protein kinase C as a possible receptor protein of tumor-promoting phorbol esters, *J Biol Chem 258*, 11442-11445.

(6) Hug, H., and Sarre, T.F. (1993) Protein kinase C isoenzymes: divergence in signal transduction?, *Biochem J 291 (Pt 2)*, 329-343.

(7) Churchill, E., Budas, G., et al. (2008) PKC isozymes in chronic cardiac disease: possible therapeutic targets?, *Annu Rev Pharmacol Toxicol 48*, 569-599.

(8) Drosatos, K., Bharadwaj, K.G., et al. (2011) Cardiomyocyte lipids impair beta-adrenergic receptor function via PKC activation, *Am J Physiol Endocrinol Metab 300*, E489-499.

(9) Khan, T.K., Nelson, T.J., et al. (2009) A cellular model of Alzheimer's disease therapeutic efficacy: PKC activation reverses Abeta-induced biomarker abnormality on cultured fibroblasts, *Neurobiol Dis 34*, 332-339.

(10) Griner, E.M., and Kazanietz, M.G. (2007) Protein kinase C and other diacylglycerol effectors in cancer, *Nature Reviews Cancer 7*, 281-294.

(11) Kim, J., Thorne, S.H., et al. (2011) Sustained inhibition of PKCalpha reduces intravasation and lung seeding during mammary tumor metastasis in an in vivo mouse model, *Oncogene 30*, 323-333.

(12) Mandil, R., Ashkenazi, E., et al. (2001) Protein kinase Calpha and protein kinase Cdelta play opposite roles in the proliferation and apoptosis of glioma cells, *Cancer Res 61*, 4612-4619.

(13) Pham, T.N.D., Perez White, B.E., et al. (2017) Protein kinase C alpha enhances migration of breast cancer cells through FOXC2-mediated repression of p120-catenin, *BMC Cancer 17*, 832.

(14) Clark, A.S., West, K.A., et al. (2003) Altered protein kinase C (PKC) isoforms in non-small cell lung cancer cells: PKCdelta promotes cellular survival and chemotherapeutic resistance, *Cancer Res 63*, 780-786.

(15) Abrial, E., Lucas, G., et al. (2011) A role for the PKC signaling system in the pathophysiology and treatment of mood disorders: involvement of a functional imbalance?, *Mol Neurobiol 44*, 407-419.

(16) Markovac, J., and Goldstein, G.W. (1988) Picomolar concentrations of lead stimulate brain protein kinase C, *Nature 334*, 71-73.

(17) Beyersmann, D., Block, C., et al. (1994) Effects of cadmium on nuclear protein kinase C, *Environ Health Perspect 102 Suppl 3*, 177-180.

(18) Long, G.J. (1997) The effect of cadmium on cytosolic free calcium, protein kinase C, and collagen synthesis in rat osteosarcoma (ROS 17/2.8) cells, *Toxicol Appl Pharmacol 143*, 189-195.

(19) Sun, X., Tian, X., et al. (1999) Analysis of differential effects of Pb2+ on protein kinase C isozymes, *Toxicol Appl Pharmacol 156*, 40-45.

(20) Anilkumar, N., Parsons, M., et al. (2003) Interaction of fascin and protein kinase Calpha: a novel intersection in cell adhesion and motility, *EMBO J. 22*, 5390-5402.

(21) Dempsey, E.C., Newton, A.C., et al. (2000) Protein kinase C isozymes and the regulation of diverse cell responses, *Am. J. Physiol. Lung Cell Mol. Physiol. 279*, L429-438.

(22) Poole, A.W., Pula, G., et al. (2004) PKC-interacting proteins: from function to pharmacology, *Trends Pharmacol. Sci. 25*, 528-535.

(23) Nishikawa, K., Toker, A., et al. (1997) Determination of the specific substrate sequence motifs of protein kinase C isozymes, *J Biol Chem 272*, 952-960.

(24) House, C., and Kemp, B.E. (1987) Protein kinase C contains a pseudosubstrate prototope in its regulatory domain, *Science 238*, 1726-1728.

(25) Pears, C.J., Kour, G., et al. (1990) Mutagenesis of the pseudosubstrate site of protein kinase C leads to activation, *Eur J Biochem 194*, 89-94.

(26) Young, S., Rothbard, J., et al. (1988) A monoclonal antibody recognising the site of limited proteolysis of protein kinase C. Inhibition of down-regulation in vivo, *Eur J Biochem 173*, 247-252.

(27) Kishimoto, A., Kajikawa, N., et al. (1983) Proteolytic activation of calcium-activated, phospholipid-dependent protein kinase by calcium-dependent neutral protease, *J Biol Chem 258*, 1156-1164.

(28) Parente, J.E., Walsh, M.P., et al. (1992) Effects of the constitutively active proteolytic fragment of protein kinase C on the contractile properties of demembranated smooth muscle fibres, *J Muscle Res Cell Motil 13*, 90-99.

(29) Kazanietz, M.G. (2002) Novel "nonkinase" phorbol ester receptors: the C1 domain connection, *Mol Pharmacol 61*, 759-767.

(30) Zhang, G., Kazanietz, M.G., et al. (1995) Crystal structure of the cys2 activator-binding domain of protein kinase C delta in complex with phorbol ester, *Cell 81*, 917-924.

(31) Stewart, M.D., and Igumenova, T.I. (2012) Reactive Cysteine in the Structural Zn2+ Site of the C1B Domain from PKCα, *Biochemistry 51*, 7263-7277.

(32) Solution structure of the second Phorbol esters/diacylglycerol binding domain of human Protein kinase C alpha type FAU - Tochio, N., Koshiba, S., Saito, K., Tomizawa, T., Watanabe, S., Harada, T., Kigawa, T., Yokoyama, S. CRDT - 2007/03/27 12:00 AID - 10.2210/pdb2eli/pdb [doi].

(33) Xu, R.X., Pawelczyk, T., et al. (1997) NMR Structure of a Protein Kinase C-γ Phorbol-Binding Domain and Study of Protein−Lipid Micelle Interactions, *Biochemistry 36*, 10709-10717.

(34) Solution structure of the second C1 domain from human protein kinase C theta FAU - Nagashima, T., Hayashi, F., Yokoyama, S. CRDT - 2007/03/28 12:00 AID - 10.2210/pdb2enz/pdb [doi].

(35) Bittova, L., Stahelin, R.V., et al. (2001) Roles of ionic residues of the C1 domain in protein kinase C-alpha activation and the origin of phosphatidylserine specificity, *J Biol Chem 276*, 4218-4226.

(36) Pu, Y., Garfield, S.H., et al. (2009) Characterization of the differential roles of the twin C1a and C1b domains of protein kinase C-delta, *J Biol Chem 284*, 1302-1312.

(37) Ananthanarayanan, B., Stahelin, R.V., et al. (2003) Activation mechanisms of conventional protein kinase C isoforms are determined by the ligand affinity and conformational flexibility of their C1 domains, *J Biol Chem 278*, 46886-46894.

(38) Irie, K., Oie, K., et al. (1998) Molecular Basis for Protein Kinase C Isozyme-Selective Binding: The Synthesis, Folding, and Phorbol Ester Binding of the Cysteine-Rich Domains of All Protein Kinase C Isozymes, *Journal of the American Chemical Society 120*, 9159-9167.

(39) Stahelin, R.V., Digman, M.A., et al. (2004) Mechanism of diacylglycerol-induced membrane targeting and activation of protein kinase Cdelta, *J Biol Chem 279*, 29501-29512.

(40) Dries, D.R., Gallegos, L.L., et al. (2007) A single residue in the C1 domain sensitizes novel protein kinase C isoforms to cellular diacylglycerol production, *J Biol Chem 282*, 826-830.

(41) Giorgione, J.R., Lin, J.H., et al. (2006) Increased membrane affinity of the C1 domain of protein kinase Cdelta compensates for the lack of involvement of its C2 domain in membrane recruitment, *J Biol Chem 281*, 1660-1669.

(42) Perin, M.S., Brose, N., et al. (1991) Domain structure of synaptotagmin (p65), *J Biol Chem 266*, 623-629.

(43) Shao, X., Davletov, B.A., et al. (1996) Bipartite Ca2+-binding motif in C2 domains of synaptotagmin and protein kinase C, *Science 273*, 248-251.

(44) Cho, W., and Stahelin, R.V. (2006) Membrane binding and subcellular targeting of C2 domains, *Biochim Biophys Acta 1761*, 838-849.

(45) Ono, Y., Fujii, T., et al. (1989) Phorbol ester binding to protein kinase C requires a cysteine-rich zinc-finger-like sequence, *Proc Natl Acad Sci U S A 86*, 4868-4871.

(46) Davletov, B.A., and Südhof, T.C. (1993) A single C2 domain from synaptotagmin I is sufficient for high affinity Ca2+/phospholipid binding, *Journal of Biological Chemistry 268*, 26386-26390.

(47) Sutton, R.B., Davletov, B.A., et al. (1995) Structure of the first C2 domain of synaptotagmin I: a novel Ca2+/phospholipid-binding fold, *Cell 80*, 929-938.

(48) Medkova, M., and Cho, W. (1998) Mutagenesis of the C2 domain of protein kinase C-alpha. Differential roles of Ca2+ ligands and membrane binding residues, *J Biol Chem 273*, 17544-17552.

(49) Kohout, S.C., Corbalan-Garcia, S., et al. (2002) C2 domains of protein kinase C isoforms alpha, beta, and gamma: activation parameters and calcium stoichiometries of the membrane-bound state, *Biochemistry 41*, 11411-11424.

(50) Morales, K.A., Lasagna, M., et al. (2011) Pb2+ as modulator of protein-membrane interactions, *J Am Chem Soc 133*, 10599-10611.

(51) Morales, K.A., Yang, Y., et al. (2013) Cd2+ as a Ca2+ surrogate in protein-membrane interactions: isostructural but not isofunctional, *J Am Chem Soc 135*, 12980-12983.

(52) Landgraf, K.E., Malmberg, N.J., et al. (2008) Effect of PIP2 binding on the membrane docking geometry of PKC alpha C2 domain: an EPR site-directed spin-labeling and relaxation study, *Biochemistry 47*, 8301-8316.

(53) Guerrero-Valero, M., Marin-Vicente, C., et al. (2007) The C2 domains of classical PKCs are specific PtdIns(4,5)P2-sensing domains with different affinities for membrane binding, *J Mol Biol 371*, 608-621.

(54) Guerrero-Valero, M., Ferrer-Orta, C., et al. (2009) Structural and mechanistic insights into the association of PKCalpha-C2 domain to PtdIns(4,5)P2, *Proc Natl Acad Sci U S A 106*, 6603-6607.

(55) Evans, J.H., Murray, D., et al. (2006) Specific translocation of protein kinase Calpha to the plasma membrane requires both Ca2+ and PIP2 recognition by its C2 domain, *Mol Biol Cell 17*, 56-66.

(56) Antal, C.E., Violin, J.D., et al. (2014) Intramolecular conformational changes optimize protein kinase C signaling, *Chem Biol 21*, 459-469.

(57) Stahelin, R.V., Wang, J., et al. (2005) The origin of C1A-C2 interdomain interactions in protein kinase Calpha, *J Biol Chem 280*, 36452-36463.

(58) Slater, S.J., Seiz, J.L., et al. (2002) Regulation of PKC alpha activity by C1-C2 domain interactions, *J Biol Chem 277*, 15277-15285.

(59) Yang, Y., Shu, C., et al. (2018) Structural Basis of Protein Kinase Calpha Regulation by the C-Terminal Tail, *Biophys J 114*, 1590-1603.

(60) Stensman, H., and Larsson, C. (2007) Identification of acidic amino acid residues in the protein kinase C alpha V5 domain that contribute to its insensitivity to diacylglycerol, *J Biol Chem 282*, 28627-28638.

(61) Leonard, T.A., Rozycki, B., et al. (2011) Crystal structure and allosteric activation of protein kinase C betaII, *Cell 144*, 55-66.

(62) Huang, S.M., Leventhal, P.S., et al. (1999) Calcium and phosphatidylserine stimulate the self-association of conventional protein kinase C isoforms, *Biochemistry 38*, 12020-12027.

(63) Swanson, C.J., Ritt, M., et al. (2014) Conserved modular domains team up to latch-open active protein kinase Calpha, *J Biol Chem 289*, 17812-17829.

(64) Swanson, C.J., Sommese, R.F., et al. (2016) Calcium Stimulates Self-Assembly of Protein Kinase C alpha In Vitro, *PLoS One 11*, e0162331.

(65) Abadin, H., Ashizawa, A., et al. (2007) In *Toxicological Profile for Lead*, Atlanta (GA).

(66) Faroon, O., Ashizawa, A., et al. (2012) In *Toxicological Profile for Cadmium*, Atlanta (GA).

(67) Jarup, L., Berglund, M., et al. (1998) Health effects of cadmium exposure--a review of the literature and a risk estimate, *Scand. J. Work. Environ. Health 24 Suppl 1*, 1-51.

(68) Waalkes, M.P. (2003) Cadmium carcinogenesis, *Mutat. Res. 533*, 107-120.

(69) Waalkes, M.P., and Rehm, S. (1992) Carcinogenicity of oral cadmium in the male Wistar (WF/NCr) rat: effect of chronic dietary zinc deficiency, *Fundam Appl Toxicol 19*, 512-520.

(70) Needleman, H.L., Schell, A., et al. (1990) The long-term effects of exposure to low doses of lead in childhood. An 11-year follow-up report, *N. Engl. J. Med. 322*, 83-88.

(71) Murakami, K., Feng, G., et al. (1993) Inhibition of brain protein kinase C subtypes by lead, *J Pharmacol Exp Ther 264*, 757-761.

(72) Long, G.J., Rosen, J.F., et al. (1994) Lead activation of protein kinase C from rat brain. Determination of free calcium, lead, and zinc by 19F NMR, *J Biol Chem 269*, 834-837.

(73) Rajanna, B., Chetty, C.S., et al. (1995) Modulation of protein kinase C by heavy metals, *Toxicol Lett 81*, 197-203.

(74) Speizer, L.A., Watson, M.J., et al. (1989) Inhibition of phorbol ester binding and protein kinase C activity by heavy metals, *J Biol Chem 264*, 5581-5585.

(75) Dailianis, S., and Kaloyianni, M. (2004) Cadmium induces both pyruvate kinase and Na+/H+ exchanger activity through protein kinase C mediated signal transduction, in isolated digestive gland cells of Mytilus galloprovincialis (L.), *Journal of Experimental Biology 207*, 1665.

(76) Hecker, E. (1968) Cocarcinogenic principles from the seed oil of Croton tiglium and from other Euphorbiaceae, *Cancer Res 28*, 2338-2349.

(77) Boutwell, R.K. (1974) The function and mechanism of promoters of carcinogenesis, *CRC Crit Rev Toxicol 2*, 419-443.

(78) Betz, A., Ashery, U., et al. (1998) Munc13-1 is a presynaptic phorbol ester receptor that enhances neurotransmitter release, *Neuron 21*, 123-136.

(79) Castagna, M., Takai, Y., et al. (1982) Direct activation of calcium-activated, phospholipid-dependent protein kinase by tumor-promoting phorbol esters, *J Biol Chem 257*, 7847-7851.

(80) Giorgione, J., Hysell, M., et al. (2003) Contribution of the C1A and C1B domains to the membrane interaction of protein kinase C, *Biochemistry 42*, 11194-11202.

(81) Ziemba, B.P., Li, J., et al. (2014) Single-molecule studies reveal a hidden key step in the activation mechanism of membrane-bound protein kinase C-alpha, *Biochemistry 53*, 1697-1713.

(82) Pu, Y., Perry, N.A., et al. (2005) A novel diacylglycerol-lactone shows marked selectivity in vitro among C1 domains of protein kinase C (PKC) isoforms alpha and delta as well as selectivity for RasGRP compared with PKCalpha, *The Journal of biological chemistry 280*, 27329-27338.

(83) Bell, M.R., Engleka, M.J., et al. (2013) To fuse or not to fuse: what is your purpose?, *Protein science : a publication of the Protein Society 22*, 1466-1477.

(84) Roffey, J., Rosse, C., et al. (2009) Protein kinase C intervention: the state of play, *Curr Opin Cell Biol 21*, 268-279.

(85) Benes, C.H., Wu, N., et al. (2005) The C2 domain of PKC delta is a phosphotyrosine binding domain, *Cell 121*, 271-280.

(86) Stahelin, R.V., Kong, K.F., et al. (2012) Protein Kinase C theta C2 Domain Is a Phosphotyrosine Binding Module That Plays a Key Role in Its Activation, *Journal of Biological Chemistry 287*, 30518-30528.

(87) House, C., and Kemp, B.E. (1987) Protein Kinase C contains a pseudosubstrate prototype in its regulatory domain, *Science 238*, 1726-1728.

(88) Nishikawa, K., Toker, A., et al. (1997) Determination of the specific substrate sequence motifs of protein kinase C isozymes, *Journal of Biological Chemistry 272*, 952-960.

(89) Orr, J.W., and Newton, A.C. (1994) Intrapeptide regulation of Protein Kinase C, *Journal of Biological Chemistry 269*, 8383-8387.

(90) Pears, C.J., Kour, G., et al. (1990) Mutagenesis of the pseudosubstrate site of Protein Kinase C leads to activation, *European Journal of Biochemistry 194*, 89-94.

(91) Parissenti, A.M., Kim, S.A., et al. (1996) Regulatory domain of human protein kinase C alpha dominantly inhibits protein kinase C beta-I-regulated growth and morphology in Saccharomyces cerevisiae, *J Cell Physiol 166*, 609-617.

(92) Schultz, A., Jonsson, J.I., et al. (2003) The regulatory domain of protein kinase Ctheta localises to the Golgi complex and induces apoptosis in neuroblastoma and Jurkat cells, *Cell Death Differ 10*, 662-675.

(93) Zeidman, R., Lofgren, B., et al. (1999) PKCepsilon, via its regulatory domain and independently of its catalytic domain, induces neurite-like processes in neuroblastoma cells, *J Cell Biol 145*, 713-726.

(94) Irie, K., Nakahara, A., et al. (2002) Establishment of a binding assay for protein kinase C isozymes using synthetic C1 peptides and development of new medicinal leads with protein kinase C isozyme and C1 domain selectivity, *Pharmacology & Therapeutics 93*, 271-281.

(95) Cho, W., Digman M., et al. (2003) Bacterial expression and purification of C1 and C2 domains of protein kinase C isoforms, In *Protein Kinase C Protocols* (Newton, A. C., Ed.), pp 291-298.

(96) Medkova, M., and Cho, W. (1999) Interplay of C1 and C2 domains of protein kinase C-alpha in its membrane binding and activation, *J. Biol. Chem. 274*, 19852-19861.

(97) Cole, T.R., and Igumenova, T.I. (2015) Expression and purification of the N-terminal regulatory domain of Protein Kinase C for biophysical studies, *Protein Expr Purif 110*, 14-21.

(98) Mori, S., Abeygunawardana, C., et al. (1995) Improved sensitivity of HSQC spectra of exchanging protons at short interscan delays using a new fast HSQC (FHSQC) detection scheme that avoids water saturation, *Journal of Magnetic Resonance Series B 108*, 94-98.

(99) Butt, T.R., Edavettal, S.C., et al. (2005) SUMO fusion technology for difficult-to-express proteins, *Protein Expression and Purification 43*, 1-9.

(100) Marley, J., Lu, M., et al. (2001) A method for efficient isotopic labeling of recombinant proteins, *Journal of Biomolecular Nmr 20*, 71-75.

(101) Kumar, R. (2009) Role of naturally occurring osmolytes in protein folding and stability, *Archives of Biochemistry and Biophysics 491*, 1-6.

(102) Matthews, S., and Leatherbarrow, R. (1993) The use of osmolytes to facilitate protein NMR spectroscopy, *Journal of Biomolecular NMR 3*, 597-600.

(103) Stewart, M.D., Morgan, B., et al. (2011) Probing the determinants of diacylglycerol binding affinity in the C1B domain of protein kinase Calpha, *J Mol Biol 408*, 949-970.

(104) Stewart, M.D., Cole, T.R., et al. (2014) Interfacial partitioning of a loop hinge residue contributes to diacylglycerol affinity of conserved region 1 domains, *Journal of Biological Chemistry pii: jbc.M114.585570*.

(105) Islam, M.M., Khan, M.A., et al. (2012) Analysis of amino acid contributions to protein solubility using short peptide tags fused to a simplified BPTI variant, *Biochimica Et Biophysica Acta-Proteins and Proteomics 1824*, 1144-1150.

(106) Kato, A., Maki, K., et al. (2007) Mutational analysis of protein solubility enhancement using short peptide tags, *Biopolymers 85*, 12-18.

(107) Golovanov, A.P., Hautbergue, G.M., et al. (2004) A simple method for improving protein solubility and long-term stability, *J Am Chem Soc 126*, 8933-8939.

(108) Rabinowitz, M.B. (1991) Toxicokinetics of bone lead, *Environ. Health Perspect. 91*, 33-37.

(109) Sigel, A., Sigel, H., et al. (2013) *Cadmium : from toxicity to essentiality*, Springer, Dordrecht ; New York.

(110) Habermann, E., Crowell, K., et al. (1983) Lead and Other Metals Can Substitute for Ca-2+ in Calmodulin, *Arch. Toxicol. 54*, 61-70.

(111) Ouyang, H., and Vogel, H.J. (1998) Metal ion binding to calmodulin: NMR and fluorescence studies, *Biometals 11*, 213-222.

(112) Bouton, C.M., Frelin, L.P., et al. (2001) Synaptotagmin I is a molecular target for lead, *J. Neurochem. 76*, 1724-1735.

(113) Pan, T., Freedman, L.P., et al. (1990) Cadmium-113 NMR studies of the DNA binding domain of the mammalian glucocorticoid receptor, *Biochemistry 29*, 9218-9225.

(114) Michalek, J.L., Lee, S.J., et al. (2012) Cadmium coordination to the zinc binding domains of the non-classical zinc finger protein Tristetraprolin affects RNA binding selectivity, *J. Inorg. Biochem. 112*, 32-38.

(115) Huang, M., Krepkiy, D., et al. (2004) Zn-, Cd-, and Pb-transcription factor IIIA: properties, DNA binding, and comparison with TFIIIA-finger 3 metal complexes, *J. Inorg. Biochem. 98*, 775-785.

(116) Malgieri, G., Zaccaro, L., et al. (2011) Zinc to cadmium replacement in the A. thaliana SUPERMAN Cys(2) His(2) zinc finger induces structural rearrangements of typical DNA base determinant positions, *Biopolymers 95*, 801-810.

(117) Ghering, A.B., Jenkins, L.M., et al. (2005) Spectroscopic and functional determination of the interaction of Pb2+ with GATA proteins, *J. Am. Chem. Soc. 127*, 3751-3759.

(118) Block, C., Freyermuth, S., et al. (1992) Role of cadmium in activating nuclear protein kinase C and the enzyme binding to nuclear protein, *J. Biol. Chem. 267*, 19824-19828.

(119) Lawal, A.O., and Ellis, E.M. (2011) Nrf2-mediated adaptive response to cadmium-induced toxicity involves protein kinase C delta in human 1321N1 astrocytoma cells, *Environ. Toxicol. Pharmacol. 32*, 54-62.

(120) Suszkiw, J.B. (2004) Presynaptic disruption of transmitter release by lead, *Neurotoxicology 25*, 599-604.

(121) Shindo, M., Irie, K., et al. (2003) Analysis of the non-covalent interaction between metal ions and the cysteine-Rich domain of protein kinase C eta by electrospray ionization mass spectrometry, *Biorg. Med. Chem. 11*, 5075-5082.

(122) Ahmed, S., Kozma, R., et al. (1991) The cysteine-rich domain of human proteins, neuronal chimaerin, protein kinase C and diacylglycerol kinase binds zinc. Evidence for the involvement of a zinc-dependent structure in phorbol ester binding, *Biochem. J. 280 (Pt 1)*, 233-241.

(123) Newton, A.C. (2001) Protein kinase C: structural and spatial regulation by phosphorylation, cofactors, and macromolecular interactions, *Chem. Rev. 101*, 2353-2364.

(124) Morales, K.A., Yang, Y., et al. (2013) Cd2+ as a Ca2+ Surrogate in Protein-Membrane Interactions: Isostructural but Not Isofunctional, *J. Am. Chem. Soc. 135*, 12980-12983.

(125) Morales, K.A., and Igumenova, T.I. (2012) Synergistic effect of Pb(2+) and phosphatidylinositol 4,5-bisphosphate on C2 domain-membrane interactions, *Biochemistry 51*, 3349-3360.

(126) Morales, K.A., Lasagna, M., et al. (2011) Pb2+ as Modulator of Protein-Membrane Interactions, *J. Am. Chem. Soc. 133*, 10599-10611.

(127) Colon-Gonzalez, F., and Kazanietz, M.G. (2006) C1 domains exposed: from diacylglycerol binding to protein-protein interactions, *Biochim. Biophys. Acta 1761*, 827-837.

(128) Nalefski, E.A., and Falke, J.J. (1996) The C2 domain calcium-binding motif: structural and functional diversity, *Protein Sci. 5*, 2375-2390.

(129) Hurley, J.H., Newton, A.C., et al. (1997) Taxonomy and function of C1 protein kinase C homology domains, *Protein Sci. 6*, 477-480.

(130) Marley, J., Lu, M., et al. (2001) A method for efficient isotopic labeling of recombinant proteins, *J. Biomol. NMR 20*, 71-75.

(131) Delaglio, F., Grzesiek, S., et al. (1995) NMRPipe: a multidimensional spectral processing system based on UNIX pipes, *J. Biomol. NMR 6*, 277-293.

(132) Si, Y.X., Lee, J., et al. (2015) Molecular dynamics simulations integrating kinetics for Pb2+-induced arginine kinase inactivation and aggregation, *Process Biochem. 50*, 729-737.

(133) Yamazaki, T., Lee, W., et al. (1994) A Suite of Triple-Resonance Nmr Experiments for the Backbone Assignment of N-15, C-13, H-2 Labeled Proteins with High-Sensitivity, *J. Am. Chem. Soc. 116*, 11655-11666.

(134) Muhandiram, D.R., and Kay, L.E. (1994) Gradient-Enhanced Triple-Resonance 3-Dimensional Nmr Experiments with Improved Sensitivity, *J. Magn. Reson., Ser B 103*, 203-216.

(135) Classen, S., Hura, G.L., et al. (2013) Implementation and performance of SIBYLS: a dual endstation small-angle X-ray scattering and macromolecular crystallography beamline at the Advanced Light Source, *J. Appl. Crystallogr. 46*, 1-13.

(136) Rambo, R.P., and Tainer, J.A. (2013) Accurate assessment of mass, models and resolution by small-angle scattering, *Nature 496*, 477-481.

(137) Durand, D., Vives, C., et al. (2010) NADPH oxidase activator p67(phox) behaves in solution as a multidomain protein with semi-flexible linkers, *J. Struct. Biol. 169*, 45-53.

(138) Atkins, C.G., Banu, L., et al. (2009) Structure of [Pb(Gly-H)]+ and the monosolvated water and methanol solvated species by infrared multiple-photon dissociation spectroscopy, energy-resolved collision-induced dissociation, and electronic structure calculations, *J Phys Chem B 113*, 14457-14464.

(139) Nikol, H., Alexander Becht and Arnd Vogler. (1992) Photoluminescence of Germanium(II), Tin(II), and Lead(II) Chloride Complexes in Solution., *Inorganic Chemistry 31*, 3211-3219.

(140) Demeler, B., and van Holde, K.E. (2004) Sedimentation velocity analysis of highly heterogeneous systems, *Anal. Biochem. 335*, 279-288.

(141) Demeler, B. (2005) UltraScan - A Comprehensive Data Analysis Software Package for Analytical Ultracentrifugation Experiments, In *Analytical Ultracentrifugation: Techniques and Methods*, pp 210-230.

(142) Valentine, R.C., Shapiro, B.M., et al. (1968) Regulation of Glutamine Synthetase .12. Electron Microscopy of Enzyme from Escherichia Coli, *Biochemistry 7*, 2143-+.

(143) Johnson, J.E., Giorgione, J., et al. (2000) The C1 and C2 domains of protein kinase C are independent membrane targeting modules, with specificity for phosphatidylserine conferred by the C1 domain, *Biochemistry 39*, 11360-11369.

(144) Busenlehner, L.S., Cosper, N.J., et al. (2001) Spectroscopic properties of the metalloregulatory Cd(II) and Pb(II) sites of S. aureus pI258 CadC, *Biochemistry 40*, 4426-4436.

(145) Clapp, L.A., Siddons, C.J., et al. (2006) The amide oxygen donor. Metal ion coordinating properties of the ligand nitrilotriacetamide. A thermodynamic and crystallographic study, *Dalton Trans*, 2001-2007.

(146) Payne, J.C., ter Horst, M.A., et al. (1999) Lead Fingers: Pb2+ Binding to Structural Zinc-Binding Domains Determined Directly by Monitoring Lead−Thiolate Charge-Transfer Bands, *J. Am. Chem. Soc. 121*, 6850-6855.

(147) Stewart, M.D., and Igumenova, T.I. (2017) Toggling of Diacylglycerol Affinity Correlates with Conformational Plasticity in C1 Domains, *Biochemistry 56*, 2637-2640.

(148) Tomsig, J.L., and Suszkiw, J.B. (1995) Multisite interactions between Pb2+ and protein kinase C and its role in norepinephrine release from bovine adrenal chromaffin cells, *J Neurochem 64*, 2667-2673.

(149) Hubbard, S.R., Bishop, W.R., et al. (1991) Identification and characterization of zinc binding sites in protein kinase C, *Science 254*, 1776-1779.

(150) Magyar, J.S., Weng, T.C., et al. (2005) Reexamination of lead(II) coordination preferences in sulfur-rich sites: implications for a critical mechanism of lead poisoning, *J. Am. Chem. Soc. 127*, 9495-9505.

(151) Friedman, R. (2014) Structural and computational insights into the versatility of cadmium binding to proteins, *Dalton T 43*, 2878-2887.

(152) Zhu, H.L., Meng, S.R., et al. (2011) Fibrillization of Human Tau Is Accelerated by Exposure to Lead via Interaction with His-330 and His-362, *PLoS One 6*.

(153) Hayakawa, A., Hayes, S.J., et al. (2004) Structural basis for endosomal targeting by FYVE domains, *J. Biol. Chem. 279*, 5958-5966.

(154) Katti, S., Nyenhuis, S.B., et al. (2017) Non-Native Metal Ion Reveals the Role of Electrostatics in Synaptotagmin 1-Membrane Interactions, *Biochemistry 56*, 3283-3295.

(155) Mochly-Rosen, D., and Koshland, D.E., Jr. (1987) Domain structure and phosphorylation of protein kinase C, *J. Biol. Chem. 262*, 2291-2297.

(156) Kirberger, M., and Yang, J.J. (2008) Structural differences between Pb2+- and Ca2+-binding sites in proteins: implications with respect to toxicity, *J Inorg Biochem 102*, 1901-1909.

(157) Bonny, M., Hui, X., et al. (2016) C2-domain mediated nano-cluster formation increases calcium signaling efficiency, *Sci. Rep. 6*, 36028.

(158) Garcia, R.A., and Godwin, H.A. (2004) High metal concentrations are required for self-association of synaptotagmin II, *Biophys. J. 86*, 2455-2466.

(159) Kirberger, M., Wong, H.C., et al. (2013) Metal toxicity and opportunistic binding of Pb(2+) in proteins, *J. Inorg. Biochem. 125*, 40-49.

(160) Erskine, P.T., Duke, E.M., et al. (2000) MAD analyses of yeast 5-aminolaevulinate dehydratase: their use in structure determination and in defining the metal-binding sites, *Acta Crystallogr D Biol Crystallogr 56*, 421-430.

(161) Bertini, I., Ferella, L., et al. (2012) MaxOcc: a web portal for maximum occurrence analysis, *J Biomol NMR 53*, 271-280.

(162) Luchinat, C., Nagulapalli, M., et al. (2012) Maximum occurrence analysis of protein conformations for different distributions of paramagnetic metal ions within flexible two-domain proteins, *J Magn Reson 215*, 85-93.

(163) Tria, G., Mertens, H.D., et al. (2015) Advanced ensemble modelling of flexible macromolecules using X-ray solution scattering, *IUCrJ 2*, 207-217.

(164) Bista, M., Wolf, S., et al. (2013) Transient protein states in designing inhibitors of the MDM2-p53 interaction, *Structure 21*, 2143-2151.

(165) Joerger, A.C., Bauer, M.R., et al. (2015) Exploiting Transient Protein States for the Design of Small-Molecule Stabilizers of Mutant p53, *Structure 23*, 2246-2255.

(166) Teague, S.J. (2003) Implications of protein flexibility for drug discovery, *Nat Rev Drug Discov 2*, 527-541.

(167) Igumenova, T.I. (2015) Dynamics and Membrane Interactions of Protein Kinase C, *Biochemistry 54*, 4953-4968.

(168) Stewart, M.D., and Igumenova, T.I. (2012) Reactive cysteine in the structural Zn(2+) site of the C1B domain from PKCalpha, *Biochemistry 51*, 7263-7277.

(169) Findeisen, M., Brand, T., et al. (2007) A 1H-NMR thermometer suitable for cryoprobes, *Magn Reson Chem 45*, 175-178.

(170) Farrow, N.A., Muhandiram, R., et al. (1994) Backbone dynamics of a free and phosphopeptide-complexed Src homology 2 domain studied by 15N NMR relaxation, *Biochemistry 33*, 5984-6003.

(171) Ferrage, F., Reichel, A., et al. (2010) On the measurement of (1)(5)N-{(1)H} nuclear Overhauser effects. 2. Effects of the saturation scheme and water signal suppression, *J Magn Reson 207*, 294-303.

(172) Ferrage, F., Cowburn, D., et al. (2009) Accurate sampling of high-frequency motions in proteins by steady-state (15)N-{(1)H} nuclear Overhauser effect measurements in the presence of cross-correlated relaxation, *J Am Chem Soc 131*, 6048-6049.

(173) Gong, Q., and Ishima, R. (2007) 15N-{1H} NOE experiment at high magnetic field strengths, *J Biomol NMR 37*, 147-157.

(174) Berlin, K., Longhini, A., et al. (2013) Deriving quantitative dynamics information for proteins and RNAs using ROTDIF with a graphical user interface, *J Biomol NMR 57*, 333-352.

(175) Tjandra, N., Feller, S.E., et al. (1995) Rotational diffusion anisotropy of human ubiquitin from 15N NMR relaxation, *Journal of the American Chemical Society 117*, 12562-12566.

(176) Garcia de la Torre, J., Huertas, M.L., et al. (2000) HYDRONMR: prediction of NMR relaxation of globular proteins from atomic-level structures and hydrodynamic calculations, *J Magn Reson 147*, 138-146.

(177) Bernado, P., Fernandes, M.X., et al. (2004) Interpretation of NMR relaxation properties of Pin1, a two-domain protein, based on Brownian dynamic simulations, *J Biomol NMR 29*, 21-35.

(178) Jacobs, D.M., Saxena, K., et al. (2003) Peptide binding induces large scale changes in inter-domain mobility in human Pin1, *J Biol Chem 278*, 26174-26182.

(179) Rinaldelli, M., Carlon, A., et al. (2015) FANTEN: a new web-based interface for the analysis of magnetic anisotropy-induced NMR data, *J Biomol NMR 61*, 21-34.

(180) Iwahara, J., Tang, C., et al. (2007) Practical aspects of (1)H transverse paramagnetic relaxation enhancement measurements on macromolecules, *J Magn Reson 184*, 185-195.

(181) Andralojc, W., Luchinat, C., et al. (2014) Exploring regions of conformational space occupied by two-domain proteins, *J Phys Chem B 118*, 10576-10587.

(182) Bertini, I., Giachetti, A., et al. (2010) Conformational space of flexible biological macromolecules from average data, *J Am Chem Soc 132*, 13553-13558.

(183) Morales, K.A., Yang, Y., et al. (2016) Dynamic Response of the C2 Domain of Protein Kinase Calpha to Ca(2+) Binding, *Biophys J 111*, 1655-1667.

(184) Scott, A.M., Antal, C.E., et al. (2013) Electrostatic and Hydrophobic Interactions Differentially Tune Membrane Binding Kinetics of the C2 Domain of Protein Kinase C alpha, *Journal of Biological Chemistry 288*, 16905-16915.

(185) Antal, C.E., Callender, J.A., et al. (2015) Intramolecular C2 Domain-Mediated Autoinhibition of Protein Kinase C betaII, *Cell Rep 12*, 1252-1260.

(186) Sommese, R.F., Ritt, M., et al. (2017) The Role of Regulatory Domains in Maintaining Autoinhibition in the Multidomain Kinase PKCalpha, *J Biol Chem 292*, 2873-2880.

(187) Newton, A.C. (1995) Protein kinase C: structure, function, and regulation, *J Biol Chem 270*, 28495-28498.

(188) Luo, J.H., and Weinstein, I.B. (1993) Calcium-dependent activation of protein kinase C. The role of the C2 domain in divalent cation selectivity, *J Biol Chem 268*, 23580-23584.

(189) Orr, J.W., and Newton, A.C. (1992) Interaction of protein kinase C with phosphatidylserine. 2. Specificity and regulation, *Biochemistry 31*, 4667-4673.

(190) Nelson, T.J., and Alkon, D.L. (2009) Neuroprotective versus tumorigenic protein kinase C activators, *Trends in biochemical sciences 34*, 136-145.

(191) Haughian, J.M., Reno, E.M., et al. (2009) Protein kinase C alpha-dependent signaling mediates endometrial cancer cell growth and tumorigenesis, *Int J Cancer 125*, 2556-2564.

(192) Pervushin, K., Riek, R., et al. (1997) Attenuated T2 relaxation by mutual cancellation of dipole-dipole coupling and chemical shift anisotropy indicates an avenue

to NMR structures of very large biological macromolecules in solution, *Proc Natl Acad Sci U S A 94*, 12366-12371.

(193) Ottiger, M., Delaglio, F., et al. (1998) Measurement of J and dipolar couplings from simplified two-dimensional NMR spectra, *J Magn Reson 131*, 373-378.

(194) Grzesiek, S., Anglister, J., et al. (1993) Correlation of Backbone Amide and Aliphatic Side-Chain Resonances in 13C/15N-Enriched Proteins by Isotropic Mixing of 13C Magnetization, *Journal of Magnetic Resonance, Series B 101*, 114-119.

(195) Montelione, G.T., Lyons, B.A., et al. (1992) An efficient triple resonance experiment using carbon-13 isotropic mixing for determining sequence-specific resonance assignments of isotopically-enriched proteins, *Journal of the American Chemical Society 114*, 10974-10975.

(196) Schoenmakers, T.J., Visser, G.J., et al. (1992) CHELATOR: an improved method for computing metal ion concentrations in physiological solutions, *Biotechniques 12*, 870-874, 876-879.

(197) Giorgione, J., and Newton, A.C. (2003) Measuring the Binding of Protein Kinase C to Sucrose-Loaded Vesicles, In *Protein Kinase C Protocols* (Newton, A. C., Ed.), pp 105-113, Humana Press, Totowa, NJ.

(198) Bjorneras, J., Nilsson, M., et al. (2015) Analysing DHPC/DMPC bicelles by diffusion NMR and multivariate decomposition, *Biochim Biophys Acta 1848*, 2910-2917.

(199) Li, J., Ziemba, B.P., et al. (2014) Interactions of protein kinase C-alpha C1A and C1B domains with membranes: a combined computational and experimental study, *J Am Chem Soc 136*, 11757-11766.

(200) Chauhan, A., Chauhan, V.P., et al. (1991) Activation of protein kinase C by phosphatidylinositol 4,5-bisphosphate: possible involvement in Na+/H+ antiport down-regulation and cell proliferation, *Biochem Biophys Res Commun 175*, 852-857.

(201) Lee, M.H., and Bell, R.M. (1991) Mechanism of protein kinase C activation by phosphatidylinositol 4,5-bisphosphate, *Biochemistry 30*, 1041-1049.

(202) Bian, X., and De Camilli, P. (2019) In Vitro Assays to Measure the Membrane Tethering and Lipid Transport Activities of the Extended Synaptotagmins, *Methods Mol Biol 1949*, 201-212.

(203) Liu, T.Y., Bian, X., et al. (2015) Cis and trans interactions between atlastin molecules during membrane fusion, *Proc Natl Acad Sci U S A 112*, E1851-1860.

(204) Xu, R.X., Pawelczyk, T., et al. (1997) NMR structure of a protein kinase C-gamma phorbol-binding domain and study of protein-lipid micelle interactions, *Biochemistry 36*, 10709-10717.

(205) Kortmansky, J., and Schwartz, G.K. (2003) Bryostatin-1: a novel PKC inhibitor in clinical development, *Cancer Invest 21*, 924-936.

(206) Miana, G.A., Riaz, M., et al. (2015) Prostratin: An Overview, *Mini Rev Med Chem 15*, 1122-1130.

(207) Knape, M.J., Ballez, M., et al. (2017) Divalent metal ions control activity and inhibition of protein kinases, *Metallomics 9*, 1576-1584.